2014

Characterization of the Transporter Protein Sodium-Potassium Adenosine Triphosphatase in the Myelin Membrane

Dara E C Schaefer
Wilfrid Laurier University, scha1850@mylaurier.ca

Characterization of the Transporter Protein Sodium-Potassium Adenosine Triphosphatase In the Myelin Membrane

By

Dara Schaefer
B.Sc. Biomedical Toxicology, University of Guelph, 2011

THESIS
Submitted to the Department of Chemistry and Biochemistry
Faculty of Science
In partial fulfillment of the requirements for
Master of Science in Chemistry
Wilfrid Laurier University

2014

Abstract

Sodium-potassium adenosine triphosphatase (Na^+/K^+-ATPase) is an integral membrane protein with known involvement in the maintenance of resting membrane potentials, nutrient uptake, cellular signal transduction, and cell-cell adhesion. The functional enzyme contains a catalytic alpha subunit and a glycosylated beta subunit, of which three isoforms of each are known to exist in the central nervous system (CNS). Altered expression and/or activity of Na^+/K^+-ATPase subunit isoforms has been previously implicated in the pathophysiology of several neurological disorders. This study characterized Na^+/K^+-ATPase expression and distribution in the myelin membrane, identified its specific heterodimeric forms and binding partners, and explored its possible involvement in demyelinating disorders, such as multiple sclerosis. For the first time, Na^+/K^+-ATPase α_1, α_2, and α_3, as well as the β_1, β_2, and β_3 subunits, were shown to co-express within a tissue of the CNS. These six isoforms, in addition to six isozymes ($\alpha_1\beta_1$, $\alpha_2\beta_1$, $\alpha_2\beta_3$, $\alpha_3\beta_1$, $\alpha_3\beta_2$, and $\alpha_3\beta_3$), of Na^+/K^+-ATPase were identified in myelin isolated from mouse brain; this expression shared both similarities and differences with neurons, astrocytes and/or oligodendrocytes. The major isozymes of Na^+/K^+-ATPase identified in myelin were $\alpha_1\beta_1$, $\alpha_2\beta_3$, and $\alpha_3\beta_1$. Co-immunoprecipitation (co-IP) assays demonstrated that the three alpha isoforms of Na^+/K^+-ATPase in the myelin sheath can interact with other Na^+/K^+-ATPase alpha and beta subunit isoforms, in addition to associating with certain myelin-specific proteins and other protein types. These protein binding partners of Na^+/K^+-ATPase have known cellular functions, including RNA splicing, involvement in cell-cell migration and adhesion, the mediation of cytoskeletal

interactions, and the regulation of protein degradation and apoptosis; they also suggested localization of Na$^+$/K$^+$-ATPase to the adherens junctions, tight junctions, caveolin-1 enriched microdomains, lipid rafts and tetraspanin-enriched microdomains of myelin. Western blot analysis indicated that Na$^+$/K$^+$-ATPase expression varies over post-natal development. Distinct differences in protein expression were observed between healthy and diseased myelin. In particular, demyelinating ND4 mice exhibited severe impairment of Na$^+$/K$^+$-ATPase β_1 subunit maturation. Overall, this study has provided a comprehensive look into Na$^+$/K$^+$-ATPase expression and interactions within the myelin sheath, emphasizing its importance to both myelin structure and function.

Acknowledgements

Firstly, I would like to give recognition and many thanks to my supervisor, Dr. Lillian DeBruin, for this opportunity. Her valuable advice and guidance made this project possible, and only further bolstered my scientific curiosity. Secondly, I would like to thank the members of my Supervisory and Examining committees, Dr. Geoff Horsman, Dr. Scott Smith, and Dr. George Harauz, for taking the time to read this document. It has certainly been my greatest academic achievement, in addition to being the longest thing I have ever written (and hopefully ever will write!).

A big thank you to Joe Meissner; your help was much appreciated, as was the comic relief you provided on those stressful grad school days. Thanks to my lab mates Mehak Bhatia, Afshan Sohail, Devang Nijsure, Joanne Liang, Bridget McDonald, Maya Ashoka, and Michael Wolfe for your assistance and companionship. I would also like to thank the entire grad office crew; Tara Tait, Petrease Patton, Tyler Auld, Holly Gray, Alexandra Carvajal, Katie Psutka, Adrian Adamescu, everyone! You provided me with hours of entertainment, and taught me a lifetime's worth of lessons (some academic and some not). I couldn't have asked for better people to work all those long hours with!

I am grateful for all the love and support from my family and friends. Thanks for sticking by my side and continuing to encourage me, even when I was stressed beyond belief and ready to pull out all my hair. A special thanks to my mother for her patience and understanding, but especially for cheering me on in everything that I do. Tyler

Declaration

The data presented and discussed in this thesis are the results of my own work. I hereby declare that I am the sole author of this thesis, including all final revisions, as accepted by my examiners.

Table of Contents

List of Tables

List of Figures

List of Abbreviations

A-domain	Actuator domain
AMOG	Adhesion molecule on glia
APS	Ammonium persulfate
ATP	Adenosine triphosphate
BASP1	Brain acid soluble protein 1
BCA	Bicinchoninic acid
BSA	Bovine serum albumin
CAND1	Cullin-associated NEDD8-dissociated protein 1
CHAPS	3-[(3-Cholamidopropyl)dimethylammonio]-1-propanesulfonate
CIS	Clinically isolated syndrome
CNP	2',3'-cyclic nucleotide 3'-phosphodiesterase
CNS	Central nervous system
Co-IP	Protein complex immunoprecipitation
DM-20	Deletion mutant of proteolipid protein
DRM	Detergent resistant membrane
DTT	Dithiothreitol
EAE	Experimental autoimmune encephalomyelitis
ECM	Extracellular matrix
EDTA	Ethylene diamine tetraacetic acid
EGTA	Ethylene glycol tetraacetic acid
ESI	Electrospray ionization

FDR	False detection rate
HCl	Hydrochloric acid
HRP	Horseradish peroxidase
IgG	Immunoglobulin G
I_{max}	Maximal inhibition
IP	Individual protein immunoprecipitation
K^+	Potassium ion
KCl	Potassium chloride
kDa	Kilodalton
KLF6	Krueppel-like factor 6
LC-MS/MS	Liquid chromatography coupled with tandem mass spectrometry
L_d	Liquid-disordered phase
L_o	Liquid-ordered phase
MAG	Myelin-associated glycoprotein
MALDI	Matrix-assisted laser desorption ionization
MAPK	Mitogen-activated protein kinase
MBP	Myelin basic protein
MCT1	Monocarboxylate transporter 1
MEK	MAPK kinase
$MgCl_2$	Magnesium chloride
MOG	Myelin oligodendrocyte glycoprotein
MRVI1	Protein Mrvi1

MS	Multiple sclerosis
m/z	Mass-to-charge ratio
Na^+	Sodium ion
NaCl	Sodium chloride
NAD(P)H	Nicotinamide adenine dinucleotide phosphate
Na^+/K^+-ATPase	Sodium-potassium adenosine triphosphatase
NaN_3	Sodium azide
NaOH	Sodium hydroxide
Na_3VO_4	Sodium vanadate
N-domain	Nucleotide binding domain
NF-κB	Nuclear factor kappa light-chain-enhancer of activated B cells
NQO1	NAD(P)H quinone oxidoreductase 1
OMgp	Oligodendrocyte myelin glycoprotein
OPCs	Oligodendrocyte-astrocyte glial progenitor cells
P-domain	Phosphorylation domain
P0	Myelin protein zero
PhosSTOP	Phosphatase inhibitor cocktail
PIC	Protease inhibitor cocktail
PLP	Proteolipid protein
PMD	Pelizaeus Merzbacher Disease
PMSF	Phenylmethanesulfonylfluoride
PMP-22	Peripheral myelin protein 22

pNPP	*p*-nitrophenyl phosphate
PNS	Peripheral nervous system
PPMS	Primary progressive multiple sclerosis
PRMS	Progressive relapsing multiple sclerosis
PVDF	Polyvinylidene difluoride
R_f	Rate relative to front
RRMS	Relapsing remitting multiple sclerosis
SDS	Sodium dodecyl sulfate
SDS-PAGE	Sodium dodecyl sulfate polyacrylamide gel electrophoresis
SPAT7	Spermatogenesis-associated protein 7
SPMS	Secondary progressive multiple sclerosis
SRRM2	Serine/arginine repetitive matrix protein 2
TBS	Tris-buffered saline
TEMED	Tetramethylethylenediamine
TMEV	Theiler's murine encephalomyelitis virus
TOF	Time of flight
TTBS	Tris-buffered saline with tween-20
TX-100	Triton-X 100
VDAC	Voltage-dependent anion channel

Chapter 1 – Introduction

1.1 The Nervous System

The nervous system is a complex network of cells which transmit both motor and sensory signals between different parts of the body. It allows the body to respond to changes in its internal and external environments [1]. The nervous system is divided into two distinct, but mutually supporting, branches: the central nervous system (CNS) and the peripheral nervous system (PNS). These systems, as well as their subdivisions, are described in Figure 1.1. Consisting of the brain and spinal cord, the CNS is responsible for higher mental functions and is recognized as the processing center for all of the received stimuli. Alternatively, the PNS is fundamental in reacting to stimuli and uses nerves to conduct the electrical signals between nerve cell bodies outside of the CNS, called ganglia, with the CNS itself [1]. Collaboration between these two divisions is critical for the conscious and unconscious processes required to sustain life.

To facilitate signal transmission throughout the body, specialized cells called neurons receive stimuli and conduct electrochemical waves to other parts of the system. These waves are traditionally called action potentials. Neurons, or nerve cells, receive information via specialized processes called dendrites, which extend from its cell body. Receipt of stimuli will trigger an electrical impulse (action potential), originating in the cell body and propagating along the axon of the neuron. This process is typically the longest extension of the cell, and most neurons generally only have one [1]. Neurotransmitters allow the signal to be passed from one neuron to another, via

specialized contact points called synapses [1]. A synapse will connect the axon of the

pre-synaptic neuron with the post-synaptic cell, often the dendrites of another neuron.

Post-synaptic cells may become excited or inhibited depending on the neurotransmitter

in effect.

```
                              Nervous System
                     ┌──────────────┴──────────────┐
        Central Nervous System (CNS)        Peripheral Nervous System (PNS)
         ┌──────────┴──────────┐              ┌──────────┴──────────┐
       Brain              Spinal Cord        Motor              Sensory
   • Receives and      • Conducts neural     Neurons            Neurons
     processes           signals to and    • Connect CNS to   • Connect sensory
     sensory             from the brain      muscles and        organs to the
     information       • Responsible for     glands of the      CNS
   • Generates           reflex actions      body
     responses                                   │
   • Stores memories           ┌────────────────┴─────────────────┐
   • Responsible for    Somatic Nervous System        Autonomic Nervous System
     higher-order     • Controls voluntary responses • Controls involuntary responses
     thinking                                                     │
     processes                                         ┌──────────┴──────────┐
                                                  Sympathetic        Parasympathetic
                                               • "Fight or flight"  • "Rest and digest"
                                                 responses            responses
```

Figure 1.1 The divisions of the nervous system

The nervous system is divided into the CNS and PNS. The CNS comprises the brain and spinal cord, and processes the neural information that is transmitted. The PNS reacts to stimuli and uses nerves to conduct the electrical signals between nerve cell bodies outside of the CNS to the spinal cord and brain. The peripheral nervous system accommodates both motor and sensory functions; motor responses may be either voluntary or involuntary and therefore are further divided into the somatic and autonomic systems, respectively. Involuntary motor responses include those which prime the body to react to stressful stimuli or trigger the activities that occur in the resting state.

The non-conductive cells of the nervous system are often designated as

supporting cells. They can provide protection of the delicate neuronal processes,

insulation of electrical impulses, and connect the nervous system to the vasculature [1].

2

In the CNS, these cells are commonly referred to as glia, or glial cells. Astrocytes are the most abundant cell type in the nervous system and the largest of all neuroglial cells [1]. They are essential in maintenance of the blood-brain barrier, in addition to maintaining ionic homeostasis, they provide metabolic support to neurons and respond to injurious stimuli [2]. Interestingly, astrocytes have the ability to express voltage-gated sodium channels, despite being classically considered inexcitable [2]. Oligodendrocytes are another glial cell type; their PNS equivalents are called Schwann cells. Both oligodendrocytes and Schwann cells are much smaller in size when compared with astrocytes, and are responsible for the formation of and maintenance of the myelin sheath. Finally, microglia and ependymal cells are two other types of neuroglia. The former possesses phagocytic properties which are often employed in cases of disease or tissue damage, whereas the latter forms the lining of the ventricles and canals of the CNS [1].

1.2 The Myelin Membrane

1.2.1 Structure, Function and Morphology

The propagation of action potentials along a neuronal axon is significantly increased when the axon has been electrically insulated [3]. This insulation can be provided by oligodendrocytes in the CNS or Schwann cells in the PNS, in the form of myelin; however, the formation of the myelin sheath in the CNS is more complicated, as a single oligodendrocyte can myelinate several axons [1]. As shown in Figure 1.2, myelination of an axon is achieved by the wrapping of cytoplasmic extensions of the

supporting cell to form concentric layers of oligodendrocyte or Schwann cell plasma membrane [1;4;5]. During this process, cytoplasm within the wrapping processes of the myelinating cell becomes extruded such that the lipid bilayers are side by side; the intracellular space is compacted to produce the major dense line of myelin, while the extracellular space becomes the intraperiod line of myelin [4]. Neighbouring segments of myelin, along the same neuronal axon, are generated by different oligodendrocytes [6]. The result of myelination is a multi-layered, lipid rich membrane, called the myelin sheath, which protects and insulates the axons of vertebrates for rapid neural transmission. Action potentials generated in myelinated axons are restricted to the nodes of Ranvier; these are segments of the neuron which are not insulated by myelin. Consequently, action potentials travel more rapidly via myelinated axons, as they do not need to travel the full length of the axon; this phenomenon is referred to as saltatory conduction [1].
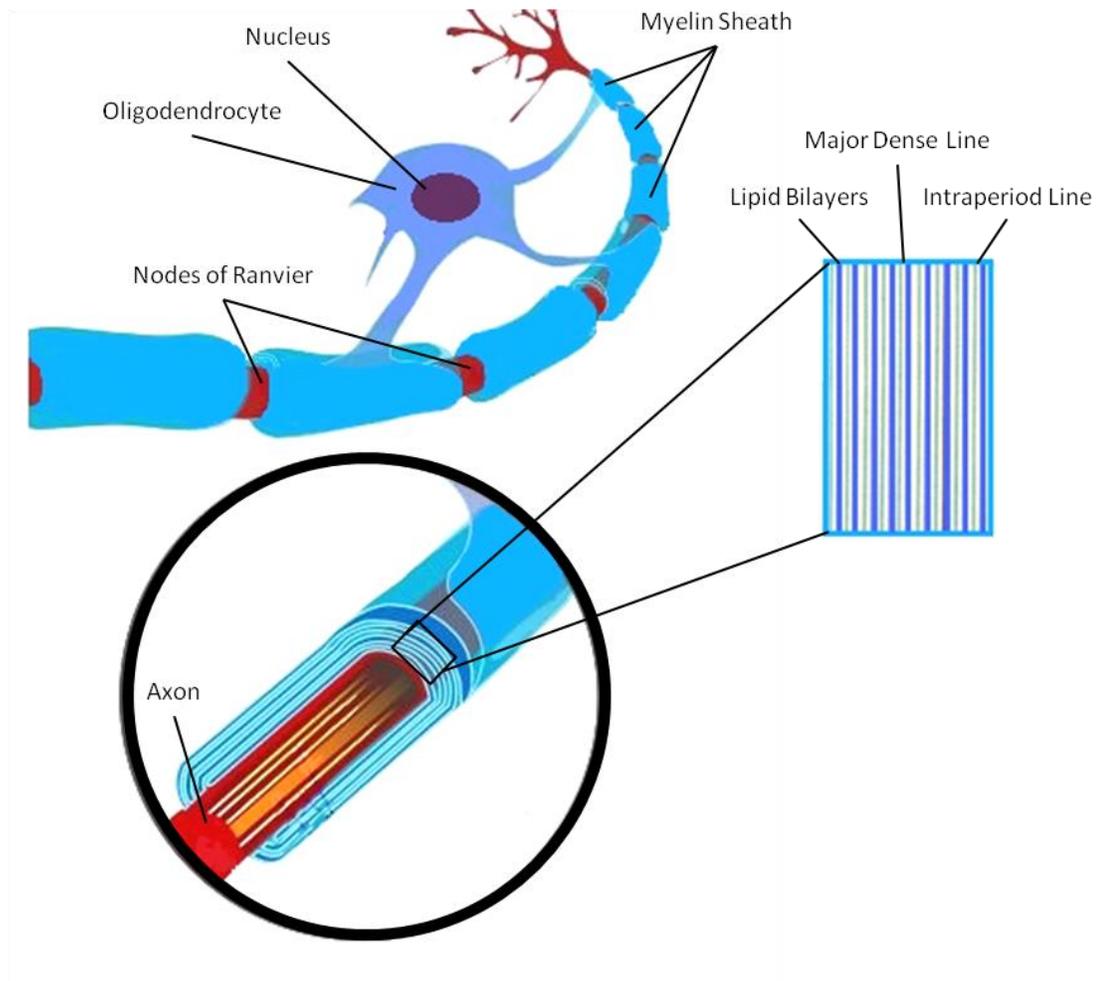
Figure 1.2 The process of myelination by oligodendrocytes

Oligodendrocytes can myelinate multiple axons, and multiple segments of a single axon, by repeatedly wrapping extensions of their cytoplasm around the neuronal axons, forming concentric layers of cell plasma membrane. The cytoplasm and extracellular space of the myelinating cell become extruded such that the lipid bilayers are side by side. The intracellular space is compacted to produce the major dense line of myelin. The extracellular space becomes the intraperiod line of myelin. Image adapted from references [1;7].

The biogenesis of oligodendrocytes begins with their conception from migratory and mitotic precursors; these become progenitor cells, specifically oligodendrocyte-astrocyte glial progenitor cells (OPCs), and mature into post-mitotic myelin-producing cells [6;8]. The maturation of the oligodendroglial cell lineage, and differentiation into myelin-forming cells, is accompanied by corresponding changes in protein expression; in

particular, cell surface antigens which can be recognized by monoclonal antibodies and act as markers of the oligodendrocyte cell lineage [6]. The OPCs are generated in waves, beginning in early embryonic development and continuing after birth [9]. These progenitors migrate throughout the CNS prior to maturation; they are guided by extracellular matrix (ECM) molecules. For example, tenascin-C has proposed inhibitory effects on oligodendrocyte migration, as increased expression at the rat retina-optic nerve junction coincides with an absence of oligodendrocytes [6]. Oligodendrocyte maturation into myelinating cells predominately occurs in the early post-natal life of mammals. Post-migration, the progenitor cells become established along the neural tracts of the CNS that are destined to become white matter; here they differentiate further into preoligodendrocytes [6]. These immature oligodendrocytes, or preoligodendrocytes, express 2',3'-cyclic nucleotide 3'-phosphodiesterase (CNP), which is the first myelin-specific protein that is known to be produced by oligodendrocytes. Finally, the expression of myelin basic protein (MBP), myelin-associated glycoprotein (MAG), and proteolipid protein (PLP) indicate fully matured oligodendrocytes [6].

1.2.2 Lipid and Protein Composition and Membrane Microdomains

The myelin sheath has a high lipid to protein ratio, with its protein composition classically perceived as low in complexity. An estimated 70-80% of the dry weight of myelin is lipid [10;11]. The lipid content is composed of a 2:2:1:1 molar ratio of cholesterol to phospholipid to galactolipid to plasmalogen [11]. It is unclear how cholesterol and these other lipids are enriched to such an unparalleled degree, in myelin. With regards to protein content, oligodendrocytes and Schwann cells express

different myelin-specific proteins [1]. In the PNS, Schwann cells express myelin protein zero (P0) and peripheral myelin protein 22 (PMP-22) during myelination; PLP, myelin oligodendrocyte glycoprotein (MOG), oligodendrocyte myelin glycoprotein (OMgp), and other proteins act as proxies in the CNS [1]. PLP and its isoforms represent 30-45% of the total myelin protein in the CNS [11]. It is believed that PLP provides structural support for the maintenance of the compact lamellar structure of myelin; though it has also been speculated to act as an ionophore [12]. The second most abundant protein found in CNS myelin is MBP; 22-35% of total myelin protein consists of a combination of MBP isoforms [11]. Finally, CNP makes up 4-15% of the total protein in myelin, while the remaining 5-25% is a combination of a variety of different proteins [11]. Transporter proteins and ion channels have not been extensively studied in the myelin membrane.

The myelin sheath, like any biological membrane, is fluid in nature. Molecules within the lipid bilayer are not static; instead, they are dynamic and capable of diffusion within the membrane itself. The fluid mosaic model, proposed by Singer and Nicolson in 1972, describes the ability of proteins and lipids to move via rotational or translational diffusion [13]. Consequently, cellular membranes are heterogeneous and exhibit phase separation. Two coexisting phases, specifically the liquid-disordered (L_d) and liquid-ordered (L_o) phases, are identifiable and can be differentiated by their lipid components; this compartmentalization is observed in the lipid bilayer of model membranes. The liquid-disordered phase is cholesterol-poor and primarily composed of unsaturated lipids, or those with short acyl chains, resulting in a more fluid and disordered membrane [14;15]. In contrast, cholesterol and other sterols are intrinsic to the liquid-

ordered phase [14;15]. This phase is often enriched in sphingolipids, while containing few transmembrane proteins. Cholesterol and sphingolipids become tightly packed, along with saturated lipids, within the L_o phase, creating a thickened, less fluid and more ordered membrane.

Although biological membranes, including the myelin sheath, are fluid, the lipid bilayer is maintained by hydrophobic and hydrophilic interactions; hydrogen bonding, electrostatic interactions, and van der Waals forces also contribute to the arrangement of lipids and proteins in the membrane [13]. These intermolecular forces are involved in the maintenance of L_o and L_d phases, as well as the formation of membrane microdomains, which are basis for many membrane-associated cellular processes [15]. Membrane microdomains, often termed lipid rafts, are enriched in cholesterol and other lipids with longer, highly saturated fatty acid chains; these are characteristic of the L_o phase. Experimentally, in biological membranes, lipid rafts are isolated as detergent resistant membranes (DRMs) using non-ionic detergents at 4^oC. Numerous integral and peripheral membrane proteins are incorporated amongst these lipids, and they impart significant functional roles in biological membranes, including signal transduction, cellular transport, secretion and endocytosis [1;14;16]. The close proximity of interacting proteins within lipid rafts offers efficient signal transduction and has defined these microdomains as "signaling platforms" within biological membranes [1;14]. Proteins identified in the microdomains of myelin have demonstrated developmental regulation that is essential for maintenance of the myelin sheath; similarly, lipid rafts in

oligodendrocyte progenitors have been noted to contain proteins that provide vital

roles in the signaling cascades necessary for their maturation and differentiation [16].

1.3 Demyelinating Diseases

1.3.1 Multiple Sclerosis

Multiple sclerosis (MS) is a chronic disease of the central nervous system. It is

characterized by the destruction of the myelin sheath; a consequence of myelin

detachment from the axon of neurons [1]. These two processes are termed

demyelination and intramyelinic edema, respectively [4]. The loss of myelin is usually

coupled with damage to the oligodendrocytes which generate and maintain the myelin

sheath [1]. Consequently, MS is a model example of a myelinopathy, in which the myelin

sheath is damaged either directly or incidentally as a result of injury to the myelinating

cells [4]. Grinker myelinopathy and Guillain-Barré syndrome are two other well-known

myelinopathies. Figure 1.3 illustrates the typical pattern of myelinopathy, in addition to

depicting other types of neurotoxic injury. The disruption of the myelin sheath, and the

fundamental changes in its protein and lipid chemistry, contributes to the presentation

of plaques which are customarily found in the white matter of individuals afflicted with

MS [1]. In general, the disease manifests in recurring episodes of neurological

insufficiency; symptoms differ according to the regions of the CNS which are affected

[1]. Ultimately, the problem remains a consequence of impaired, or non-existent,

transmission of action potentials. Schwann cells in the PNS are able to remyelinate

neuronal axons, thereby restoring the transmission of electrical impulses; unfortunately,

remyelination in the CNS is more complicated and only occurs to a limited extent [4].

Without adequate cell division of the myelinating cells, the axon remains exposed and

can initiate undesirable cross-talk with adjacent axons [4].
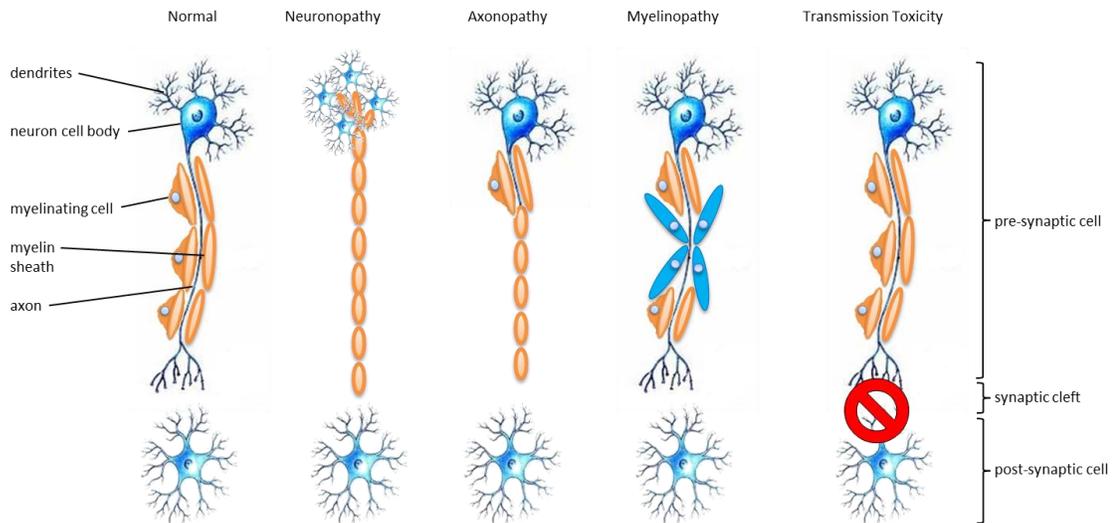
Figure 1.3 Patterns of injury in the cells of the nervous system

Several different processes can result in injury to the cells of the nervous system; these include neuronopathy, axonopathy, myelinopathy and transmission toxicity. Neuron death is termed neuronopathy, and often causes the proliferation of astrocytes. Axonopathy occurs when the axon degenerates, despite neuron survival; the axon is the primary site of injury. Damage to the myelin sheath is termed myelinopathy. Myelinopathies may develop as a consequence of injury to the oligodendrocytes in the CNS, or Schwann cells in the PNS. In cases where cells are uninjured, transmission toxicity can still occur; excitation may be blocked, or cells may become excessively stimulated. Communication between neurons and their post-synaptic cells is disrupted. Image adapted from reference [4].

MS varies in its presentation of symptoms; as such, it has been clinically divided

into four different types. Relapsing-remitting MS (RRMS) is diagnosed in individuals who

experience random episodes of symptom flare-ups, followed by periods of recovery or

remission [18;19]. These so-called attacks may introduce new symptoms or simply a

worsening of existing ones. Both symptomatic episodes and remission periods can last

anywhere from a few hours to several months. RRMS is most common in MS patients,

with more than 80% of cases initially presenting as this type [19]. Two subgroups of

RRMS exist; benign MS and clinically isolated syndrome. Cases in which remission

reaches near completion, and in which there is limited progression in physical disability

15-20 years post-diagnosis, are described as benign MS [18]. Alternatively, patients who

experience only single episodes of neurological symptoms are often diagnosed with

clinically isolated syndrome (CIS), sometimes called 'probable MS' [18]. The second main

classification is primary progressive MS (PPMS). It affects roughly 10-15% of MS patients

and is characterized by the continued advancement of symptoms and escalation of

physical disability [18;19]. This form of the disease often presents later in life, and is the

only type of MS which equally affects both men and women [18]. In all other types,

women appear to be most vulnerable to the manifestation of MS. Secondary

progressive MS (SPMS) initially presents as RRMS, with distinct episodes and periods of

remission; unfortunately, over time the disease evolves such that the disability no

longer improves but continues to gradually worsen [18;19]. Approximately 50% of

patients with RRMS will progress to SPMS within 10 years of their initial diagnosis [18].

Finally, progressive-relapsing MS (PRMS) is a rare diagnosis, in which the patient

experiences a persistent worsening of symptoms combined with acute attacks of

greater severity [18;19]. Although RRMS, PPMS, SPMS and PRMS are clinically discrete,

the development and symptoms of multiple sclerosis range over a spectrum which can

ultimately make for a challenging diagnosis. Disease-modifying treatments, in addition

to those for symptom management, are available; however, the etiology of MS remains

unclear and there is no known cure.

1.3.2 Models for Demyelination

An animal model utilizes non-human organisms as a representation of the pathology, symptoms, and/or prognosis of a human disease. Animal models have been developed not only as tools for investigating human diseases and disorders, but are key to the advancement of therapeutics. They provide a means for examining and manipulating disease processes, such as the development of MS, without unnecessarily harming actual humans. Although it would be ideal to directly study MS in people, tissue samples are hard to come by since patients are rarely biopsied [20]. Samples collected post-mortem provide limited information, as they are often representative of late-stage lesions and the chronic effects of MS; they do not provide much information regarding the generation and development of lesions or mechanisms of demyelination [20]. Typical models of MS demonstrate (1) immune-mediated demyelination, (2) viral-induced demyelination, (3) genetic defects leading to demyelination, or (4) toxin-induced demyelination [21;22]. Well-known examples of each include experimental autoimmune encephalomyelitis (EAE), Theiler's murine encephalomyelitis virus (TMEV), DM-20 (deletion mutant of PLP), and the cuprizone model, respectively.

Pelizaeus Merzbacher Disease (PMD) is an X-linked dysmyelinating disorder of the CNS that is characterized by hypomyelination and a reduction in the total number of mature oligodendrocytes. This human leukodystrophy has been successfully modelled in mice, rats, rabbits, and dogs; each exhibiting spontaneous mutations [21]. More specifically, it was discovered that roughly 25% of patients with PMD possess a mutation in the DM-20 gene which codes for a myelin PLP. DM-20 has proposed roles in

myelinogenesis; its expression has been shown in the normal embryonic development of mice, despite being a minor myelin protein in mature adults [23]. Individuals with increased protein expression demonstrated a more severe phenotype [21]. This discovery guided the development of ND4 transgenic mice, which are now used to model MS. The transgenic ND4 mice contain 70 copies of the DM-20 gene [23]. These mice are clinically normal up to 3 months of age; however, they develop neurological deficits which increase in severity as the animals mature. The transgenic mice die shortly after 8-10 months of age, when neurological symptoms are marked and include tremors and unsteady gait [23]. It is postulated that as the myelin membrane matures in ND4 mice, the overexpression of DM-20 impedes the formation of compact myelin and triggers spontaneous demyelination.

1.4 Sodium-Potassium Adenosine Triphosphatase

1.4.1 Structure, Function, and Localization

Sodium-potassium adenosine triphosphatase (Na^+/K^+-ATPase), also known as the sodium-potassium pump, is an integral plasma membrane protein responsible for the maintenance of the resting potential of cells, including oligodendrocytes, astrocytes, and microglia [24;25]. It belongs to the P-type ATPase family [26]. It specifically utilizes the energy generated from the hydrolysis of adenosine triphosphate (ATP), in order to import two potassium ions into the cell for every three sodium ions the enzyme exports out of the cell [24;27]. The resultant sodium ion gradient produced by the enzyme has been associated with the cellular uptake of nutrients, such as sugars and amino acids

[24]. At rest, the sodium-potassium pump utilizes 20-30% of ATP generated [28]. This active transport of sodium and potassium ions, performed by Na$^+$/K$^+$-ATPase, is a Mg^{2+}-dependent process [29]. Like other P-type ATPases, Na$^+$/K$^+$-ATPase forms an acyl phosphate intermediate; ATP binds to an aspartate residue in the enzyme, via the terminal phosphate of ATP [27]. All P-type ATPase family members contain a 7 amino acid motif that include the necessary aspartate residue; this sequence follows the format of D-K-T-G-T-[LIVM]-[TIS] [27]. The most common version of this DKTG motif is DKTGTLT [27]. P-type ATPases can be further classified according to their structure and function. P$_1$-ATPases transport alkali metal cations, and P$_2$-ATPases transport transition metals or metalloid cations [27]. The P$_3$-ATPase subfamily only has a single member; KdpB is a protein which specifically transports K$^+$ ions [27;30]. Members of each of these subfamilies vary in their arrangement of three key amino acid motifs; the DKTG, TGES, and GDGXNDXP sequences. The TGES motif is located in front of phosphorylation site of the protein, while the GDGXNDXP motif directly follows the ATP binding domain [27].

Generally there are three protein subunits which assemble together via non-covalent bonds to produce the active form of the sodium-potassium pump [29]. These include a catalytic α subunit, a glycosylated β subunit, and a proteolipid γ subunit [29]. The subunits are roughly 110 kDa, 45-55 kDa, and 10 kDa, respectively [29]. The α subunit is polytopic, whereas the β subunit is a type II membrane protein [26]. Alternatively, the γ subunit is a transmembrane protein belonging to the FXYD family [25]. It is not required for functional expression of Na$^+$/K$^+$-ATPase; as a result, Na$^+$/K$^+$-ATPase is commonly identified as a heterodimeric enzyme, composed of a αβ complex.

Several isoforms of the α and β Na^+/K^+-ATPase subunits exist. Each isoform may demonstrate variations in ion, ATP or ligand affinities [24]. Likewise, particular isoforms can be distinguished according to their location in the plasma membrane, their ability to couple with other transporters, or the way in which they are regulated [24].

In mammalian cells, studies have successfully identified four isoforms of the α subunit [24]. Each of these isoforms is roughly 1000 amino acid residues in length [27]. The divergence in amino acid sequences between the isoforms is minor, and it is unclear how these changes influence the functional roles of the subunits [27]. The amino acid sequences of Na^+/K^+-ATPase α_1, α_2, and α_3 are available in Appendix B. The α_1 subunit is the most prominent isoform, with ubiquitous expression in mammalian cells, and it is typically the dominant or exclusive isoform found in epithelia and kidney cells [24;27]. Alternatively, the α_2 subunit is found in specific tissues including brain, muscle, adipose, osteoblasts, retina, choroid plexus, lung, and the optic nerve [24]. It regulates muscle contractility, and is involved in responding to stress by adjusting blood pressure [31]. The α_3 and α_4 subunits demonstrate significant tissue specificity. The α_3 subunit is expressed in the neural tissue of most animals, though it has also been identified in human cardiac tissue [24]. With restriction to the testis, the α_4 subunit has only been identified in spermatogonia and sperm [24;27]. It was demonstrated that inhibition of the α_4 subunit results in immotile sperm, and mutations can ultimately impair fertility [27;31]. Diversity in Na^+, K^+, ATP and cardiac glycoside affinity has been noted among the α subunit isoforms [24]. For example, the rat α_3 isoform has demonstrated a reduced affinity for Na^+ in comparison to α_1 and α_2, whereas α_1 exhibits a greater K^+

affinity than its α_2 and α_3 counterparts [24]. The isoforms of the α subunit have displayed a minimum of 85% conserved sequences, across species [32]. Neurological diseases such as familial hemiplegic migraine type 2 and rapid-onset dystonia-parkinsonism have been associated with human mutations of the α_1- and α_2-subunits [31].

The C- and N-termini of the α subunit are both intracellular, and the subunit also possesses five extracellular and four intracellular loops [27]. Consequently, the α subunit of Na^+/K^+-ATPase has 10 transmembrane domains, as shown in Figure 1.4. This observation is consistent with other P-type ATPases, as all family members have at least six transmembrane helices (M1-M6); also, the P_2-type ATPase subclass, of which Na^+/K^+-ATPase belongs, have 10 transmembrane helices (M1-M10) [33]. These transmembrane regions accommodate the ion binding sites for Na^+ and K^+ [32]. Three major cytoplasmic domains have also been identified in the α subunits; these include the actuator (A-), nucleotide binding (N-), and phosphorylation (P-) domains [32]. The actuator domain is composed of the N-terminal and second cytoplasmic domain (CD2) connecting helices M2 and M3; it contains the TGES motif [27]. Alternatively, the third cytoplasmic domain (CD3) connecting M4 and M5 accommodates the nucleotide binding and phosphorylation domains, with the N-domain being inserted in the P-domain [32]. The conserved aspartate residue, and its associated DKTG sequence, is located within the P-domain [27].
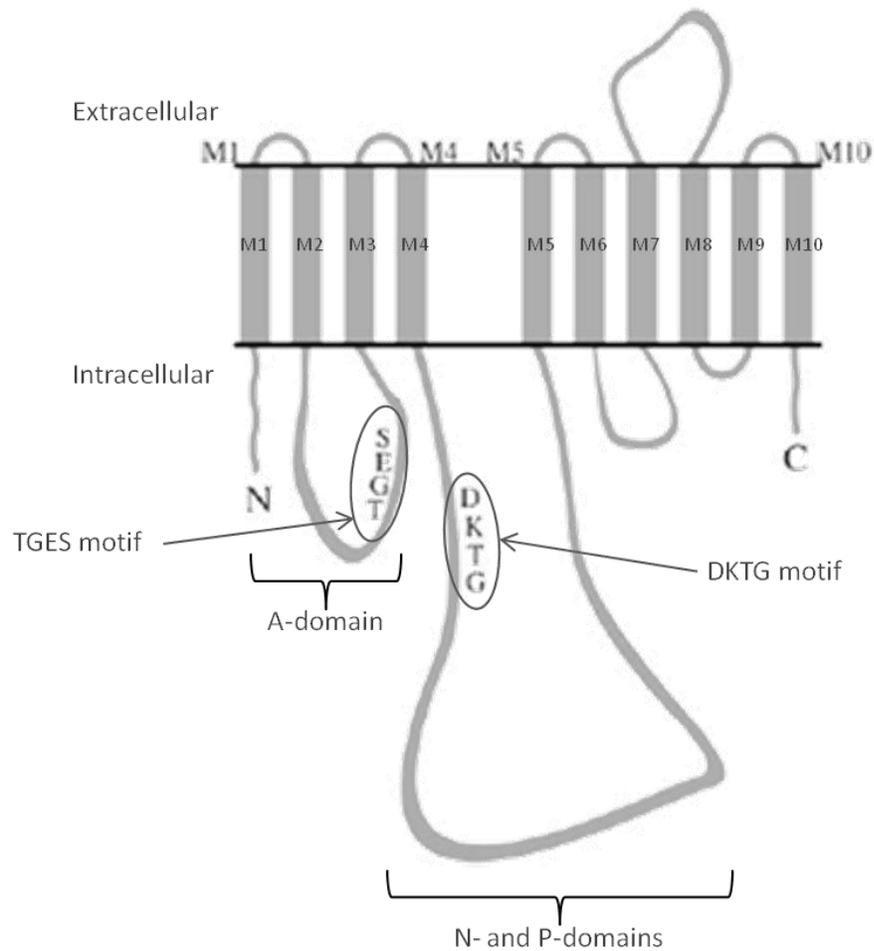
Figure 1.4 The typical structure of the α subunit of Na$^+$/K$^+$-ATPase

The α subunit of Na$^+$/K$^+$-ATPase has 10 transmembrane domains, with both N and C-termini located on the cytoplasmic side of the plasma membrane. Image modified from reference [27].

To date, four isoforms of the 370 amino acid long β subunit have been discovered [27]. Only three of the isoforms (β$_1$, β$_2$, β$_3$) have been shown to occur in mammalian cells [24]. Limited information is available regarding the β$_4$ subunit, at this time. Similar to the α$_1$ subunit, the β$_1$ subunit is found in most tissues [24]. It is intimately involved in the intracellular adhesion of epithelial cells [31]. Alternatively, the β$_2$ subunit is limited primarily to neural tissue, whereas the β$_3$ subunit can be found in a broader range of tissues [27;34]. The β$_2$ subunit, sometimes referred to as the adhesion

molecule on glia (AMOG), plays an important role in the adhesion and subsequent migration of neurons on glial cells [31]. The N-terminus of the β subunit and roughly 30 amino acid residues reside in the cytoplasm [27]. All isoforms of the β subunit are heavily glycosylated, with the extracellular portion of the β subunit containing N-linked glycosylation sites, either NXS or NXT [3;27]. Each isoform varies in its number of potential N-glycosylation sequences; this value also depends on the species of origin. For example, the mammalian β_1 subunit has three possible extracellular N-glycosylation sites; alternatively, the β_2 subunit may have eight or nine potential N-glycosylation sites if derived from a human or mouse, respectively [3]. The β_1 subunit extracellular domain is also the site of several disulfide bridges; enzyme activity is lost if these disulfide bridges are disrupted [3;27]. The structure of the mammalian β_1 subunit is illustrated in Figure 1.5. Conservation of amino acid sequences is much lower for the isoforms of the β subunit when compared to the α subunit, with β_3 subunits being as low as 50% identical across species [32]. The amino acid sequences of Na^+/K^+-ATPase β_1, β_2, and β_3 are available in Appendix B. A decrease in β_1 subunit expression has been linked to certain forms of cancer, whereas disturbances in β_2 subunit expression and distribution within cells and/or tissues have been associated with gliomas and epilepsy [31].
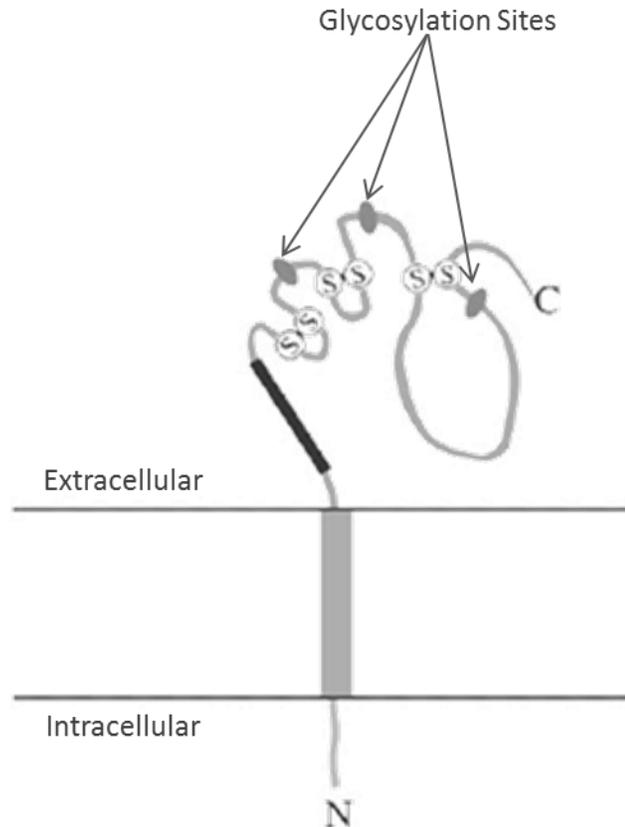
Figure 1.5 The structure of the mammalian β_1 subunit of Na$^+$/K$^+$-ATPase

The β_1 subunit of Na$^+$/K$^+$-ATPase has a single transmembrane segment, with a large extracellular region. The N-terminal is located with the cytoplasm, while the C-terminal, 3 N-glycosylation sequences and 3 disulfide bridges are found on the extracellular portion of the protein. Image modified from reference [27].

1.4.2 Altered and Proposed Functions

Both α and β subunits are vital for cardiac glycoside-sensitive Na$^+$/K$^+$-ATPase

activity; separation of these components results in a loss of enzymatic activity [27]. It

has been unmistakably shown that the β subunit is responsible for the transport and

placement of the α subunit into the plasma membrane; nonetheless, the β subunit can

be expressed in the membrane without α expression [27]. These components are

combined in the endoplasmic reticulum, where independent production of the subunits

also occurs [27]. Despite the obvious tissue-specific distribution of both the α and β

isoforms of Na^+/K^+-ATPase, little is known regarding specific αβ heterodimers [31].

Members of the FXYD family have been closely associated with Na^+/K^+-ATPase;

these proteins modulate the kinetic activity of the enzyme [25]. Currently, all

crystallized structures of the αβ complex of Na^+/K^+-ATPase have been shown to

associate with an FXYD protein; nonetheless this γ subunit is not essential for the

functional expression of the αβ complex [32]. It is for this reason that the sodium

potassium pump is commonly classified as a heterodimeric protein. Regardless, it is

important to recognize the influence these proteins have on the enzymatic activity of

Na^+/K^+-ATPase. The various isoforms of the γ subunit, FXYD1-7, are summarized in Table

1.1. These variants differ in their localization and have distinct structural divergence in

their N-terminal sequences [25]. The γ subunit has been shown to influence the catalytic

function of Na^+/K^+-ATPase in two distinct ways; it increases the affinity between ATP

and the enzyme, in addition to increasing antagonism between sodium and potassium

ions [35]. The sodium and potassium ions will compete for Na^+ activation sites on the

cytoplasmic side of the plasma membrane [25].

Table 1.1 FYXD Proteins

This table provides the distribution of FXYD proteins which associate with Na^+/K^+-ATPase, in addition to providing the known effects that these proteins have on its enzymatic activity. Table modified from reference [36].

Isoform	Distribution	Function
FXYD1	• Known to combine with Na^+/K^+-ATPase $α_1, α_2$, and $α_3$ in the cerebellum • Most abundant in Purkinje cells, choroid plexus and ependymal cells • Present in neurons and glia	• Decreased affinity of Na^+/K^+-ATPase for Na^+ and K^+

	• Limited expression identified in Allan Atlas rat brain	
FXYD2	• Moderate expression identified in Allan Atlas rat brain	• Decreased affinity of Na^+/K^+-ATPase for Na^+ and K^+
FXYD3	• No expression in Allan Atlas rat brain	• Decreased affinity of Na^+/K^+-ATPase for Na^+ and K^+
FXYD4	• No expression in Allan Atlas rat brain	• Decreased affinity of Na^+/K^+-ATPase for Na^+ and K^+
FXYD5	• Limited expression identified in Allan Atlas rat brain	• Increased Na^+/K^+-ATPase maximum enzyme inhibition (I_{max})
FXYD6	• Abundant expression identified in Allan Atlas rat brain	• Decreased affinity of Na^+/K^+-ATPase for Na^+ and K^+
FXYD7	• Almost exclusive to brain • Abundant expression identified in Allan Atlas rat brain	• Decreased affinity of Na^+/K^+-ATPase for Na^+ and K^+

The general reaction mechanism for Na^+/K^+-ATPase is depicted in Figure 1.6.

Na^+/K^+-ATPase exists largely in two enzymatic states. These states, E_1 and E_2, are due to

extreme conformational changes which occur during the catalytic process [33]. E_1 is the

high affinity state for the primary transported ion (Na^+ in this case), whereas E_2 is the

low affinity state for sodium ions [33]. It has been suggested that a minimum of four of

these steps are voltage-dependent. In particular, the cytoplasmic Na^+ binding, the E_1 to

E_2 conformational change, the extracellular release of Na^+, and the extracellular binding

of K^+, are all thought to be voltage dependent [37].

Extracellular

E_2P ouabain

E_2P ⬤⬤ → → ⬤⬤ → E_2P → → E_2P ⬤⬤

P_i

E_2 ⬤⬤

E_1P ⬤⬤⬤

E_2ATP ⬤⬤

ADP

E_1ATP ⬤⬤⬤ ← ← E_1ATP ← ← E_1ATP ⬤⬤

Intracellular

⬤ Sodium Ion
⬤ Potassium Ion
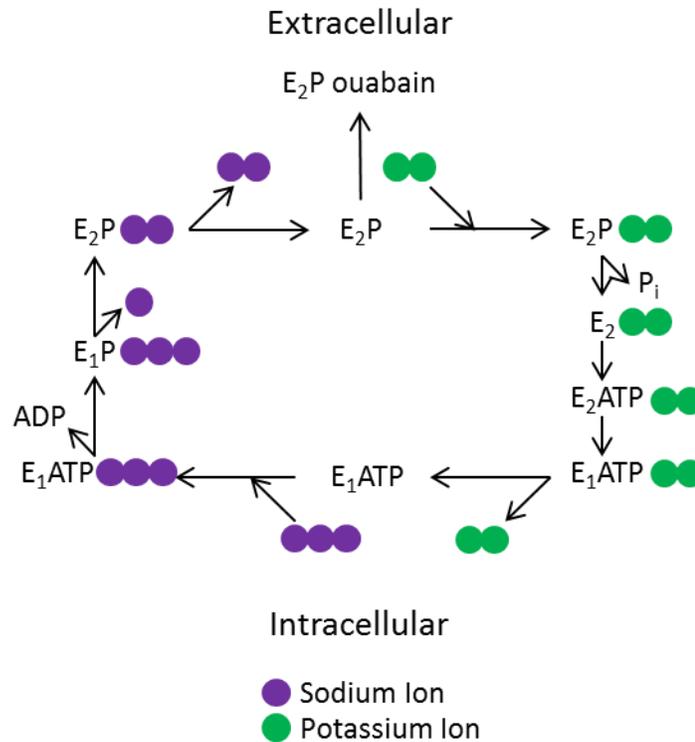
Figure 1.6 The Na$^+$/K$^+$-ATPase reaction cycle

Sodium and potassium ions are represented by purple and green dots, respectively. The E_1 state has a high affinity for sodium ions, while the E_2 state has a low affinity for sodium ions. Sodium and potassium ions are exchanged across the plasma membrane by Na$^+$/K$^+$-ATPase, using the energy captured from the hydrolysis of ATP. Image adapted from reference [27].

There are two main categories within which Na$^+$/K$^+$-ATPase inhibitors can be classified; these include glycoside inhibitors and non-glycoside inhibitors. Glycoside inhibitors, otherwise known as cardiac glycosides, are characterized by the union of an aglycone, or genin, and one to four sugars [38]. The aglycone is pharmacologically active, with a chemical structure similar to steroids or bile acids; conversely, the sugars determine the potency and duration of action of the inhibitor by managing its solubility [38]. Examples of cardiac glycosides include digoxin and ouabain. Like all cardiac glycosides, these compounds can be further divided into two classes of glycoside inhibitors: the cardenolides and the bufadienolides. In contrast, non-glycoside inhibitors

22

have distinctive chemical structures from the glycosides, or have a modified aglycone component. For example, cassaine is a non-glycoside inhibitor, in which the steroid ring is broken [38].

Though ion transport is the primary function of Na^+/K^+-ATPase, several unrelated functions have been proposed. It has demonstrated a role in cellular signalling pathways. Exposure to low levels of the glycoside inhibitor ouabain, at concentrations which do not affect ion gradients, has been associated with increased cellular growth [24]. Na^+/K^+-ATPase appears to be involved in two Ras-dependent signalling cascades, which are activated by ouabain inhibition of the enzyme. In the first pathway, Ras promotes the formation of reactive oxygen species which in turn activate nuclear factor kappa light-chain-enhancer of activated B cells (NF-κB); while in the second pathway, the induced Ras protein initiates a Raf/MEK/MAPK cascade [24]. MAPK refers to the mitogen-activated protein kinase, and MEK is the MAPK kinase. It is unclear if the induction of these signalling cascades is due to the inhibition of a specific α subunit, or if several isoforms are affected. The effect has been demonstrated in kidney and HeLa cells which only express the α_1 subunit; however, ouabain-induced signalling and cell growth has also been witnessed in cardiac myocytes and smooth muscle cells which express both α_1 and α_2 subunits [24].

1.5 Purpose of the Study

Disrupted Na^+/K^+-ATPase activity has already been implicated in a variety of disorders, such as male infertility, rapid onset dystonia Parkinsonism, essential

hypertension, migraine headaches, and epilepsy [24;27;39;40]. Decreased Na^+/K^+-ATPase expression has also been previously recognized in bladder, kidney, colon, breast and pancreatic cancers [41]. Changes in the activity or expression of Na^+/K^+-ATPase within the central nervous system may designate this protein as a biomarker of certain neurological conditions, including MS. The three CNS neural cell types, specifically neurons, astrocytes and oligodendrocytes, do not demonstrate equivalent expression of either the α or β isoforms of Na^+/K^+-ATPase [36]. In addition, neither the $α_4$ or $β_4$ isoforms are known to exist in the central nervous system of humans. The role of Na^+/K^+-ATPase in the myelin membrane, and its potential as a biomarker of MS, has not been previously investigated. MS affects people of all age demographics, emphasizing the value in successfully treating this condition. Likewise, it is one of the main causes of permanent disability in not only paediatric and elderly populations, but also young adults [17].

The main purpose of this study was to characterize sodium-potassium adenosine triphosphatase in the myelin membrane, using a mouse model. In order to achieve this feat, three primary objectives were defined:

- The first objective of this study was to identify which Na^+/K^+-ATPase subunit isoforms exist in mouse myelin, determine how they are distributed among the various microdomains, and to characterize their expression.
- The second objective was to determine:
  - The heterodimeric forms of Na^+/K^+-ATPase in mouse myelin.

24

- The specific binding partners of Na^+/K^+-ATPase in mouse myelin.

- The third objective was to evaluate any differences in the expression of Na^+/K^+-ATPase, and its individual subunit isoforms, in healthy mouse myelin and in diseased mouse myelin, specifically using ND4 mice to model MS.

The realization of these objectives will provide insight into the structural and functional roles of Na^+/K^+-ATPase within the myelin sheath. Establishing the normal protein interactions of Na^+/K^+-ATPase and its expression in healthy, intact myelin will provide the basis for its comparison in models of myelinopathies such as MS. Although Na^+/K^+-ATPase is an integral membrane protein, making its use as a biomarker more challenging, understanding its role in demyelination will also provide crucial information for the development of therapies for neurological diseases. Determining the contribution of Na^+/K^+-ATPase to either demyelination or remyelination processes, and identifying its binding partners, will indicate possible ways that the protein can be manipulated for preventative or therapeutic purposes.

Chapter 2 – Materials, Experimental Techniques, and Methodology

2.1 Materials

Mouse brains, collected from CD1 strain mice, were purchased from Rockland Inc. (Gilbertsville, PA, USA) and Bioreclamation LLC (Liverpool, NY, USA). The transgenic ND4 mouse brains were provided by Dr. George Harauz, from the University of Guelph (Guelph, ON, Canada). All animal tissues were stored at -80°C. The Pierce Micro Bicinchoninic acid (BCA) Protein Assay Kit used in this study was from ThermoScientific (Rockford, IL, USA). Protease Inhibitor Cocktail (PIC) and Phosphatase Inhibitor Cocktail (PhosSTOP) tablets were from Roche (Mannheim, Germany). Grade 703 blotting paper was from VWR International (Mississauga, ON, Canada), while 0.45 µm nitrocellulose membrane was purchased from both Bio-Rad Laboratories Ltd. (Mississauga, ON, Canada) and Santa Cruz Biotechnology (Dallas, TX, USA).

Ethyl ether and ammonium bicarbonate were purchased from EMD Chemicals (Gibbstown, NJ, USA). Anhydrous alcohol and acetonitrile were from Mallinckrodt Baker, Inc. (Philipsburg, NJ, USA). Methanol was from Fischer Scientific (Fair Lawn, NJ, USA) and acetone was purchased from Caledon Laboratories Ltd. (Georgetown, ON, Canada). Sodium thiosulfate, silver nitrate, 37% formaldehyde, sodium carbonate, triton X-100 (TX-100), and 3-[(3-Cholamidopropyl)dimethylammonio]-1-propanesulfonate (CHAPS) detergent were purchased from Sigma-Aldrich (St. Louis, MO, USA). TX-100 10% (w/v) solution was also purchased from ThermoScientific (Rockford, IL, USA) as Surfact-Amps

X-100. Sodium dodecyl sulfate (SDS) was purchased from Bio Basic Inc. (USA) and Fluka Chemie (Switzerland). Additionally, AccuGENE 10% (w/v) SDS was obtained from Lonza (Rockland, ME, USA). Tetramethylethylenediamine (TEMED) was from both Fisher Scientific (Fair Lawn, NJ, USA) and Bio-Rad Laboratories, Inc. (Hercules, CA, USA). Acrylamide/bis 30% solution (37.5:1) was purchased from Bio-Rad Laboratories, Inc. (Japan). Tween-20 10% solution, Precision Plus Protein Dual Color Standards, and Coomassie G-250 BioSafe stain were from Bio-Rad Laboratories, Inc. (Hercules, CA, USA). Hydrochloric acid (HCl) was purchased from VWR Scientific Products (West Chester, PA, USA) and from EM Science (Darmstadt, Germany). Glacial acetic acid was also purchased from EM Science (Darmstadt, Germany). Ammonium persulfate (APS), glycerol and trypsin gold, mass spectrometry grade, were from MD Biochemicals, LLC (Solon, OH, USA), Sigma-Aldrich (St. Louis, MO, USA) and Promega Corporation (Madison, WI, USA), respectively.

Tris base was obtained from both BioBasic Inc. (USA) and Sigma-Aldrich (St. Louis, MO, USA). Sucrose was purchased from Fischer Scientific (Fair Lawn, NJ, USA) and Sigma-Aldrich (St. Louis, MO, USA). Potassium chloride (KCl), magnesium chloride (MgCl$_2$), sodium chloride (NaCl), ethylene diamine tetraacetic acid (EDTA), ethylene glycol tetraacetic acid (EGTA), dithiothreitol (DTT), iodoacetamide, 2-mercaptoethanol, sodium orthovanadate (Na$_3$VO$_4$), phenylmethanesulfonylfluoride (PMSF), and 2-[4-(2-hydroxyethyl)piperazin-1-yl]ethanesulfonic acid (HEPES) were also from Sigma-Aldrich. Bromophenol blue sodium salt was obtained from Fisher Scientific (Fair Lawn, NJ, USA). Percoll was from GE Healthcare (Uppsala, Sweden). Skim milk powder was from Metro

Selection (Toronto, ON, Canada). Glycine was purchased from Fischer Scientific (Fair

Lawn, NJ, USA). Formic acid was purchased under the Fluka brand of Sigma-Aldrich

(Steinheim, Germany). D-mannitol was from Acros Organics (Geel, Belgium). Cholera-

toxin B subunit peroxidase conjugate was from Sigma-Aldrich (St. Louis, MO, USA).

Table 2.1 Primary antibodies used in this study

Primary antibodies were obtained from EM Millipore (Temecula, CA, USA), Santa Cruz Biotechnology
(Dallas, TX, USA), Sigma-Aldrich (St. Louis, MO, USA) and ThermoScientific (Rockford, IL, USA).

Antibody	Type	Specificity/Epitope	Host	Supplier	Product Identifier
β-Actin	Monoclonal	N-terminal	Mouse	Sigma-Aldrich	A-1978
Na^+/K^+-ATPase α	Monoclonal	aa 551-850 of Na^+/K^+-ATPase α	Mouse	Santa Cruz	SC-48345
Na^+/K^+-ATPase α_1	Monoclonal	Purified renal outer medulla of rabbit origin	Mouse	Santa Cruz	SC-21712
Na^+/K^+-ATPase α_2	Polyclonal	Peptide mapping within a cytoplasmic domain of Na^+/K^+-ATPase α_2 of human origin	Goat	Santa Cruz	SC-31391
Na^+/K^+-ATPase α_3	Monoclonal	Na^+/K^+-ATPase α_3	Mouse	ThermoScientific	XVIF9-G10, MA3-951
Na^+/K^+-ATPase β_1	Monoclonal	External domain of Na^+/K^+-ATPase β_1	Mouse	Santa Cruz	SC-58626
Na^+/K^+-ATPase β_2	Polyclonal	aa 15-141 from the central region of human Na^+/K^+-ATPase β_2	Rabbit	ThermoScientific	PA5-26279
Na^+/K^+-ATPase β_3	Polyclonal	Internal region of Na^+/K^+-ATPase β_3 of mouse origin	Goat	Santa Cruz	SC-66343
MBP	Monoclonal	aa 82-87	Rat	Millipore	MAB386
MCT1	Polyclonal	aa 430-460	Rabbit	ThermoScientific	PA5-12335
NQO1	Polyclonal	aa 200 to C-terminus of human NQO1	Rabbit	ThermoScientific	PA5-19624
VDAC	Polyclonal	Human VDAC	Rabbit	Millipore	AB10527

EZview Red Protein A and G Affinity Gels were from Sigma-Aldrich (St. Louis, MO, USA), while the Na^+/K^+-ATPase α_1 antibody conjugated agarose (SC-21712) was acquired from Santa Cruz Biotechnology (Dallas, TX, USA). The antibodies, their suppliers, and product information, used in this study, are provided in Tables 2.1 and 2.2. The two enhanced chemiluminescent reagents, SuperSignal West Femto Substrate and VisiGlo Select HRP Chemiluminescent Substrate, were from ThermoScientific and AMRESCO (Solon, OH, USA), respectively. The water used throughout this study was filtered using a Milli-Q water purification system (Millipore).

Table 2.2 Secondary antibodies used in this study

Secondary antibodies were obtained from Rockland Inc. (Gilbertsville, PA, USA), Sigma-Aldrich (St. Louis, MO, USA) and ThermoScientific (Rockford, IL, USA).

Antibody	Type	Specificity/Epitope	Host	Supplier	Product Identifier
Anti-Goat IgG-HRP	Polyclonal	IgG	Rabbit	Sigma-Aldrich	A-5420
Anti-Mouse IgG-HRP	Polyclonal	IgG, Fc fragment	Goat	Sigma-Aldrich	A-2554
Anti-Rabbit IgG-HRP	Polyclonal	IgG	Goat	Sigma-Aldrich	A-0545
DyLight 488 Anti-Rat IgG	Polyclonal	IgG	Goat	Rockland	612-141-120
DyLight 549 Anti-Rabbit IgG	Polyclonal	IgG	Goat	ThermoScientific	35557
DyLight 649 Anti-Mouse IgG	Polyclonal	IgG	Goat	ThermoScientific	35515

Refer to Appendix A for information regarding the structure and physical and chemical properties of the detergents used in this study.

2.2 Experimental Techniques

2.2.1 Electrophoretic Separation of Proteins

Sodium dodecyl sulfate polyacrylamide gel electrophoresis (SDS-PAGE) is a commonly used biochemical technique, also known as Laemmli gel electrophoresis, which separates proteins according to their molecular mass. In this technique, the proteins are exposed to a detergent, specifically SDS, and a reducing agent, such as 2-mercaptoethanol. These compounds are responsible for the disruption of tertiary and quaternary protein structures. They denature the proteins by interacting with hydrophobic domains and breaking disulfide bonds, respectively. SDS also imparts a negative charge to proteins by coating their surfaces, which allows for separation using an electrical current. When these protein samples are applied to a discontinuous polyacrylamide gel, the now negatively charged proteins migrate towards the positive electrode; since all the proteins are linearized, they migrate according to their overall size and the smaller, lower molecular mass proteins will migrate the fastest.

A typical Laemmli SDS-PAGE gel system consists of a stacking gel of pH 6.8, a resolving gel of pH 8.8, and an electrophoresis buffer containing glycine [42]. Both the stacking and resolving gels consist of polymerized acrylamide which is formed by the addition of APS and TEMED; these ingredients initiate the polymerization of acrylamide by both introducing and stabilizing free radicals. The presence of bisacrylamide allows cross-linking between polyacrylamide chains, thereby producing the gel structure. Stacking gels generally contain a lower percentage of acrylamide; thus, they have larger

pores for the proteins to migrate through during electrophoresis. Alternatively, the resolving gels have a higher acrylamide concentration, though it can vary as needed; higher acrylamide content is necessary for the resolution of smaller molecular mass proteins, as it produces a gel with smaller pores. During electrophoretic separation, glycine from the running buffer migrates towards the cathode and becomes fully deprotonated while transitioning between the stacking and resolving gels. Chloride ions in the gel also migrate towards the cathode. In the stacking gel, glycine migrates slower, and chloride ions migrate faster, than the negatively charged sample proteins; however, once in the resolving gel, the newly deprotonated glycine ions become increasingly mobile and pass the sample proteins, thereby encouraging their separation according to molecular mass [42].

SDS-PAGE can separate proteins ranging from 20-250 kDa in size, though the scope can be altered by increasing or decreasing the acrylamide content of the resolving gel. Although it offers high resolution of protein separation, the Laemmli gel system can be inconvenient due to the time consuming gel casting procedure. Preparation and polymerization of both stacking and resolving gels can take a total of 60-90 minutes, while the running time takes roughly an additional 80 minutes [42]. Once proteins are separated, SDS-PAGE gels can be stained with Coomassie or silver; they can also be transferred to a solid support for Western blot analysis.

2.2.2 Western Blotting with Chemiluminescence and Fluorescence Detection

Western blotting was used throughout this study to qualitatively and quantitatively evaluate protein product expression. It allows for the identification of specific proteins within complex biological samples; it is a useful tool for monitoring protein expression in various tissues and under different conditions. Gel electrophoresis is used to separate proteins according to molecular mass, and these proteins can then be transferred to a solid support such that they can be probed with antibodies. Nitrocellulose or polyvinylidene difluoride (PVDF) are two types of membranes which are commonly used as the solid support in Western blotting. In this study, a wet electrotransfer procedure was used to transfer myelin proteins to nitrocellulose membranes; similar to electrophoresis, the proteins migrate from the gel towards the membrane using an electrical current.

Once the solid support membrane is prepared, it is probed with a primary antibody. Primary antibodies are designed for the unambiguous identification of a single protein; they contain paratopes which recognize and bind unique epitopes, or antigenic regions, of their respective protein targets. Epitopes which are not unique between two or more different proteins may result in non-specific binding and cross-reactivity of the antibody with other proteins in the sample or in the blocking buffer.

Antibodies can also be developed in two different ways; consequently, there are two main types of antibodies. Monoclonal antibodies are produced using identical immortalized B lymphocytes; they target a specific antigen or region of the molecule of

interest. Polyclonal antibodies, on the other hand, are developed through the immunization of animals; therefore, they are a collective of antibodies which can target different components of the same molecule [1]. Polyclonal antibodies are produced by many different B lymphocytes and since they recognize multiple epitopes of a single antigen, they are far less specific than monoclonal antibodies.

After a primary antibody has been applied, Western blots are subsequently exposed to a secondary antibody that is designed to bind the primary antibodies which are securely adhered to the proteins of interest on the solid support. Secondary antibodies may be fluorescently tagged or conjugated to an enzyme, thereby allowing the antibody bound regions of the membrane to be visualized. Alternatively, chemiluminescent blots take advantage of secondary antibodies which are conjugated to an enzyme such as horseradish peroxidase (HRP) or alkaline phosphatase [43]. These blots are incubated in a detection reagent prior to imaging; this reagent contains the substrate for these enzymes and light is emitted as a by-product of the reaction. Both fluorescent and chemiluminescent detection methods produce a signal which can be measured by densitometric analysis and used to quantify protein expression. The intensity of the measured signal is proportional to the amount of protein bound by antibody. The two methods provide extremely sensitive protein detection; for example, 2-4 pg of transferrin protein can be detected using fluorescence, whereas little as 1 pg is detectable with chemiluminescence [44].

2.2.3 Individual Protein and Protein Complex Immunoprecipitation

Individual protein, or immunoprecipitation (IP), assays are used for the purification of a specific protein from a complex mixture. Alternatively, protein complex, or co-immunoprecipitation (co-IP), studies are used for the purification of a group of interacting proteins; it is also an effective way to examine indirect protein-protein interactions [45]. Co-IP procedures use an antibody to specifically isolate a bait protein and its respective targets. The bait is the protein of interest, while its binding partners or associated proteins are the targets [45]. In contrast, IP studies directly capture only the target protein. In either scenario, a solid support, such as agarose or other polymeric beads which are covalently bonded to Protein A or G, are used to bind an antibody specific for the protein of interest; Protein A and G bind antibodies at either the Fc portion or Fab fragments of Immunoglobulin G (IgG) [46]. Protein A and G are able to interact with antibodies of various species and subclasses; however, not every antibody is capable of immunoprecipitation and therefore may require use of a polyclonal antibody or the addition of a bridging antibody which is reactive with the primary antibody but also has a higher affinity for Protein A or G.

When the biological sample (i.e., complex mixture) is introduced to the beads, the target or bait/target protein complexes will bind to the antibody and become immobilized. Unbound proteins can then be washed away, and the bait and/or targets can be eluted using detergents or by boiling. Non-specific binding by undesirable proteins can be prevented by altering the wash buffer; salt or detergent content will affect the stringency of IP/co-IP studies. The antibody may also co-elute, resulting in

immunoglobulin light and heavy chains appearing in the final product. Softer elution

methods, which avoid boiling, can be developed; these may reduce the likelihood of

antibody contamination. In situations where IP/co-IP experiments are paired with

Western blotting, antibody contamination poses a problem since many secondary

antibodies are raised against immunoglobulins. The signal may become overwhelmingly

high if the IP/co-IP capture antibody and the Western primary antibodies were

produced in the same species; thus, it is important to use antibodies from different

species or minimize contamination [45]. Similarly, the light and heavy immunoglobulin

chains of the antibody may mask unique protein bands in the eluted product, if

examined using Coomassie or silver staining.

2.2.4 Protein Identification by Mass Spectrometry

Mass spectrometry is a popular analytical technique for the identification of

biological molecules. It is highly sensitive and allows for the identification of compounds

based on their mass spectrum. A mass spectrum is a graph of ion intensity versus mass-

to-charge ratio (m/z); in essence, it illustrates the distribution of ions, generated from a

sample, according to their mass. All mass spectrometers are made up of three distinct

part components: the source in which ions are produced from the input sample, an

analyzer which separates the ions according to their m/z, and a detector which turns the

ions into a signal.

Ion sources vary depending on the chemical properties of the analytes under

investigation; for protein identification, electrospray ionization (ESI) is typically used. It

is a soft ionization method, which minimizes fragmentation of the molecular or parent

ions generated. Furthermore, it permits the detection of high mass compounds and is easily coupled to liquid chromatography. Matrix-assisted laser desorption ionization (MALDI) is another ionization technique that is effective for the analysis of peptides, proteins, and other biological molecules. The analyzed sample is co-crystallized with an excess of a solid matrix, which absorbs light from a pulsed laser; unfortunately, the matrix-related ions generate an increased background signal which impairs the analysis of smaller molecules. In addition, it cannot be readily coupled with liquid chromatography for chemical separation.

Mass analyzers have three major features: a mass limit which represents the highest m/z that is measurable, its ability to successfully transmit ions from the source to the detector, and the resolving power to distinguish between ions of minimal mass difference. Quadrupole mass analyzers are commonly paired with ESI, while time-of-flight (TOF) mass spectrometers are matched with MALDI. The quadrupole mass spectrometer can operate in a scanning mode which allows a range of m/z ratios to be monitored; alternatively, it can monitor for selected ions, thereby targeting only a few m/z ratios. Selected ion monitoring is possible when analyte masses are known in advance, and this allows for more rapid detection. TOF systems provide higher resolution, superior ion transmission and can analyze a greater range of masses; however, TOF is limited when compared with quadrupole mass analyzers, as it does not have tandem mass spectrometry capabilities.

Protein identification is often achieved by following a bottom-up approach; proteins are digested with proteolytic enzymes and then the resultant peptides are

separated and analyzed by liquid chromatography coupled with tandem mass

spectrometry (LC-MS/MS) [47]. The identified peptides can then be compared with

protein databases and/or peptide libraries; alternatively, programs are available that

perform de novo sequencing on LC-MS/MS data, and search the results against specific

databases. Collision-induced dissociation of digested peptides is commonly used to

generate fragment ions for the database searches; the primary fragments are b-ions

which represent the N-terminus of the peptide, and y-ions that are generated from the

C-terminus [47]. The fragment b- and y-ions can be used to obtain the actual amino acid

sequence of the peptides being analyzed (refer to Appendix F). Unfortunately, the

bottom-up approach can result in the loss of post-translational modifications during

fragmentation, and sequence coverage is often between 5-70% [47].

When using a top-down approach for proteomic analysis, intact proteins are

directly examined using mass spectrometry. The direct measurement of the intact

molecular protein species allows its molecular form to be established. Use of alternative

dissociation techniques, such as electron-capture dissociation, allows for the generation

of c- and z-ions from cleavage of the N-C(R) bond; this type of fragmentation preserves

post-translational modifications [47]. Post-translational modifications of particular

importance include glycosylation and phosphorylation; however, ubiquitylation,

deamidation, acetylation and methylation also occur in proteins. These modifications

are critically important to the structural and functional features of proteins, and can

control biological processes. The top-down approach can provide 100% sequence

coverage, including these modifications, but it is not readily coupled to liquid

chromatography; all protein purification must be performed offline [47].

2.3 Methodology

2.3.1 Myelin Isolation

Myelin was isolated from mouse brains using a modified version of the method

developed by Norton [48]. Whole brains were homogenized with a Dounce

homogenizer, on ice, in 10.5% sucrose in TNE (25 mM Tris-HCl, pH 7.4, 150 mM NaCl, 5

mM EDTA) containing 1 mM Na_3VO_4, 1X PIC, 1X PhosSTOP and 1 mM PMSF. The

homogenate was overlaid on top of an equal volume of 30% sucrose in TNE, in 5 mL

centrifuge tubes. In order to separate the myelin from the remaining brain tissue, the

homogenate was subjected to a series of centrifugation steps using the Optima Max

Ultracentrifuge (Beckman Coulter). The MLS-50 rotor for this ultracentrifuge was used.

First, the sucrose gradient was centrifuged for 60 minutes at 35,000 rpm. The middle

myelin layer, at the 10.5%-30% sucrose interface, was removed. This fraction was

diluted with an equal volume of ice cold water and gently vortexed. Centrifugation for

30 minutes at 35,000 rpm was subsequently used to pellet the myelin membranes.

Pellets were osmotically shocked by the addition of 10 volumes of ice cold water, gentle

vortexing and incubation for 10 minutes on ice. The myelin was pelleted at 23,000 rpm

for 20 minutes, and then resuspended in 10.5% sucrose in TNE containing Na_3VO_4, PIC,

PhosSTOP and PMSF. This mixture was overlaid onto an equal volume of 30% sucrose in

TNE, and all of the centrifugation steps were repeated. The final myelin pellet was

resuspended in myelin storage buffer (25 mM Tris-HCl, pH 7.5, 140 mM NaCl, 2 mM

EDTA) containing 2 mM Na_3VO_4, 1X PIC, 1X PhosSTOP and 2 mM PMSF. The isolated

myelin was aliquoted and stored at -80°C until needed. The protein concentration of the

isolated myelin was determined, after each preparation, using the Micro BCA Protein

Assay Kit from ThermoScientific. The manufacturer's instructions were followed, using

bovine albumin standard (BSA) as the standard, and the microplate spectrophotometer

was set to measure absorbance at a wavelength of 562 nm.

A second method for isolating myelin was also used in this study. This method,

based on the protocol developed by Kristian, isolates mitochondria from the central

nervous system; myelin and synaptosomes are isolated by-products of this protocol

[49]. Rather than using a sucrose gradient, this method applies the brain homogenate to

a Percoll gradient. The two types of gradients are depicted in Figure 2.1. Percoll is made

of colloidal silica particles which have been coated with polyvinylpyrrolidone, and it has

a low viscosity. As a result, the use of Percoll, rather than sucrose, allows for the use of

lower centrifugal forces, and accelerates sedimentation rates [50]. Whole mouse brains

were homogenized with a Dounce homogenizer, on ice, in isolation medium (225 mM

sucrose, 75 mM mannitol, 1 mM EGTA, 5 mM HEPES, pH 7.4); more specifically, two

brains were homogenized in 1 mL of isolation medium, and then brought to a total

volume of 10 mL using the isolation medium. This protocol used a total of four mouse

brains, in contrast to the eight used by the sucrose gradient method. The homogenate

was centrifuged for three minutes at 1,300xg at 4°C using a F1010 fixed-angle rotor in

the Allegra 64R centrifuge (Beckman Coulter). The supernatant was set aside, and the

pellet was resuspended in 5 mL of isolation medium and centrifuged again. The pooled

supernatant was then centrifuged at 21,000xg for 10 minutes, and the resultant pellet

was resuspended in 3.5 mL of 15% Percoll containing 225 mM sucrose, 75 mM

mannitol, 1 mM EGTA, and 5 mM HEPES, pH 7.4. A Percoll gradient was prepared by

overlaying the 15% Percoll on 24% and 40% Percoll. The discontinuous gradient was

subsequently centrifuged for eight minutes at 30,700xg, using slow acceleration and

deceleration. The very top layer, above the gradient, contained the myelin. It was

collected, resuspended in 15% Percoll, and the discontinuous gradient was prepared a

second time and centrifuged as before. This time the myelin layer was removed, diluted

with 3-4 mL of ice cold water, vortexed, and centrifuged for 10 minutes at 30,700xg. The

pellet was resuspended in myelin storage buffer, aliquoted and stored at -80°C. The BCA

protein assay was performed, exactly as done for the myelin prepared using the sucrose
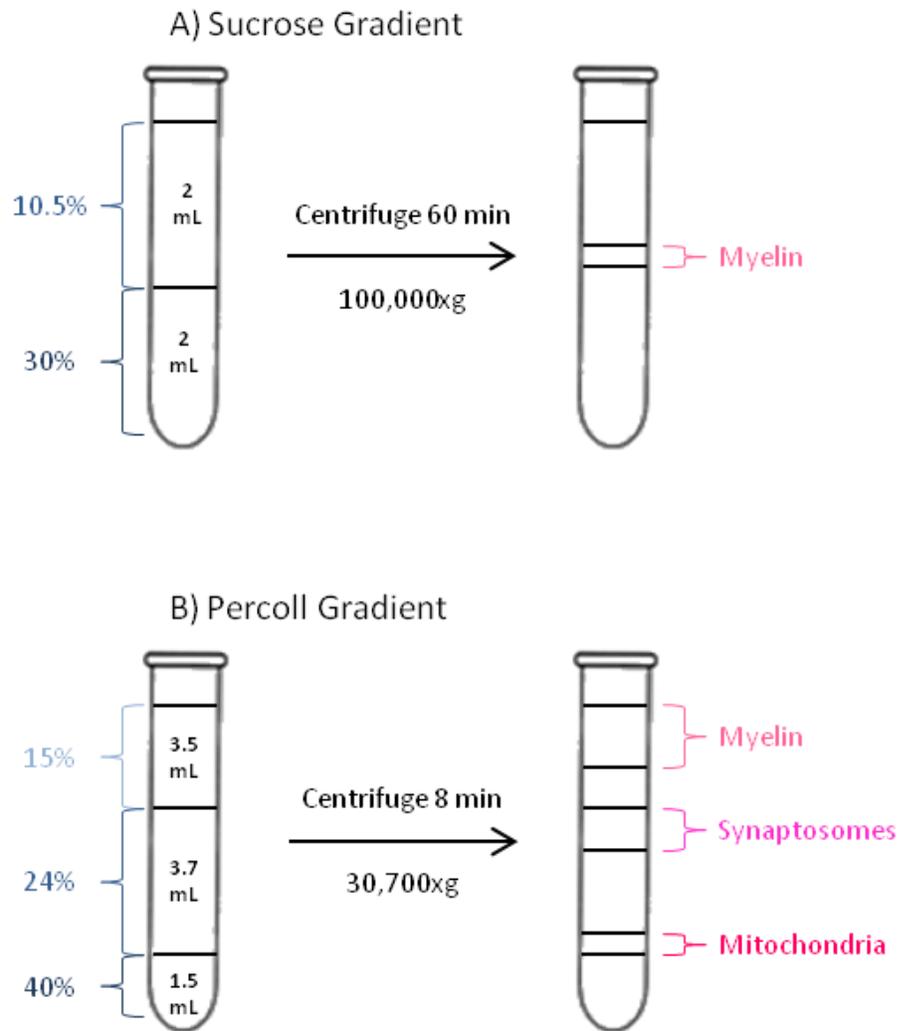
gradient method.

Figure 2.1 Schematic of sucrose and Percoll gradient myelin isolation methods

A) The sucrose gradient method; myelin membranes accumulate at the 10.5%-30% sucrose interface after 60 minutes of centrifugation at 100,000xg using the Beckman Coulter Optima Max Ultracentrifuge. **B)** The Percoll gradient method; myelin membranes accumulate in the very top layer, above the gradient, while synaptosomes and mitochondria accumulate at the 15%-24% and 24%-40% Percoll interfaces, respectively, after 8 minutes of centrifugation at 30,700xg with the Beckman Coulter Allegra 64R centrifuge.

2.3.2 Partial Delipidation of Whole Myelin

Myelin prepared using each isolation protocol, was compared by Western blot

analysis. Both preparations of whole myelin were partially delipidated prior to

electrophoretic separation, for enhanced detection. For each, 500 μg of myelin protein

was brought to a total volume of 200 μL with water. The samples were then extracted

using a 2:1 mixture of ether to ethanol. They were incubated on ice for 10 minutes, then

centrifuged at 13,000 rpm for another 10 minutes, at 4°C, using an Eppendorf centrifuge

5415 D. The supernatant was discarded, and the remaining pellets were air-dried at

room temperature and resuspended in pellet resuspension buffer (10 mM Tris-HCl, 1%

SDS, pH 8.0).

2.3.3 Detergent Extraction of Myelin

Mouse myelin, isolated from CD1 mice, was subjected to two different detergent

extraction protocols. First, a differential detergent extraction with CHAPS and TX-100

was performed. For each extraction, 500 μg of myelin protein was brought to a total of 1

mL in Tris-buffered saline (TBS; 25 mM Tris-HCl, pH 7.5, 140 mM NaCl, 2 mM EDTA),

with a final concentration of 1.5% CHAPS. This mixture, which represents the initial 1.5%

CHAPS homogenate (I), was incubated on ice for 30 minutes with occasional mixing. This

incubation was followed by centrifugation at 5,000xg for 10 minutes, at 4°C, using the

Eppendorf centrifuge 5415 D. The supernatant (S1) was set aside while the pellet (P1)

was resuspended in 1 mL of 2% TX-100 in TBS. Once again, the mixture was incubated

on ice for 30 minutes, with occasional mixing, and then centrifuged at 14,000xg for 15

minutes at room temperature using the Microfuge 18 Centrifuge (Beckman Coulter).

The supernatant (S2) was carefully removed, and the pellet (P2) was resuspended in 1

mL of 3% TX-100 in TBS. In some instances, the initial pellet (P1) was resuspended in 1

mL of 3% TX-100 in TBS, at which point the S1 and P1 fractions were directly examined;

the second extraction was completely eliminated in this case. All myelin extracts were

stored at -20°C until required.

A different detergent extraction followed by isopycnic centrifugation was

performed to isolate the DRMs, or lipid rafts, from myelin isolated from CD1 mice; this

protocol was previously described by DeBruin et $al.$ [16;51;52]. Initially, 500 μg of myelin

protein was brought to a total of 1 mL in 1.5% CHAPS in TBS with 10 mM Na_3VO_4, 10

mM PMSF, and 1X PIC solution; the myelin was added last, after 10 minutes of

incubation on ice. Once added, the myelin mixture was vortexed and incubated on ice

for 30 minutes, with occasional mixing, followed by centrifugation at 5,000xg for 10

minutes, at 4°C, using the Eppendorf centrifuge 5415 D. The pellet was resuspended in

pellet resuspension buffer, while the supernatant was combined with an equal volume

of 80% sucrose in 25 mM Tris-HCl, pH 7.5, 140 mM NaCl (Tris-buffered saline). The

resultant sample in 40% sucrose was overlaid with 30% sucrose and 5% sucrose. The

discontinuous gradients were centrifuged at 35,000 rpm for 16-18 hours, at 4°C, using

the MLS-50 rotor in the Optima Max Ultracentrifuge (Beckman Coulter). Afterwards,

samples were fractionated into approximately ten 340-μL fractions from the top of the

tube. The lipid rafts fractions were identified by GM1 dot blot. Cholera-toxin B subunit

peroxidase conjugate was used in conjunction with SuperSignal West Femto Substrate

for visualization by enhanced chemiluminescence, and imaging with the VersaDoc 4000

(Bio-Rad). Lipid raft fractions destined for analysis by Western blotting were precipitated

with acetone. A 4:1 ratio of ice-cold acetone to sample was combined, vortexed and

incubated overnight at -80°C. Later on, the acetone precipitated samples were

centrifuged at 16,100xg for 20 minutes, at 4°C, using the Eppendorf centrifuge 5415 D.

Pellets were air-dried and resuspended in 10 μL of pellet resuspension buffer. These

samples were prepared for SDS-PAGE by the addition of 5 μL of 5X sample loading

buffer (0.5 M Tris-HCl, pH 6.8, glycerol, 10% w/v SDS, 0.5% w/v bromophenol blue).

2.3.4 SDS-PAGE

In this study, protein samples were electrophoretically separated using SDS-

PAGE mini-gels, with the Mini-Protean 3 cell (Bio-Rad). Either 12% or 14% freshly cast, 1-

mm thick, resolving gels were used for protein separation. Each protein sample was

prepared for separation by combining the sample with 5X sample loading buffer in a 1:4

ratio, and heating the mixture to 65°C, unless otherwise specified. They were then run

at 90V as they passed through the stacking gel, and the voltage was increased to 120V

until separation was completed and the tracking dye had run off the gel. The gels were

often transferred to nitrocellulose for Western blot analysis, or stained with Coomassie.

For each gel, Precision Plus Protein Dual Color Standard (Bio-Rad) was used as a

molecular mass marker.

2.3.5 Coomassie and Silver Staining

In this study, protein visualization in SDS-PAGE gels was achieved with

Coomassie G-250 BioSafe Stain (Bio-Rad), as per the manufacturer's directions, or by

silver staining. The silver staining protocol was based on the original method developed

by Switzer *et al.* [53]. First, the polyacrylamide gels were fixed in 50% methanol, 10%

acetic acid for 30 minutes, with occasional shaking, and then incubated in 5% methanol,

1% acetic acid for 15 minutes. The gels were subsequently rinsed in 50% methanol and washed with ultrapure water three times, five minutes each time. After removing the water, the gels were incubated in 0.02 g/100 mL sodium thiosulfate for 90 seconds; this step was followed by three 30 second rinses with water. Next, the gels were incubated for 45 minutes in 0.2 g/100 mL ice cold silver nitrate. The gels were rinsed again in water, three times, for 60 seconds each time. Lastly, each gel was developed in 100 mL of a developing solution which contained 6.0 g of sodium carbonate, 50 μL of 37% formaldehyde, and 0.4 mg of sodium thiosulfate. Development was ceased when protein bands became stained light brown; often requiring 5 to 20 minutes of incubation. The development solution was decanted and gels were covered in 6% acetic acid, for 10 minutes, to stop development. Gels were rinsed several times with water prior to imaging.

2.3.6 Western Blotting

In this study SDS-PAGE gels were electrotransferred to nitrocellulose for 90 minutes, at 200 mA, in cold transfer buffer (25 mM Tris-HCl, pH 8.3, 192 mM glycine, 20% methanol). The membranes were subsequently blocked with 5% skim milk solution in Tris-buffered saline with Tween-20 (247 mM Tris-HCl, pH 7.6, 27 mM KCl, 1.37 mM NaCl, 0.5% Tween-20; TTBS), for at least 2 hours. After blocking, the membranes were washed for 1 minute, and again for 5 minutes, in TTBS. The specific primary antibody was then applied to the membranes, for the specified incubation period, as listed in Table 2.3. To reduce non-specific binding, membranes were washed for 1 minute, followed by three 5 minute washes, in TTBS. The corresponding secondary antibody was

subsequently applied to the membranes, as per Table 2.3. Once again, membranes were

washed for 1 minute, followed by three 5 minute washes, in TTBS, post-antibody

incubation. Detection of HRP-tagged, chemiluminescent proteins was performed by

incubating the membranes in either SuperSignal West Femto Substrate or VisiGlo Select

HRP Chemiluminescent Substrate for 5 minutes, followed by immediate imaging with

the VersaDoc 4000 (Bio-Rad). Alternatively, proteins bound to fluorescently tagged

antibodies could be imaged directly after the final wash step using specific filters on the

VersaDoc 4000; a blue LED excitation source and 530BP emission filter, or a red LED

excitation source and a 695BP emission filter, was used for the detection of the various

DyLight conjugated secondary antibodies. For all Western blots, Precision Plus Protein

Dual Color Standard was used as a molecular mass marker.

Table 2.3 Antibody dilutions used for Western blotting

This table summarizes the dilutions and incubation periods of primary antibodies used in this study, in addition to the dilutions and incubation periods of their corresponding secondary antibodies.

Primary Antibody	Dilution	Incubation Time	Secondary Antibody	Dilution	Incubation Time
β-Actin	1:2,000	2-3 hours	DyLight 649 Anti-Mouse IgG	1:12,000	1 hour
Na^+/K^+-ATPase α	1:2,000	4-5 hours	Anti-Mouse IgG-HRP	1:80,000	30 minutes
Na^+/K^+-ATPase α_1	1:500	4-5 hours	Anti-Mouse IgG-HRP	1:80,000	30 minutes
Na^+/K^+-ATPase α_2	1:500	4-5 hours	Anti-Goat IgG-HRP	1:80,000	30 minutes
Na^+/K^+-ATPase α_3	1:3,000	4-5 hours	Anti-Mouse IgG-HRP	1:80,000	30 minutes
Na^+/K^+-ATPase β_1	1:500	4-5 hours	Anti-Mouse IgG-HRP	1:80,000	30 minutes
Na^+/K^+-ATPase β_2	1:500	4-5 hours	Anti-Rabbit IgG-HRP	1:80,000	30 minutes
Na^+/K^+-ATPase β_3	1:500	4-5 hours	Anti-Goat IgG-HRP	1:80,000	30 minutes
MBP	1:500	4-5 hours	DyLight 488	1:12,000	1 hour

			Anti-Rat IgG		
MCT1	1:100	4-5 hours	Anti-Rabbit IgG-HRP	1:80,000	30 minutes
NQO1	1:100	4-5 hours	Anti-Rabbit IgG-HRP	1:80,000	30 minutes
VDAC	1:1,000	4-5 hours	Anti-Rabbit IgG-HRP	1:80,000	30 minutes

When β-actin was used as a protein loading control for Western blots, the
membranes were stripped after imaging of the target protein. Each membrane was
stripped twice, 5 minutes each time, in stripping buffer (25 mM glycine-HCl, pH 2.2, 1%
SDS). The membranes were rinsed several times with water, and then washed in TTBS
for 5 minutes. The nitrocellulose membranes were then reblocked with 5% skim milk
solution, for 2 hours. The primary and secondary antibodies used for the detection of β-
actin are specified in Table 2.3. The same antibody incubation procedure, as described
earlier, was followed.

2.3.7 Quantification of Protein Expression by Densitometric Analysis

Protein expression levels in myelin samples were quantified by densitometric
analysis of prepared Western blots, using Image Lab Version 5.0 (Bio-Rad). Volumes for
each fluorescent or chemiluminescent signal were measured and compared with
corresponding samples of equivalent area (mm^2). Volume was adjusted using local
background subtraction.

2.3.8 Immunoprecipitation Assays

An individual protein immunoprecipitation assay was used to identify the heterodimeric forms, or isozymes, of Na^+/K^+-ATPase. This IP method used the antibodies for each β isoform, to capture the αβ complexes present in mouse myelin. EZview Red Protein A and/or G affinity gels were used as the antibody binding matrix for these IPs; the affinity gel and amount of each antibody used are summarized in Table 2.4. For each IP, 25 µL of the corresponding 50% slurry suspension of the affinity gel was washed and equilibrated in 50 mM Tris-HCl, pH 7.6, on ice. Isolated CD1 mouse myelin was extracted with 1.5% CHAPS, as per first step of the differential detergent extraction protocol. A sample of the initial 1.5% CHAPS homogenate (I) was set aside for comparison, while 2 µg of the $β_1$, $β_2$ and $β_3$ antibodies were each added to separate 100 µL aliquots of the 1.5% CHAPS supernatant (S1). These antibody-sample mixtures were rotated for 2-4 hours, at 4^oC, after which they were introduced to their respective affinity gels and rotated, at 4^oC, overnight. Each sample was subsequently centrifuged for 30 seconds at 1,500xg using the Microfuge 18 Centrifuge (Beckman Coulter). The unretained material was removed and the affinity gels were washed with 50 mM Tris-HCl, pH 7.6. The αβ complexes were eluted from the affinity gel by the addition of 10 µL of pellet resuspension buffer and 10 µL of 5X sample loading buffer. The eluted material was heated to 50^oC for 5 minutes, and then cooled, pulse centrifuged, and examined using Western blotting. Specifically, 20 µL of each β subunit IP elution were electrophoretically separated on 12% SDS-PAGE gels, along with 20 µL of the initial 1.5% CHAPS homogenate in sample loading buffer. Eluted material was otherwise stored at

-20°C until required.

Table 2.4 Affinity gel and antibodies for individual protein immunoprecipitations.

Target	Sample	Antibody Introduced	Amount of Antibody Used	Affinity Gel Used
β_1	1.5% CHAPS supernatant (S1)	Mouse monoclonal Na$^+$/K$^+$-ATPase β_1	2 µg	50/50 mixture of EZview Red Protein A and Protein G
β_2	1.5% CHAPS supernatant (S1)	Rabbit polyclonal Na$^+$/K$^+$-ATPase β_2	2 µg	EZview Red Protein A
β_3	1.5% CHAPS supernatant (S1)	Goat polyclonal Na$^+$/K$^+$-ATPase β_3	2 µg	EZview Red Protein G

Protein complex immunoprecipitations were used to identify the specific binding partners of Na$^+$/K$^+$-ATPase in the myelin membrane. Similar to the beta subunit IP, this co-IP used the antibodies for each α isoform to capture the protein complexes which include the catalytic component of Na$^+$/K$^+$-ATPase. A non-specific binding control was also used to identify which proteins interact with the affinity gel, without the presence of an antibody. For these co-IPs, EZview Red Protein G Affinity Gel was used as the antibody binding matrix, in addition to use of an α_1 antibody-conjugated agarose for the α_1 subunit co-IP; the affinity gel and amount of each antibody used are summarized in Table 2.5. The EZview Red Protein G Affinity Gel was prepared as above with the beta subunit IPs. The antibodies mentioned in Table 2.5 were each combined with 150 µL of the 1.5% CHAPS supernatant and rotated for 2-4 hours, at 4°C; no antibody was added to the control sample. For the α_1 subunit co-IP, this step was omitted as the antibody was conjugated to the agarose beads prior to use. Afterwards, the antibody-sample mixtures were added to their respective affinity gels, and 150 µL of the 1.5% CHAPS

supernatant was combined with the α_1 antibody-conjugated agarose; these samples

were then rotated, at 4°C, overnight. Samples were spun down at 1,500xg for 30

seconds, the unretained material removed, and the matrix washed with 50 mM Tris-HCl,

pH 7.6, three times. After the removal of the final wash, protein complexes were eluted

from the affinity gel or agarose beads by the addition of 10 µL of pellet resuspension

buffer and 10 µL of 5X sample loading buffer. The eluted material was heated to 50°C

for 5 minutes, and then cooled and pulse centrifuged. The initial CHAPS homogenate (I)

was combined with sample loading buffer and 5 µL of it, and 20 µL of the non-specific

binding control and sample elutions, was run on a 12% SDS-PAGE gel and stained with

Coomassie G-250 BioSafe Stain, as per the manufacturer's directions.

Table 2.5 Affinity gel and antibodies for complex protein immunoprecipitations.

Target	Sample	Antibody Introduced	Amount of Antibody Used	Affinity Gel/Agarose Beads Used
Control	1.5% CHAPS supernatant (S1)	None	N/A	EZview Red Protein G
α_1	1.5% CHAPS supernatant (S1)	Mouse monoclonal Na$^+$/K$^+$-ATPase α_1	N/A	Na$^+$/K$^+$-ATPase α_1 antibody-conjugated agarose
α_2	1.5% CHAPS supernatant (S1)	Goat polyclonal Na$^+$/K$^+$-ATPase α_2	2 µg	EZview Red Protein G

α_3	1.5% CHAPS supernatant (S1	Mouse monoclonal Na$^+$/K$^+$-ATPase α_3	2 µg	EZview Red Protein G

2.3.9 Trypsin Digestion and Proteomic Analysis

Unique protein bands from the α subunit co-IPs, identified on the Coomassie stained SDS-PAGE, were cut from the gels and digested with trypsin for protein identification by mass spectrometry. A negative control band was also cut and trypsin digested. The in-gel trypsin digestion was performed as outlined by the SPARC BioCentre at the Hospital for Sick Children (Toronto, ON, Canada). The predicted trypsin cleavage sites of Na$^+$/K$^+$-ATPase α_1, α_2, and α_3, and β_1, β_2, and β_3, are available in Appendix B. Excised protein bands were washed with 50 µL of 50 mM ammonium bicarbonate, for 5 minutes. The gel was shrunk with 50 µL of 50% acetonitrile/25 mM ammonium bicarbonate for 10 minutes, and dried to completeness at ambient temperature in a Labconco CentriVap Benchtop Concentrator. Each band was then reduced with 30 µL of 10 mM DTT for 30 minutes, at 56°C, alkylated with 30 µL of 100 mM iodoacetamide for 15 minutes, at room temperature, in the dark, shrunk with 50 µL of 50% acetonitrile/25 mM ammonium bicarbonate for 15 minutes, and then completely dried again in the vacuum centrifuge at ambient temperature. Gel pieces were covered in 13 ng/µL trypsin in 50 mM ammonium bicarbonate, and incubated on ice for 30-45 minutes. After that, any remaining solution was removed and 50 mM ammonium bicarbonate was added to cover the gel pieces while they were incubated, at 37°C, for 16-18 hours. The peptide

extraction was performed after incubation; first, by sonicating the samples for 5 minutes in cool water. The supernatant of each gel piece was collected and combined with the supernatants from the following incubation steps. Each gel piece was incubated in 20 μL of 25 mM ammonium bicarbonate for 10 minutes, then 20 μL of 5% formic acid for 10 minutes, 20 μL of 100% acetonitrile for 10 minutes, 20 μL of 5% formic acid for 10 minutes, and finally 20 μL of 100% acetonitrile for 10 minutes. The final solution was evaporated to dryness in the vacuum centrifuge, at 44-48°C. The samples were stored at -20°C until sent for analysis by LC-MS/MS.

The LC-MS/MS samples were analyzed using both Sequest version 1.4.0.288 (ThermoFisher Scientific, San Jose, CA, USA) and X!Tandem version CYCLONE (The GPM, thegpm.org). Sequest was set up to search Mouse-UniProt-Jan-09-2013.fasta (unknown version, 50272 entries) assuming the digestion enzyme trypsin. X!Tandem was set up to search the Uniprot_Mus_musculus_May222014.fasta database (unknown version, 43362 entries) also assuming trypsin digestion. Sequest and X!Tandem were searched with a fragment ion mass tolerance of 0.60 Da and a parent ion tolerance of 2.0 Da. Deamidation of asparagine and glutamine, oxidation of methionine and carbamidomethyl of cysteine were specified in Sequest as variable modifications. Glu->pyro-Glu of the N-terminus, ammonia-loss of the N-terminus, Gln->pyro-Glu of the N-terminus, deamidation of asparagine and glutamine, oxidation of methionine and carbamidomethylation of cysteine were specified in X!Tandem as variable modifications.

Mass spectrometry peptide and protein identifications were validated using Scaffold, version 4.3.2, proteome software (Proteome Software Inc., Portland, OR, USA).

Peptide identifications were accepted if they could be established at greater than 20.0% probability to achieve a false detection rate (FDR) less than 1.0%. Peptide Probabilities from Sequest were assigned by the Scaffold Local FDR algorithm. Peptide probabilities from X!Tandem were assigned by the Peptide Prophet algorithm with Scaffold delta-mass correction [54]. Protein identifications were accepted if they could be established at greater than 95.0% probability to achieve an FDR less than 1.0% and contained at least 2 identified peptides. Protein probabilities were assigned by the Protein Prophet algorithm [55]. Proteins that contained similar peptides and could not be differentiated based on LC-MS/MS analysis alone were grouped to satisfy the principles of parsimony. Proteins sharing significant peptide evidence were grouped into clusters.

Chapter 3 – Results

3.1 Identification of Na$^+$/K$^+$-ATPase in the Myelin Membrane

3.1.1 Expression of Na$^+$/K$^+$-ATPase Subunit Isoforms

Understanding the distribution of proteins within tissues, as well as identifying changes in their expression over a lifespan, is central to comprehending their involvement in both developmental and disease processes [56]. Many methods exist for the identification of temporal and spatial gene or protein expression; in this study, protein expression of each Na$^+$/K$^+$-ATPase subunit isoform, present in the myelin membrane, was evaluated by the Western blot analysis of myelin from mouse brain. Myelin was isolated from brains of euthanized mice from different age groups, thereby allowing examination of changes in protein expression during post-natal development. The myelin produced in mature CD1 mice was also investigated; this initial survey of protein expression was informative and outlined which Na$^+$/K$^+$-ATPase subunit isoforms exist in mouse myelin, and should therefore be further examined.

The products of both sucrose-gradient and Percoll-gradient isolated CD1 mouse myelin were partially delipidated, and subsequently examined by Western blot analysis. Ultimately, it was shown that Na$^+$/K$^+$-ATPase is expressed in the myelin membrane, and can be successfully detected using this analysis technique. As illustrated in Figure 3.1, Na$^+$/K$^+$-ATPase α_1, α_2, and α_3, as well as the complementary β_1, β_2, and β_3 subunits, were readily detected in both myelin preparations. These three alpha and three beta subunits represent all known isoforms of Na$^+$/K$^+$-ATPase in the CNS.

All subsequent analyses of Na^+/K^+-ATPase were performed using myelin isolated by the sucrose-gradient method. Both the sucrose-gradient and Percoll-gradient isolation protocols generated myelin with detectable levels of each subunit isoform, in addition to MBP, voltage-dependent anion channel (VDAC), monocarboxylate transporter 1 (MCT1) and NAD(P)H quinone oxidoreductase 1 (NQO1) (refer to Appendix G). Nevertheless, when these myelin preparations were compared with a brain homogenate sample, of equal protein content, the myelin produced using the Percoll-gradient method appeared less purified although it had a greater yield.
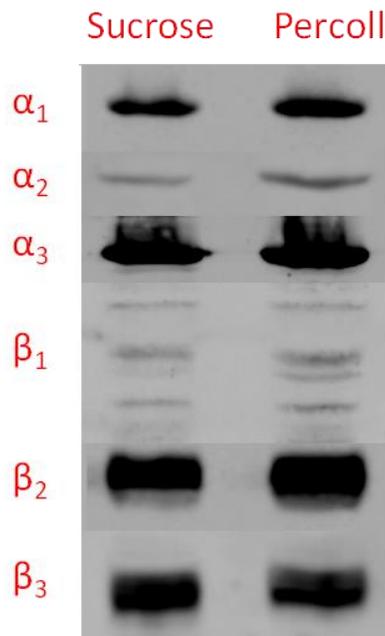
Figure 3.1 Detection of Na^+/K^+-ATPase subunit isoforms in partially delipidated sucrose-gradient and Percoll-gradient isolated CD1 mouse myelin

Enhanced chemiluminescent Western blot detection of each alpha and beta isoform of Na^+/K^+-ATPase in partially delipidated myelin samples, of equivalent protein content, from sucrose-gradient and Percoll-gradient isolation methods. Equal volumes (15 μL), and therefore equal protein (approximately 60 μg of total myelin protein), of each sample were separated on 12% SDS-PAGE and transferred to nitrocellulose membrane. The corresponding primary and secondary antibodies used are described in Table 2.3. Each Western blot was imaged using the VersaDoc 4000 (Bio-Rad) with an exposure time of 30-400 seconds, ensuring non-saturation.

3.1.2 Detergent Solubility of Na^+/K^+-ATPase

Non-ionic detergents, such at TX-100, have formerly proven incapable of solubilizing certain regions, or microdomains, of plasma membranes. These DRMs are enriched in cholesterol, sphingomyelin, and lipid-anchored proteins. They show

similarities to the L_o phase (refer to section 1.2.2) of model membranes, and may

represent membrane microdomains such as lipid rafts, caveolae and/or cellular

junctions [14;16]. Consequently, the detergent-insolubility of these coalesced lipid rafts

became the basis for the isolation and characterization of both raft proteins and lipids

[57]. As earlier studies of Na^+/K^+-ATPase have demonstrated its localization within

various membrane microdomains, such as the caveolae of kidney cells, detergent

extraction has proven essential in the successful characterization of this protein in other

tissue and cell types [58].

The initial extraction of Na^+/K^+-ATPase from the myelin membrane using the

differential detergent extraction procedure with 1.5% CHAPS, followed by 2% TX-100,

indicated that limited protein was detectable in the TX-100 supernatant (S2) and pellet

(P2) fractions. Each of the Na^+/K^+-ATPase subunit isoforms was observed in the initial

pellet (P1), but preferentially partitioned into the 1.5% CHAPS supernatant (S1) fraction;

refer to Figure 3.2. Densitometric data indicated that Na^+/K^+-ATPase α_1, β_1, β_2, and β_3

were highly enriched in the CHAPS supernatant; more than 90% of all Na^+/K^+-ATPase α_1,

β_1, β_2, and β_3 was detected in this S1 fraction. Alternatively, the P1 fraction contained

approximately 20-30% of all Na^+/K^+-ATPase α_2 and α_3.
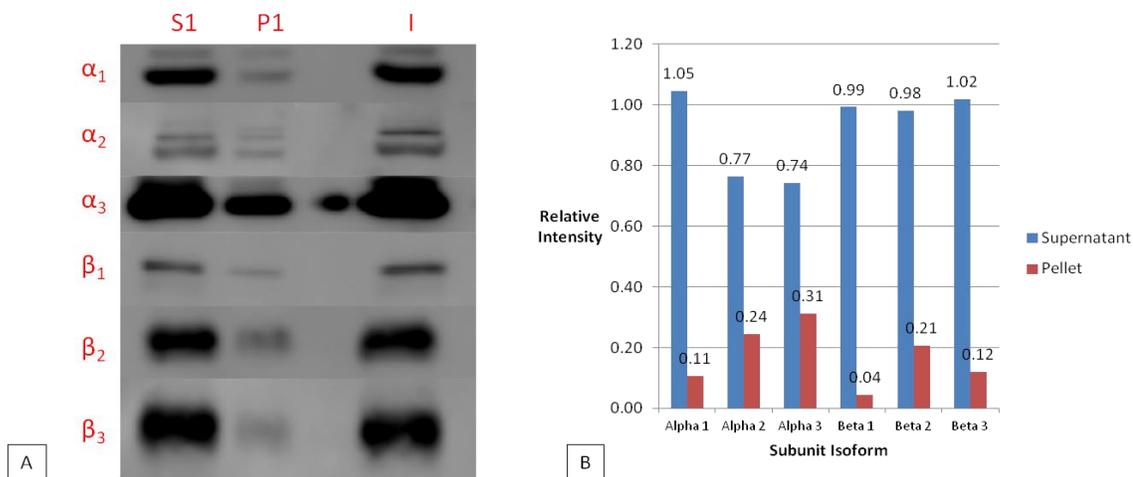
Figure 3.2 Detection of Na$^+$/K$^+$-ATPase subunit isoforms in detergent extracted CD1 mouse myelin

A) Enhanced chemiluminescent Western blot detection of each alpha and beta isoform of Na$^+$/K$^+$-ATPase in the 1.5% CHAPS supernatant (S1), pellet (P1) and the initial CHAPS homogenate (I). Equal volumes (20 µL) of each sample were separated on 12% SDS-PAGE and transferred to nitrocellulose membrane. The corresponding primary and secondary antibodies used are described in Table 2.3. Each Western blot was imaged using the VersaDoc 4000 (Bio-Rad) with an exposure time of 30-200 seconds, ensuring non-saturation. **B)** Relative intensity of each Na$^+$/K$^+$-ATPase subunit isoform in the 1.5% CHAPS supernatant and pellet, ensuring non-saturation and subtracting background. Each value was corrected by normalization with the initial CHAPS homogenate.

The propensity of Na$^+$/K$^+$-ATPase to become solubilized in 1.5% CHAPS detergent suggested that its subunit isoforms may be present in the myelin lipid rafts. DRMs, coalesced lipid rafts, were isolated from CD1 mouse myelin by treatment with 1.5% CHAPS detergent, followed by separation with a discontinuous sucrose density gradient. Larger fragments of the myelin membrane, as well as subcellular organelles, were compacted by low speed centrifugation of the 1.5% CHAPS mixture; whereas the resultant CHAPS supernatant contained the DRMs, as well as solubilized proteins and lipids [52]. When this supernatant subsequently underwent ultracentrifugation on a discontinuous sucrose density gradient, the DRMs and solubilized proteins and lipids were separated according to buoyancy. As the DRMs are rich in cholesterol and

57

glycosphingolipids, and represent the L_o phase, they are typically more buoyant and found in the lower density fractions; in contrast, solubilized proteins and lipids are detectable in the high density fractions of the density gradient. Ganglioside GM1 dot blot immunodetection was used to identify specifically which fractions contained the DRMs. All fractions were examined by Western blot analysis for each Na^+/K^+-ATPase subunit isoform, and then compared to the GM1 dot blot. All three alpha and three beta subunits of Na^+/K^+-ATPase were detected in the non-raft, high density fractions. Na^+/K^+-ATPase α_1, α_3, β_2, and β_3 were also successfully identified in the low density, raft fractions; for that reason, it is expected that these isoforms are part of the lipid rafts of the myelin membrane. Two of these Western blots are shown in Figure 3.3 below. It is unclear whether the α_2 and β_1 isoforms are also part of the DRMs, as the enhanced chemiluminescent signal was near the limit of detection (refer to Appendix G). All the same, Na^+/K^+-ATPase α_2 and β_1 are not highly enriched in the lipid rafts of myelin.
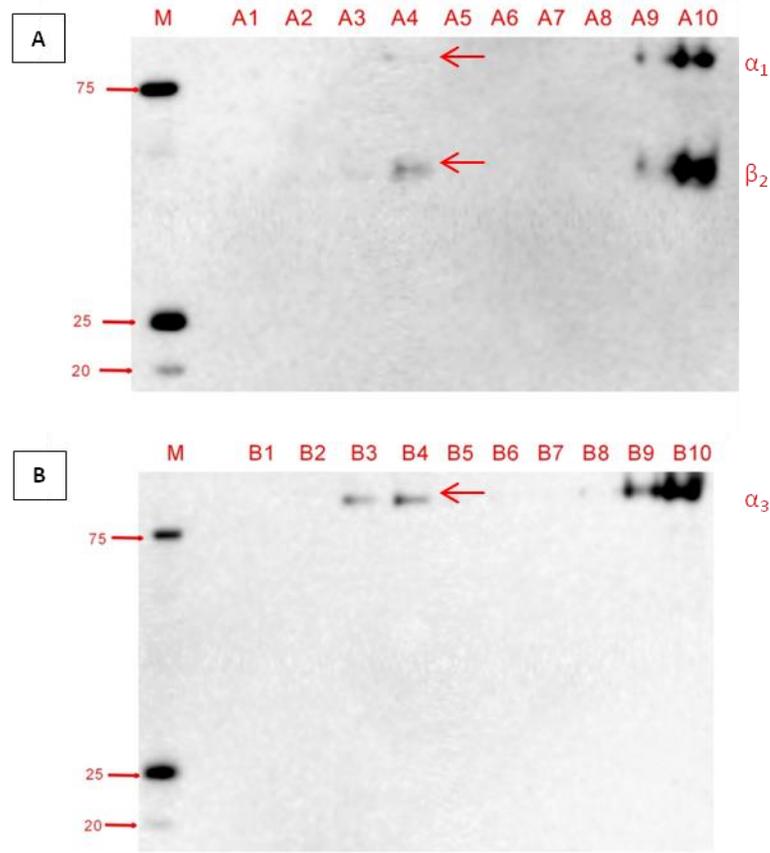
Figure 3.3 Detection of Na$^+$/K$^+$-ATPase subunit isoforms in myelin DRMs

Enhanced chemiluminescent Western blot detection of: **A)** Na$^+$/K$^+$-ATPase α_1 and β_2; **B)** Na$^+$/K$^+$-ATPase α_3. Equal volumes (20 μL) of each acetone-precipitated lipid raft fraction (A1-A10 and B1-B10), isolated as CHAPS DRMs, were separated on 12% SDS-PAGE and transferred to nitrocellulose membrane. Fractions A3, A4, B3 and B4 represent the low density, raft fractions; alternatively, fractions A9, A10, B9 and B10 represent the non-raft, high density fractions. The red arrows indicate the low density, raft fractions. The corresponding primary and secondary antibodies used are described in Table 2.3. Each Western blot was imaged using the VersaDoc 4000 (Bio-Rad) with an exposure time of 30-200 seconds, ensuring non-saturation.

3.2 Heterodimeric Forms of Na$^+$/K$^+$-ATPase in the Myelin Membrane

Determination of each heterodimeric form, or isozyme, of Na$^+$/K$^+$-ATPase in CD1 mouse myelin was performed using an IP with each beta subunit isoform. This method captures the $\alpha\beta$ complexes formed by each individual beta subunit isoform. Equal volumes of each eluted fraction were then examined for all alpha subunits by Western

blotting, using primary antibodies specific for each isoform (Figure 3.4). Six

heterodimeric forms of Na^+/K^+-ATPase were discovered; α_1 was shown to pair with β_1,

α_2 dimerized with β_1 and β_3, and α_3 was found to couple with all three beta isoforms.

These six isozymes, $\alpha_1\beta_1$, $\alpha_2\beta_1$, $\alpha_2\beta_3$, $\alpha_3\beta_1$, $\alpha_3\beta_2$, and $\alpha_3\beta_3$, were six of nine possible

functional Na^+/K^+-ATPase heterodimers; $\alpha_1\beta_2$, $\alpha_1\beta_3$ and $\alpha_2\beta_2$ were not observed in these

myelin samples. Three major isozymes, $\alpha_1\beta_1$, $\alpha_2\beta_3$, and $\alpha_3\beta_1$, were established; they

appeared to be the most abundant of each $\alpha\beta$ complex according to signal intensity.
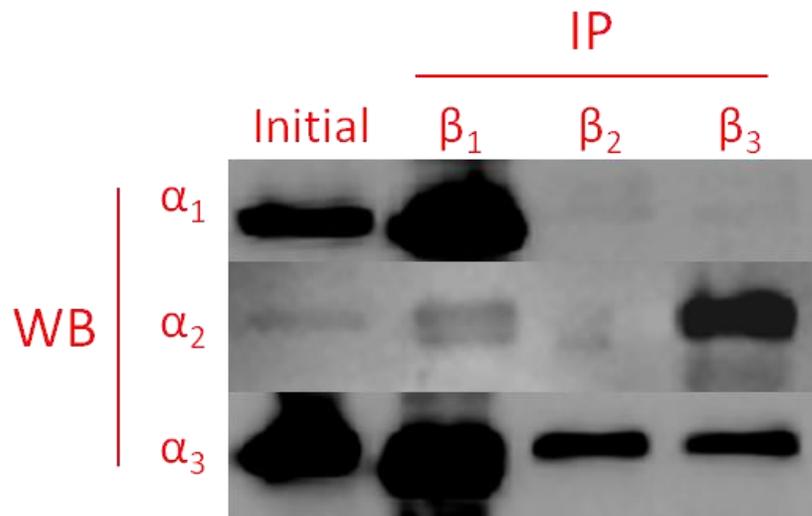
Figure 3.4 Identification of heterodimeric forms of the Na^+/K^+-ATPase in CD1 mouse myelin

Enhanced chemiluminescent Western blot detection of each alpha isoform of Na^+/K^+-ATPase in the initial CHAPS homogenate and final eluted fractions from each beta isoform immunoprecipitation. Equal volumes (20 µL) of each sample were separated on 12% SDS-PAGE and transferred to nitrocellulose membrane. The corresponding primary and secondary antibodies used are described in Table 2.3. Each Western blot was imaged using the VersaDoc 4000 (Bio-Rad) with an exposure time of 30-200 seconds, ensuring non-saturation.

3.3 Specific Binding Partners of Na⁺/K⁺-ATPase in the Myelin Membrane

Initial inspection of the proteins eluted from each Na^+/K^+-ATPase alpha subunit isoform co-IP revealed several unique protein bands, when compared to a non-specific binding control. Protein bands were identified using both silver and Coomassie G-250 BioSafe staining. These bands, in addition to those which became concentrated by the co-IP, are indicated in Figure 3.5 and Figure 3.7; they suggest that Na^+/K^+-ATPase interacts with several different proteins within the myelin membrane. Likewise, unique protein bands differed between the co-IPs of each individual alpha isoform; hence each isoform may have independent binding partners and form distinct protein complexes.
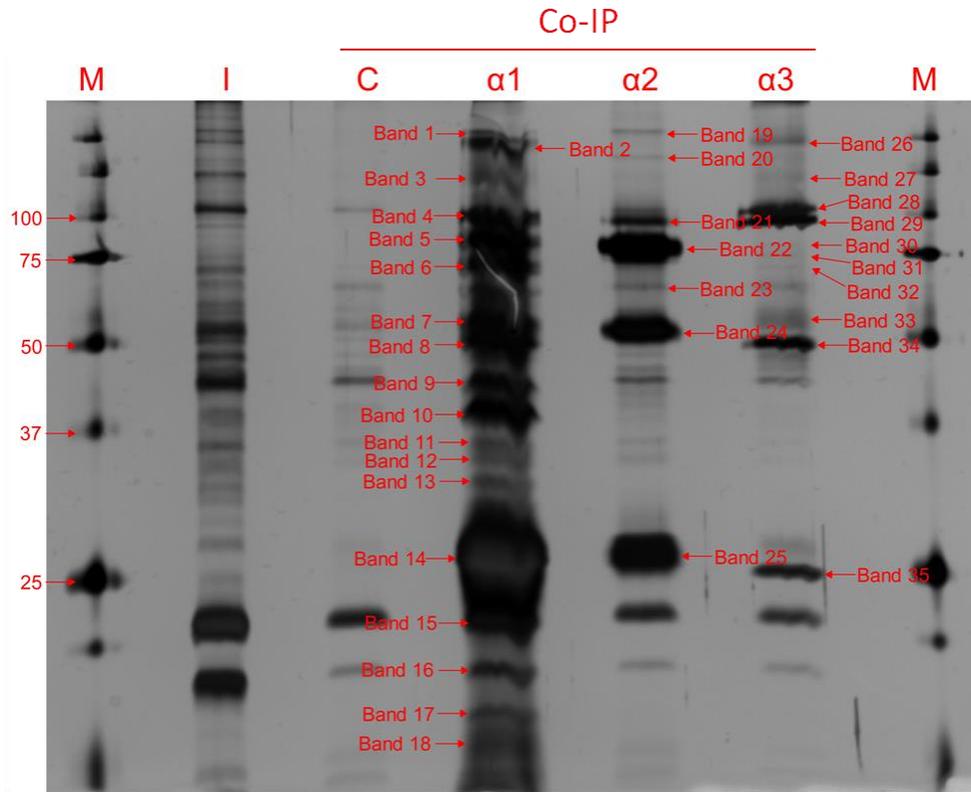
Figure 3.5 Silver stained SDS-PAGE of eluted proteins from co-immunoprecipitations of each Na$^+$/K$^+$-ATPase alpha isoform using CD1 mouse myelin

Silver stained 1-mm thick 12% SDS-PAGE, loaded with 3 µL of initial CHAPS homogenate (I) and equal volumes (20 µL) of a non-specific binding control (C) and the final eluted fraction of each alpha isoform co-immunoprecipitation. Precision Plus Protein Dual Color Standards (M) was used as a molecular mass standard. The stained gel was imaged using the VersaDoc 4000 (Bio-Rad) with an exposure time of 0.1-5 seconds, ensuring non-saturation. The indicated bands are unique when compared to the non-specific binding control, or became concentrated by the co-IP.

Each lane of the silver stain, shown in Figure 3.5, was scanned for a comparison of protein band intensities and their corresponding rate relative to front (R$_f$) values. The intensity and separation of these protein bands are illustrated in Figure 3.6. Many proteins are shown in the initial CHAPS homogenate; however, the intensity of these proteins is lesser, as only 3 µL of this sample was loaded onto the SDS-PAGE gel. Several proteins can also be identified in the non-specific binding control, according to signal intensity. By examining the separated proteins according to signal intensity, it is clear

that there are indeed both unique and shared protein bands in each Na^+/K^+-ATPase alpha subunit isoform co-IP elution. There are also non-unique protein bands which are of greater intensity in the Na^+/K^+-ATPase alpha subunit isoform co-IP elutions. It is also likely that there are a greater number of eluted proteins than identified protein bands, as the signal intensity of one protein may be masked by the signal intensity of a protein of similar molecular mass.
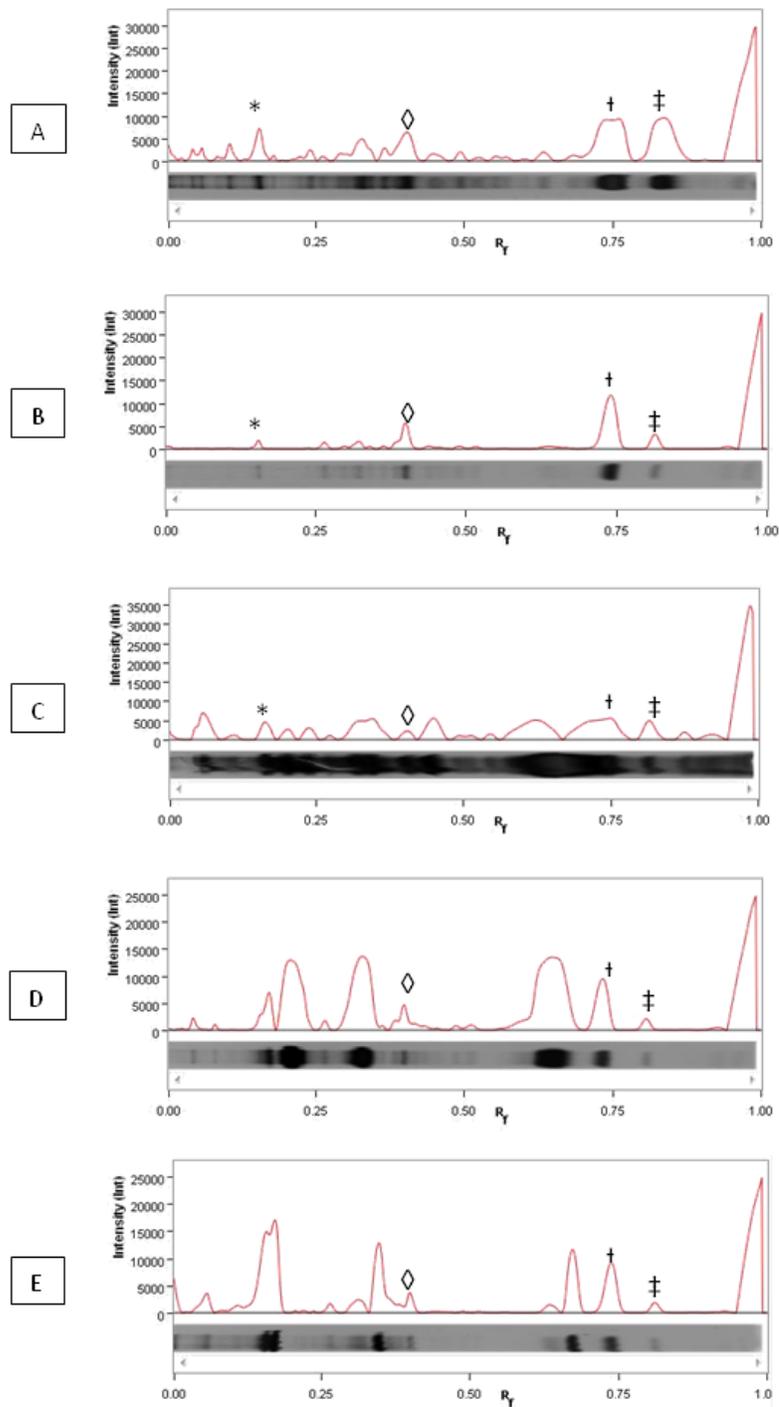
Figure 3.6 Separation of proteins eluted from Na$^+$/K$^+$-ATPase co-immunoprecipitations

Separation of proteins from: **A)** initial CHAPS homogenate; **B)** non-specific binding control; **C)** Na$^+$/K$^+$-ATPase α_1 co-IP elution; **D)** Na$^+$/K$^+$-ATPase α_2 co-IP elution; **E)** Na$^+$/K$^+$-ATPase α_3 co-IP elution. The signal intensity corresponds to the amount of protein, while the R_f value indicates the distance travelled by the protein from the origin. Larger R_f values correspond with proteins of smaller molecular mass. Analysis was completed with Image Lab Version 5.0 (Bio-Rad). The symbols (*,◊,†,‡) indicate a few of the common protein peaks observed between samples.

The unique protein bands identified in the Na$^+$/K$^+$-ATPase alpha subunit isoform co-IP elutions, by staining with Coomassie G-250 BioSafe, were examined by mass spectrometry. Ultimately, 21 bands (Figure 3.7) were excised and digested with trypsin; of these, 15 were analyzed by LC-MS/MS. Bands 10, 13, 14, 15, 17 and 19 were not sent for analysis due to the similarity of their molecular masses when compared with Bands 21, 5 and 6, 9, 1 and 11, 4, and 7, respectively. It was anticipated that the three alpha isoforms of Na$^+$/K$^+$-ATPase would share several binding partners; therefore, protein bands identified in different co-IP elutions but of similar molecular mass, were digested and stored but not sent for analysis unless necessary.
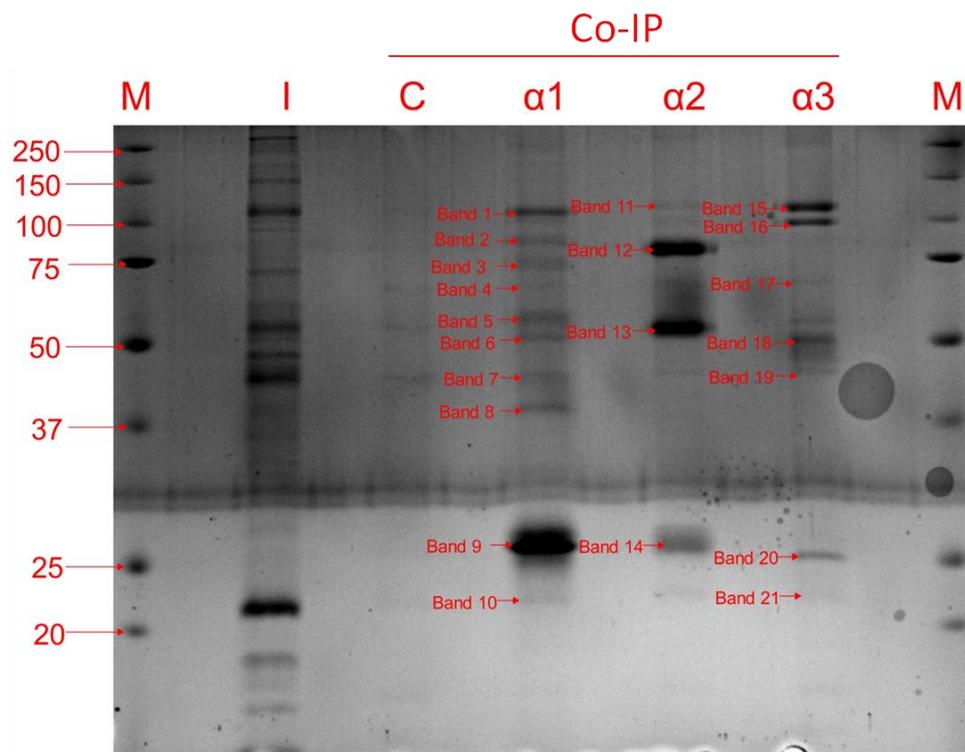
Figure 3.7 Coomassie stained SDS-PAGE of eluted proteins from co-immunoprecipitations of each Na$^+$/K$^+$-ATPase alpha isoform using CD1 mouse myelin

Coomassie G-250 BioSafe stained 1-mm thick 12% SDS-PAGE, loaded with 5 μL of initial CHAPS homogenate (I) and equal volumes (20 μL) of a non-specific binding control (C) and the final eluted

fraction of each alpha isoform co-immunoprecipitation. Precision Plus Protein Dual Color Standards (M) was used as a molecular mass standard. The stained gel was imaged using the VersaDoc 4000 (Bio-Rad) with an exposure time of 0.1-5 seconds, ensuring non-saturation. The indicated bands were excised and digested with trypsin for identification by mass spectrometry.

A total of 33 proteins were identified in the 15 digested bands; however, absolutely no proteins were detected by mass spectrometry in Band 4. Of the 33 documented proteins, positive identification was assigned to those recognized with 100% certainty using the Scaffold 4.3.2 proteome software. These proteins also required a minimum of two unique peptides to be recognized, for confirmation of identity. After applying these criteria, there were 13 major proteins identified; these are listed in Table 3.1. Several immunoglobulin chains from the antibodies used in the co-IPs were also detected by mass spectrometry; these proteins are not listed.

Table 3.1 Major proteins identified in Coomassie G-250 BioSafe stained bands from SDS-PAGE separation of Na$^+$/K$^+$-ATPase alpha co-immunoprecipitation elutions

Each band number corresponds to the indicated protein bands in Figure 3.7. Gel bands were trypsin digested and analyzed by LC-MS/MS. Each major protein was identified with 100% probability using the Scaffold 4.3.2 proteome software, in addition to having a minimum of two unique peptides identified. The ID indicated the UniProtKB/Swiss-Prot accession number, whereas Gene represents the gene name provided by NCBI. The number of unique peptides, the percent coverage, and molecular mass of each protein, as identified by LC-MS/MS, is also provided.

Band No.	Protein Identified	ID	Gene	Unique Peptides	% Coverage	MW (kDa)
1	Sodium/potassium-transporting ATPase subunit alpha-1	Q8VDN2	Atp1a1	7	19	113
	Sodium/potassium-transporting ATPase subunit alpha-3	Q6PIC6	Atp1a3	6	19	112
	Serine/arginine repetitive matrix protein 2	Q8BTI8	Srrm2	3	2	295
3	Peripheral myelin protein 22	18858	Pmp22	3	9	57
	Sodium/potassium-transporting ATPase subunit alpha-3	Q6PIC6	Atp1a3	2	3	112
5	Peripheral myelin protein 22	18858	Pmp22	2	4	57
	Spermatogenesis-associated protein 7	Q80VP2	Spat7	2	1	66

6	Sodium/potassium-transporting ATPase subunit beta-1	P14094	Atp1b1	3	12	35
7	2',3'-cyclic nucleotide 3'-phosphodiesterase	P16330	Cnp	7	16	47
9	Myelin proteolipid protein	P60202	Plp1	2	9	30
11	Sodium/potassium-transporting ATPase subunit alpha-2	Q6PIE5	Atp1a2	2	6	112
	Sodium/potassium-transporting ATPase subunit alpha-3	Q6PIC6	Atp1a3	3	7	112
12	Cullin-associated NEDD8-dissociated protein 1	Q6ZQ38	Cand1	2	2	136
18	Sodium/potassium-transporting ATPase subunit beta-1	P14094	Atp1b1	4	16	35
	Brain acid soluble protein 1	Q91XV3	Basp1	2	16	22
	Protein MRVI1	Q9WUX5	Mrvi1	2	2	100
20	Peripheral myelin protein 22	18858	Pmp22	3	5	57
21	Serine/arginine repetitive matrix protein 2	Q8BTI8	Srrm2	2	1	295
	Myelin proteolipid protein	P60202	Plp1	5	17	30
	Krueppel-like factor 6	O08584	Klf6	2	5	32

According to the mass spectrometry results, the α_1 and α_2 isoforms were confirmed to be present in their respective co-IP elutions. Similarly, Band 15 should represent the α_3 isoform, as it shares an equivalent molecular mass to Bands 1 and 11; both of which were found to contain the Na$^+$/K$^+$-ATPase α_3 subunit isoform. The α_1 subunit isoform was shown to interact with 7 other proteins in myelin; Na$^+$/K$^+$-ATPase α_3, Na$^+$/K$^+$-ATPase β_1, serine/arginine repetitive matrix protein 2 (SRRM2), PMP-22, spermatogenesis-associated protein 7 (SPAT7), CNP, and PLP1. Each of these proteins co-eluted with the α_1 subunit. In comparison, the α_2 subunit isoform was also found to interact with Na$^+$/K$^+$-ATPase α_3, in addition to cullin-associated NEDD8-dissociated

protein 1 (CAND1). Lastly, the α_3 subunit isoform co-eluted with 7 other identified proteins; Na$^+$/K$^+$-ATPase β_1, brain acid soluble protein 1 (BASP1), protein MRVI1 (MRVI1), PMP-22, SRRM2, PLP1, and krueppel-like factor 6 (KLF6). The identification of the Na$^+$/K$^+$-ATPase β_1 subunit isoform, within both the α_1 and α_3 subunit co-IP elutions, supports the previous Western blot analysis which identified $\alpha_1\beta_1$ and $\alpha_3\beta_1$ as two of the three major Na$^+$/K$^+$-ATPase isozymes present in the myelin membrane.

Potential protein binding partners of Na$^+$/K$^+$-ATPase were also identified using the STRING database. STRING version 9.1 (http://string-db.org/) was used to integrate the information from collections of experimental data and other resources, in order to provide evidence-based predictions of protein-protein interactions for each of the subunit isoforms [59]. Each alpha and beta subunit isoform was predicted to interact with all other alpha and beta subunit isoforms of Na$^+$/K$^+$-ATPase. FXYD2 was also a predicted functional partner of all Na$^+$/K$^+$-ATPase subunit isoforms. For a complete list of the predicted functional partners of Na$^+$/K$^+$-ATPase, and illustrations of the corresponding protein-protein interactions, refer to Appendix C.

3.4 Na$^+$/K$^+$-ATPase Expression in Myelin from CD1 and ND4 Mice

As previously mentioned, establishing changes in protein expression over various life stages is imperative to understanding their role in development. This knowledge also provides a basis for determining how protein expression may become altered in a diseased state, thereby offering insight regarding which biological and chemical processes could be manipulated for therapeutic benefit. In particular, ND4 transgenic

mice provide a suitable model of multiple sclerosis. In this study, myelin isolated from these mice was compared with the myelin of age- and sex-matched control CD1 mice. The animals were euthanized at 3.10, 7.65, 9.00 or 13.02 months of age; and each line was raised and sacrificed under the same conditions. Western blot analysis of equal amounts of protein from both myelin preparations, and from each age group, was performed for all three alpha and three beta subunit isoforms of Na^+/K^+-ATPase (Figure 3.8). Densitometric analysis was then carried out to evaluate changes in the expression of each isoform, from each myelin preparation, over post-natal development. All of the densitometric data, for both CD1 and ND4 myelin, can be found in Appendix D.

Western blots were performed in duplicate; samples from both myelin preparations, at each age group, were examined once without a β-actin protein loading control (refer to Appendix H) and once with a β-actin protein loading control. Without normalization to β-actin, each data set showed distinct similarities; however, the normalized densitometric data was the primary focus in this study. By using β-actin as an internal control, technical artifacts, such as pipetting errors during gel loading and inconsistent protein transfer to blotting membranes, were minimized [60]. It also permits the comparison of two different blots, when they are otherwise not directly comparable [61].
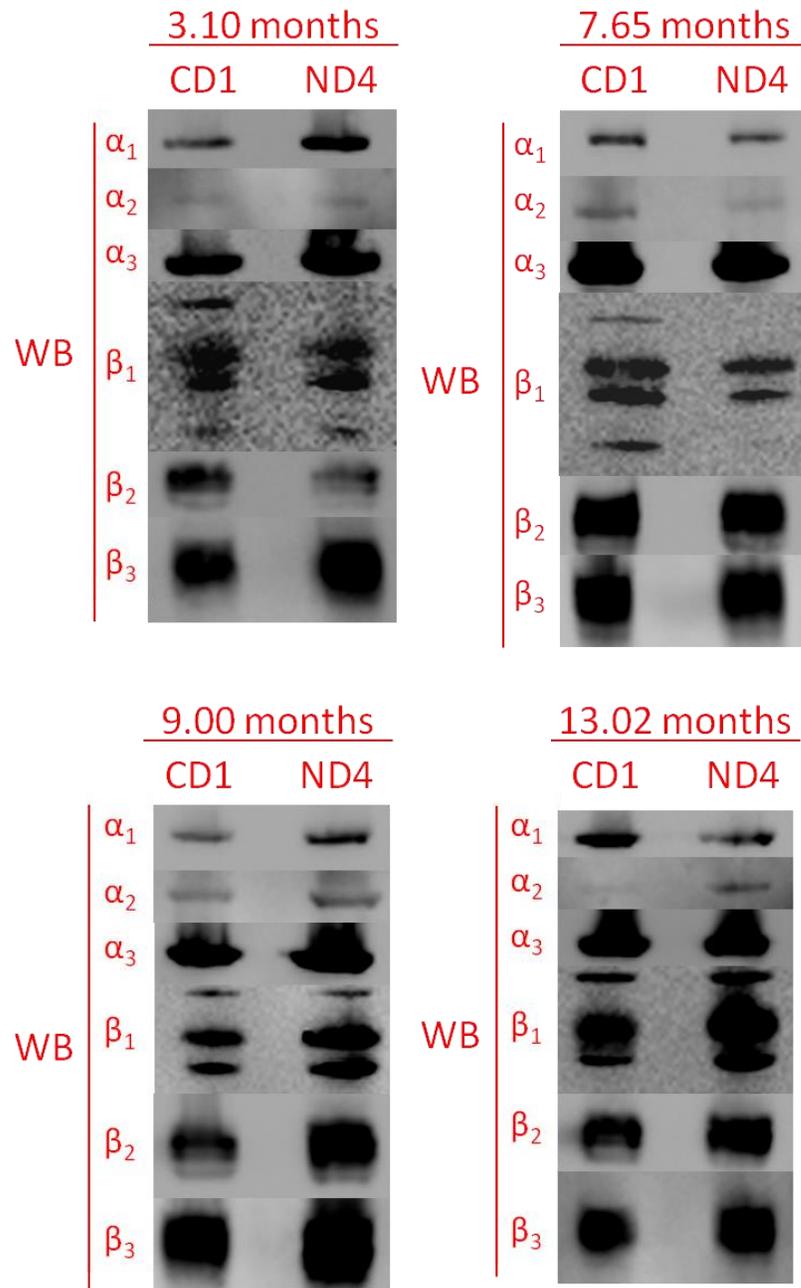
Figure 3.8 Detection of Na$^+$/K$^+$-ATPase subunit isoforms in partially delipidated CD1 and ND4 mouse myelin of varying ages

Enhanced chemiluminescent Western blot detection of each alpha and beta isoform of Na$^+$/K$^+$-ATPase in partially delipidated CD1 and ND4 mouse myelin. Equal volumes (15 μL), and therefore equal protein (approximately 60 μg of total myelin protein), of each sample were separated on 12% SDS-PAGE and transferred to nitrocellulose membrane. The corresponding primary and secondary antibodies used are described in Table 2.3. Each Western blot was imaged using the VersaDoc 4000 (Bio-Rad) with an exposure time of 30-200 seconds, ensuring non-saturation.

The normalized densitometric data in this study is represented as the relative

intensities of each Na^+/K^+-ATPase subunit isoform. Expression levels were described in

terms of the ratios of individual Na^+/K^+-ATPase subunit isoform levels, to the levels of β-

actin in each sample; this is considered a robust normalization method for Western

blotting [62]. First, the signal intensity of each β-actin control was divided by the highest

measured intensity value of all β-actin controls; this process generated a relative

intensity factor, between 0 and 1.00. The signal intensities of each Na^+/K^+-ATPase

subunit isoform were subsequently divided by their respective relative intensity factor;

the result is the relative intensity for each Na^+/K^+-ATPase subunit isoform.

3.4.1 Age-Related Protein Expression in Healthy CD1 Mouse Myelin

All three alpha and three beta subunit isoforms of Na^+/K^+-ATPase were detected

at 3.10, 7.65, 9.00 and 13.02 months of age in the CD1 control mouse myelin. These

samples represent typical, healthy myelin, and are indicative of the normal age-related

changes in protein expression. Upon the measurement of protein band intensity for

each subunit isoform, in each age group, it was noted that intensities fluctuated over

the course of normal development. These changes persisted even after each

densitometric measurement was normalized to a β-actin, as a protein loading control, in

the same sample. The adjusted values, and corresponding fluxes in the expression of

each subunit isoform, are displayed in Figure 3.9. Upon inspection, each alpha isoform

consistently exhibits an increase in expression when approaching the final 13.02 month

age group. In contrast, the beta isoforms are relatively divergent. Na^+/K^+-ATPase β_1

expression increases between 9.00 and 13.02 months but remains lesser than the initial

71

measurement at 3.10 months. Alternatively, Na^+/K^+-ATPase β_2 and β_3 expression

steadily increases or decreases, respectively, over time.
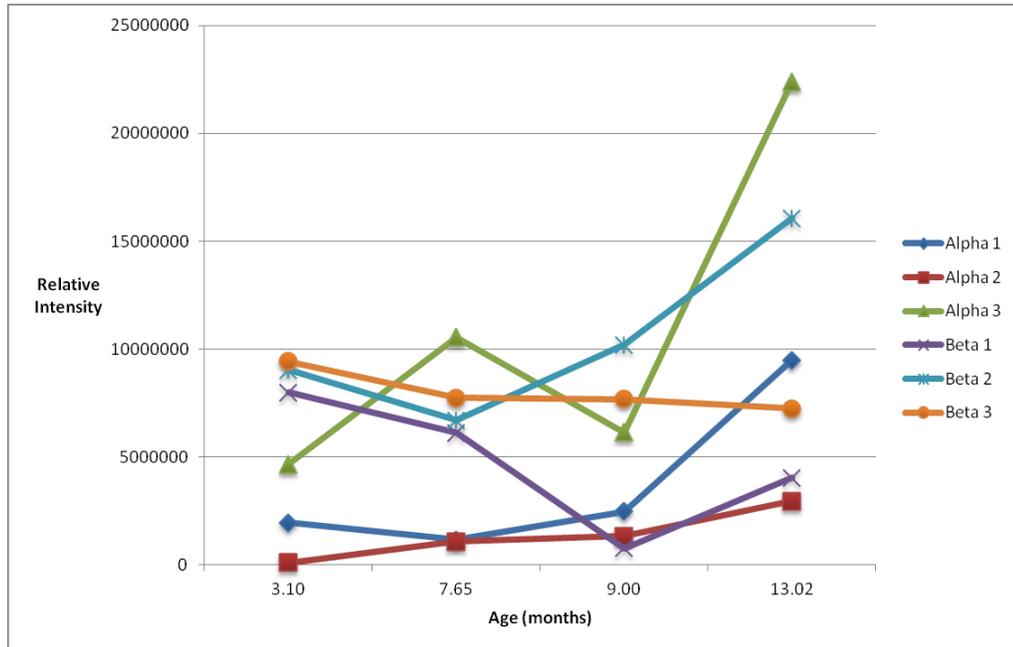
Figure 3.9 Relative Na^+/K^+-ATPase subunit isoform expression in CD1 mouse myelin with aging

Intensity of each Na^+/K^+-ATPase subunit isoform, ensuring non-saturation and subtracting background. Intensity was measured at 3.10, 7.65, 9.00 and 13.02 months of age. Each value was corrected by normalization with a β-actin protein loading control.

Beyond the observed fluctuations in the protein expression of each subunit

isoform, it was also discovered that the protein bands for each glycosylation state of

Na^+/K^+-ATPase β_1 could be detected by Western blotting (Figure 3.8). The mammalian

Na^+/K^+-ATPase β_1, such as that found in mice, can have three N-glycans or N-linked

glycosylation sites occupied; in addition to these three forms, Na^+/K^+-ATPase β_1 can also

exist as a core, unglycosylated subunit [3]. This core protein is often considered its

immature form. Three β_1 protein bands, that were approximately 60 kDa, 52 kDa and 48

kDa in size, represented the β_1 subunit with all three N-glycans, two N-glycans, and only

one N-glycan, respectively. The largest form of Na^+/K^+-ATPase β_1, with the highest

molecular mass, was designated Band 1 of the Na^+/K^+-ATPase β_1 subunit; similarly, Band

2 and Band 3 were assigned to the other glycosylated forms, from highest to lowest

molecular mass. And lastly, another small molecular mass protein band was identified

by the Na^+/K^+-ATPase β_1 antibody; it was approximately 40 kDa in size. It was designated

as Band 4 of the Na^+/K^+-ATPase β_1 subunit, and represents the β_1 core protein.
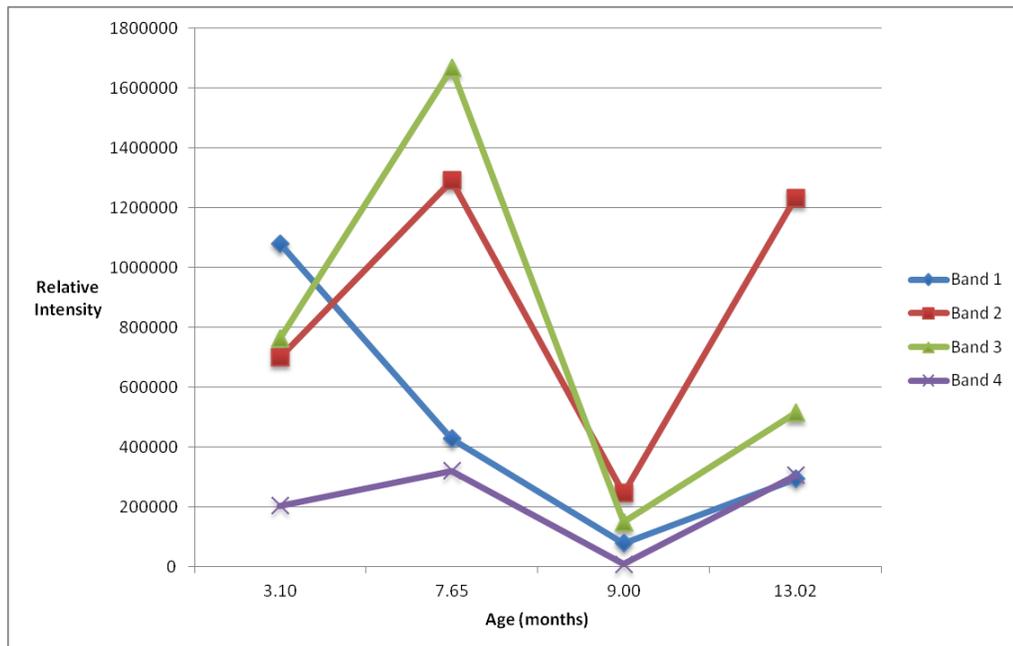
Figure 3.10 Relative Na^+/K^+-ATPase β_1 glycosylation state expression in CD1 mouse myelin with aging

Intensity of each Na^+/K^+-ATPase β_1 glycosylation state, ensuring non-saturation and subtracting background. Bands 1 to 4 represent the highest molecular mass form of Na^+/K^+-ATPase β_1 to the lowest molecular mass form (core, non-glycosylated), respectively. Intensity was measured at 3.10, 7.65, 9.00 and 13.02 months of age. Each value was corrected by normalization with a β-actin protein loading control.

Resembling the other subunit isoforms of Na^+/K^+-ATPase the protein expression

of the individual glycosylation states of Na^+/K^+-ATPase β_1 varied over the course of

development. The normalized intensities of each glycosylation state, at each age, are

illustrated in Figure 3.10. It was observed that expression levels generally increased

between 3.00 to 7.65 months, decreased after 7.65 months, and bounced back at 13.02

months of age. Band 1, the highest molecular mass form of Na^+/K^+-ATPase β_1, was

unique in the fact that its expression continually decreased from 3.00 months onward,

until rebounding at 13.02 months of age. Bands 2 and 3 were typically found in the

greatest abundance, when compared with the fully glycosylated and core forms of

Na^+/K^+-ATPase β_1. Additionally, the core, unglycosylated form of Na^+/K^+-ATPase β_1, at

both 9.00 and 13.02 months of age, was extremely difficult to perceive upon visual

inspection of the blot. These Western blots indicated that expression of the immature

form of Na^+/K^+-ATPase β_1 was extremely limited in the later months of development; it

was also the least abundant of all forms, across all four age groups.

3.4.2 Age-Related Protein Expression in Diseased ND4 Mouse Myelin

As a follow-up to studying each Na^+/K^+-ATPase subunit isoform in healthy CD1

control mouse myelin, the myelin isolated from ND4 mice, which represent a

demyelinating model of MS, was subsequently assessed. These mice were sacrificed at

the same time as the CD1 mice; either at 3.10, 7.65, 9.00 or 13.02 months of age.

Analogous to the examination of Na^+/K^+-ATPase subunit isoform expression in CD1

control mice, Western blotting in conjunction with densitometric analysis was

performed. These images are shown alongside their control counterparts in Figure 3.8.

Once again, all three alpha and three beta subunit isoforms of Na^+/K^+-ATPase were

successfully detected in the ND4 myelin from each age group. When normalized to a β-

actin protein loading control, the fluctuations in protein band intensity for each subunit

isoform closely resembled the changes which occurred in the CD1 control myelin, across

all four age groups; refer to Figure 3.11, and compare with Figure 3.9. Na$^+$/K$^+$-ATPase β_3

appeared to be an exception, as its expression within the ND4 myelin increased after

9.00 months; whereas the CD1 myelin showed a decrease in expression during this time

period.
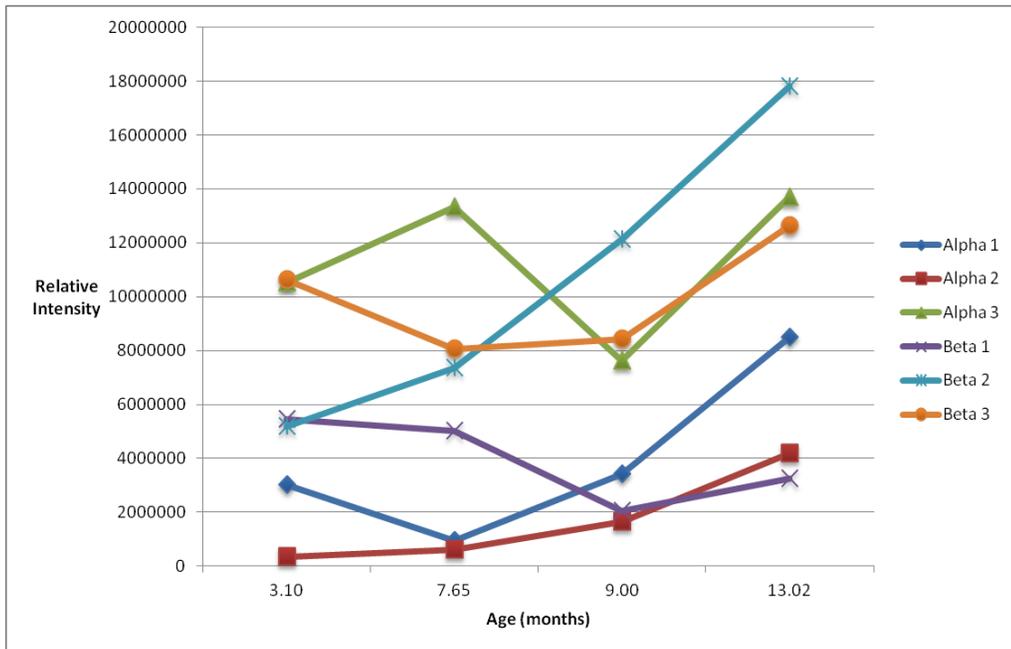
Figure 3.11 Relative Na$^+$/K$^+$-ATPase subunit isoform expression in ND4 mouse myelin with aging

Intensity of each Na$^+$/K$^+$-ATPase subunit isoform, ensuring non-saturation and subtracting background. Intensity was measured at 3.10, 7.65, 9.00 and 13.02 months of age. Each value was corrected by normalization with a β-actin protein loading control.

As with the CD1 control myelin, the three glycosylation states as well as the core,

unglycosylated form of Na$^+$/K$^+$-ATPase β_1 were evident in the ND4 myelin. In this case,

the trends of protein expression over the course of development were once again

similar to that of the CD1 myelin, with several slight differences. As shown in Figure

3.12, the fully glycosylated form of Na$^+$/K$^+$-ATPase β_1 (Band 1), rather than its core (Band

4), was the least abundant of all other Na$^+$/K$^+$-ATPase β_1 proteins. The two intermediate

molecular mass protein forms, Bands 2 and 3, remained the most abundant, as also

seen in the CD1 control myelin (Figure 3.10).
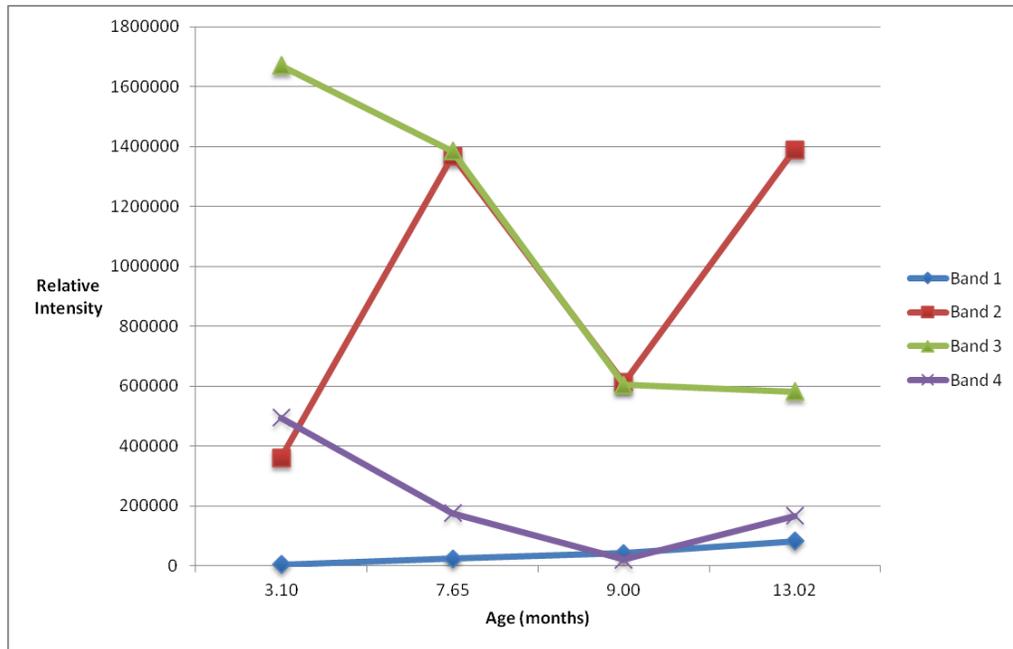
Figure 3.12 Relative Na$^+$/K$^+$-ATPase β_1 glycosylation state expression in ND4 mouse myelin with aging

Intensity of each Na$^+$/K$^+$-ATPase β_1 glycosylation state, ensuring non-saturation and subtracting background. Bands 1 to 4 represent the highest molecular mass form of Na$^+$/K$^+$-ATPase β_1 to the lowest molecular mass form (core, non-glycosylated), respectively. Intensity was measured at 3.10, 7.65, 9.00 and 13.02 months of age. Each value was corrected by normalization with a β-actin protein loading control.

3.4.3 The Effect of Demyelination on Na$^+$/K$^+$-ATPase Protein Expression

A direct comparison of the corrected intensities for each Na$^+$/K$^+$-ATPase subunit

isoform as well as the various glycosylation states of Na$^+$/K$^+$-ATPase β_1, within each

individual age group, can be found in Figure 3.13 and Figure 3.14. Certain differences

between the protein expressions of the two myelin preparations were immediately

recognized. Firstly, Na$^+$/K$^+$-ATPase α_1 initially demonstrates increased expression within

the ND4 myelin, until 13.02 months when it is lesser than, but close to, the levels of

expression detected in the CD1 myelin. Secondly, the expression of the fully

glycosylated form of Na$^+$/K$^+$-ATPase β_1 (Band 1) in the ND4 myelin was strikingly lesser

than that of the CD1 myelin, across all age groups. Na$^+$/K$^+$-ATPase β_2 also exhibited

reduced expression within the ND4 myelin at 3.00 and 7.65 months of age, but

surpassed the measured expression of the CD1 myelin at 9.00 and 13.02 months of age.

Lastly, Na$^+$/K$^+$-ATPase β_3 was consistently elevated in the ND4 myelin, across all age
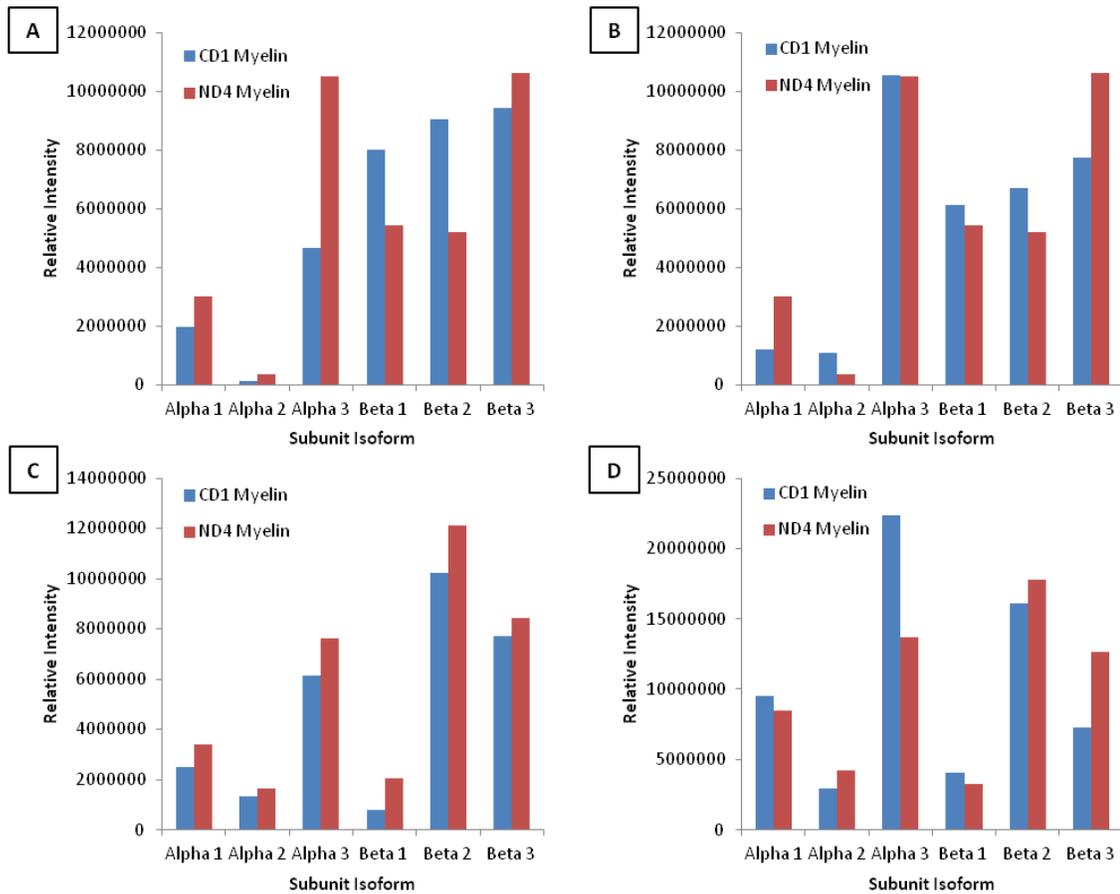
groups.

Figure 3.13 Compared relative intensities of each Na$^+$/K$^+$-ATPase subunit isoform, between CD1 and ND4 myelin, in each age group

Relative intensity of each Na$^+$/K$^+$-ATPase subunit isoform, ensuring non-saturation and subtracting background. Each value was corrected by normalization with a β-actin protein loading control. Comparisons were for CD1 (blue) and ND4 (red) myelin at: **A)** 3.00 months of age; **B)** 7.65 months of age; **C)** 9.00 months of age; **D)** 13.02 months of age.
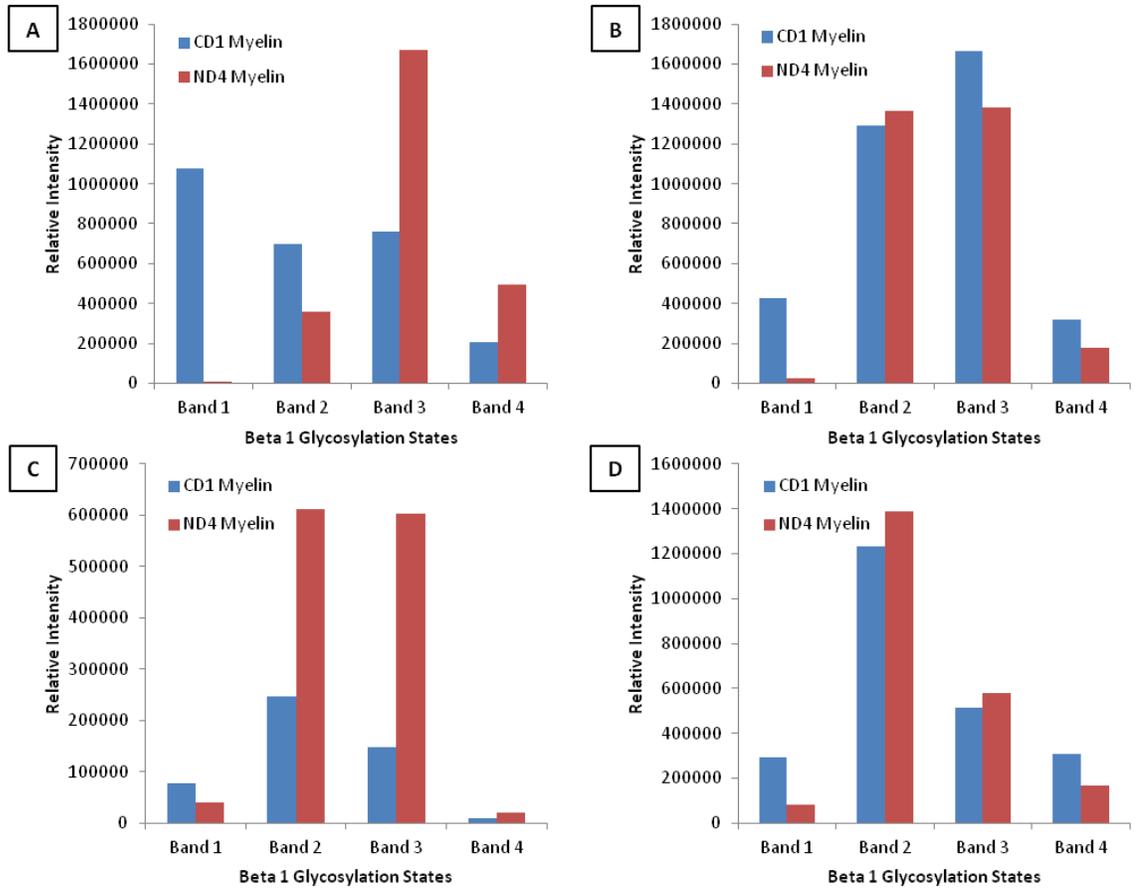
Figure 3.14 Compared relative intensities of each Na^+/K^+-ATPase β_1 glycosylation state, between CD1 and ND4 myelin, in each age group

Relative intensity of each Na^+/K^+-ATPase β_1 glycosylation state, ensuring non-saturation and subtracting background. Bands 1 to 4 represent the highest molecular mass form of Na^+/K^+-ATPase β_1 to the lowest molecular mass form (core, non-glycosylated), respectively. Each value was corrected by normalization with a β-actin protein loading control. Comparisons were for CD1 (blue) and ND4 (red) myelin at: **A)** 3.00 months of age; **B)** 7.65 months of age; **C)** 9.00 months of age; **D)** 13.02 months of age.

Chapter 4 – Discussion

4.1 Comparison of Sucrose and Percoll Gradient Isolation Methods

The biochemical analysis of specific cell types, a particular membrane, or the subcellular organelles of certain tissues, requires the successful isolation of pure cellular populations or subcellular fractions. The complex nature of the CNS, and its highly interconnected cellular processes and cell types, has prompted the development of several different isolation strategies which aid in the study of cellular neurochemistry [63]. Firstly, the successful isolation of subcellular organelles and biological membranes, such as myelin, requires a method of cell lysis or tissue homogenization which maximizes yield while minimizing cellular debris and contaminants [64]. It is also important that the procedure maintains the functional integrity of the target, as well as preserving its structure as much as possible. In this study, whole mouse brains were homogenized, using a Dounce homogenizer, in an isotonic sucrose solution of low ionic strength. Under these conditions, the myelin membrane becomes detached from neuronal axons and forms small vesicles; these myelin vesicles are similar in size to mitochondria and nuclei [65]. The high lipid to protein ratio in myelin also confers the lowest intrinsic density of any membrane fraction derived from the CNS, including mitochondria and nuclei [65].

Essentially all myelin isolation protocols exploit the size and density of the myelin vesicles generated during the homogenization of CNS tissue. Often, an isolation protocol will use differential centrifugation at low speeds to remove bulky debris from the initial

homogenate [49]. This process is then followed by the separation of the remaining cell membranes and organelles using a discontinuous density gradient. Mitochondria, synaptosomes, nuclei and other large cellular components will sediment through the denser layer of the isolation medium, while small membrane fragments and certain organelles will remain in the upper, less dense fraction; the myelin vesicles, however, will gather at the density interface due to their size and buoyancy [11;65]. After collecting the crude myelin from the interface, the sucrose is diluted out and the vesicles are osmotically shocked. By treating the isolated myelin with ice cold purified water, any residual microsomes, axoplasm or major impurities are released [65]. Myelin vesicles of higher purity can be obtained by adding supplementary centrifugation and osmotic shock steps to the methodology. A second round of density gradient centrifugation can be introduced; by doing so, further removal of large particles, which may become trapped in the crude myelin layer that forms at the density interface, is achieved [66]. Continuous density gradients can also be introduced as a way of preventing contaminating materials from becoming trapped in the crude myelin layer; this addition may be either supplementary to, or in place of, the discontinuous gradient centrifugation steps [66]. A range of myelin vesicles, of different sizes, densities, and lipid to protein ratios, can be separated by the use of continuous gradients; thereby permitting a more detailed examination of the myelin membrane to be conducted.

In this study, the myelin vesicles were separated from the remaining neural tissue using either a discontinuous sucrose or Percoll gradient; each method offered its own advantages and disadvantages. The method by Kristian used a discontinuous

Percoll gradient [49]. Percoll, like sucrose, can be prepared in an isotonic solution which allows osmolarity to be maintained throughout the isolation [67]. It has a low viscosity, as it is made of colloidal silica particles which have been coated with polyvinylpyrrolidone [67]. Consequently, the use of Percoll, rather than sucrose, allows for the use of lower centrifugal forces, and accelerates sedimentation rates [50]. More specifically, the maximum centrifugal force applied by this method was 30,700xg, and gradient separation took merely eight minutes. In fact, the entire procedure for isolating myelin, mitochondria and synaptosomes is estimated to take 90 minutes [49].

The sucrose gradient isolation method developed by Norton takes slightly over two hours to complete [48]; however, modifications used in this study increased the isolation time to 4-5 hours total. A discontinuous density gradient was applied twice; first to isolate the crude myelin, and a second time to obtain purified myelin. Unlike the Percoll gradient isolation, this method excluded an initial low speed centrifugation step to remove major debris, prior to applying the homogenized CNS tissue to a discontinuous density gradient [48]. It also required significantly greater centrifugal forces and separation times; the density gradient centrifugation steps depended upon the use of an ultracentrifuge, as forces up to 100,000xg were reached. Due to the longer isolation time, protease and phosphatase inhibitor cocktails were included in the isolation medium of the sucrose gradient method, during homogenization; they were not present in the isolation medium of the Percoll gradient method, though were incorporated into the myelin storage buffer used in each procedure. These inhibitors prevent protein denaturation which is often triggered by disturbance of the highly

81

regulated cellular environments; in so doing, total protein recovery is boosted and enzyme activity is preserved [68]. The sucrose gradient method also took advantage of two osmotic shock steps, which ensured removal of impurities from within the myelin vesicles. Unfortunately, this procedure required a greater number of mouse brains to produce an equivalent myelin yield to that generated using the Percoll method. The additional purification steps included in the sucrose gradient isolation led to the loss of some myelin vesicles; consequently, 8 mouse brains were needed to attain comparable amounts of myelin protein when judged against the product of the alternate Percoll procedure, which used only 4 mouse brains. The sucrose method was variable and yielded 2.5-14 mg of total protein, whereas the Percoll method generated approximately 5 mg of protein.

Preliminary tests indicated that both sucrose and Percoll gradient isolation protocols generated myelin with measurable levels of Na^+/K^+-ATPase α_1, α_2, and α_3, as well as their complementary β_1, β_2, and β_3 subunits. Similarly, MBP, VDAC, NQO1 and MCT1 were successfully detected by Western blotting in the products of each myelin preparation (refer to Appendix G). MBP is a known myelin-specific protein, while VDAC and NQO1 are currently being investigated in the DeBruin lab as possible myelin-associated proteins. Alternatively, MCT1, MCT2 and MCT4 have all been previously shown to localize within the CNS; MCT1 is predominately expressed in oligodendrocytes, while MCT2 and MCT4 are expressed in neurons and astrocytes, respectively [69]. Differences in the isolated myelin samples were only observed when examined side by side, along with a brain homogenate sample of equal protein content. VDAC and MCT1

were more enriched in the myelin vesicles of the Percoll gradient protocol, despite

containing equivalent levels of MBP when compared with myelin isolated using a

sucrose-gradient; therefore, the myelin produced using the sucrose-gradient method

was selected for all further analyses despite being a more timely and expensive

procedure.

4.2 Role of Na^+/K^+-ATPase Isoforms and Heterodimers in the Myelin Membrane

To date, four alpha and three beta isoforms of Na^+/K^+-ATPase have been

identified in mammalian tissues; of these, only Na^+/K^+-ATPase α_1, α_2, and α_3, and β_1, β_2,

and β_3 have been identified in CNS tissue. Each of these isoforms are encoded by

separate genes and they show a high degree of conservation, even across species

[3;70;71]. Despite any differences in sequence and/or post-translational modifications,

past studies have demonstrated that each of the four alpha subunit isoforms are

capable of forming a functional ion pump with any of the three beta subunit isoforms

[31].

4.2.1 Co-expression of Na^+/K^+-ATPase Isoforms and Isozymes

The isoforms of each subunit demonstrates spatial and temporal patterns of

expression; specifically, tissue-specific and developmental variations in protein

expression [70]. The α_1 and β_1 subunits have been classically perceived as the

"housekeeping" isoforms, as they are typically abundant and ubiquitously expressed

[24;27;31;72]. Conversely, the α_2, α_3, α_4, β_2, and β_3 subunit isoforms demonstrate

83

varying levels of tissue-specificity or variations in expression throughout the stages of development; these differences suggest that each provides unique functional roles. So far, the α_2 subunit has been primarily identified in the brain, muscle, adipose, osteoblasts, retina, choroid plexus, lung, and the optic nerve; the α_3 and β_2 subunits are found in neural tissue, with Na^+/K^+-ATPase α_3 also having been identified in human cardiac muscle; and the α_4 and β_3 subunits are expressed in spermatogonia and sperm, although Na^+/K^+-ATPase β_3 has also been noted in the brain, kidneys, lung, spleen, intestines, and liver [24;27;31;34]. With regards to the specific cell types of the CNS, the α_1 isoform distributes between neurons and glia, while the α_2 and α_3 isoforms are primarily expressed in glia or neurons, respectively; also, the β_1, β_2, and β_3 isoforms predominantly exist within neurons, both astrocytes and oligodendrocytes, or oligodendrocytes, respectively [36]. Refer to Table 4.1 and section 4.2.2 for further discussion. In this study, it was identified that all three alpha and three beta subunit isoforms of the mammalian CNS were expressed in the myelin membrane of both CD1 and ND4 mice; these represented healthy and diseased myelin, respectively.

Apart from the tissue- and organ-specific distribution of each subunit isoform, the alpha and beta subunits of Na^+/K^+-ATPase can also exhibit subplasmalemmal organization. Na^+/K^+-ATPase has the potential to reside within certain microdomains and membrane regions; therefore, it often demonstrates targeted distribution within the plasma membrane [32]. This phenomenon has been observed in cultured astrocytes and neurons, both of which have a unique and complex cellular architecture (Figure 4.1). In particular, the α_1, α_2, and α_3 subunit isoforms have demonstrated unique

patterns of expression in these cell types. Na^+/K^+-ATPase α_1 is expressed throughout

astrocytes, but appears limited to the cell bodies of neurons [72]. Alternatively, Na^+/K^+-

ATPase α_2 localizes in regions of the plasma membrane that overlap with the cellular

distribution of the endoplasmic reticulum [72]; this pattern of expression could be an

unintentional consequence of integral membrane protein synthesis and transport from

the endoplasmic reticulum to the plasma membrane, via the Golgi complex. And lastly,

Na^+/K^+-ATPase α_3 non-uniformly distributes throughout the processes (dendrites, axons,

and terminal fibers) and cell bodies of neurons; Na^+/K^+-ATPase α_3 stands apart from its

α_1 counterpart, as it is expressed in clusters or focused regions within neurons [72].
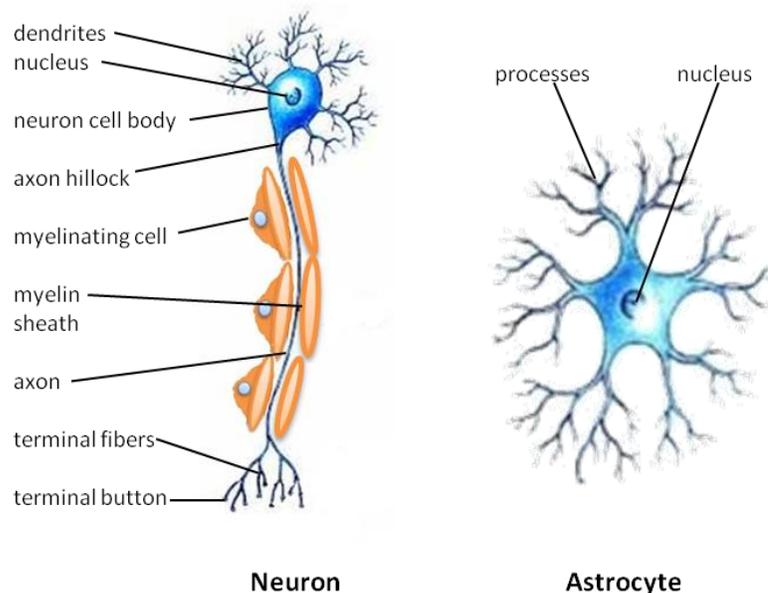
Figure 4.1 The basic structure of neurons and astrocytes

A typical neuron has a cell body, which contains the nucleus and other cellular organelles, as well as dendrites to receive impulses, and axons and fibers to transmit impulses. Astrocytes are characteristically star-shaped, and extend processes which commonly terminate on blood vessels or the axons of neurons. Image adapted from references [1;4].

Known protein-protein interactions indicated that Na^+/K^+-ATPase stabilizes

components of adherens junctions and regulates the expression of proteins found in the

tight junctions of epithelial cells [58;73;74]. These two microdomains form the apical

junctional complex, which is responsible for critical cell-cell adhesion. Na^+/K^+-ATPase has

been shown also to localize within the caveolar microdomain of renal epithelial cells;

this result was anticipated as both Na^+/K^+-ATPase and caveolae exist at the basolateral

plasma membrane of these polarized cells [32;58]. In these caveolae, oligomers of

caveolin-1, tetramers of annexin-2, and oligomers Na^+/K^+-ATPase formed large

multiprotein complexes [58]. Furthermore, when activity was investigated in both

caveolar and non-caveolar Na^+/K^+-ATPase pools, it was determined that ion transport

capabilities were retained in the caveolae; this has also been demonstrated in Na^+/K^+-

ATPase within caveolae derived from cardiac myocytes [58]. Caveolin-1 enriched

microdomains, adherens junctions and tight junctions are all found in the myelin

membrane as well; the caveolin-1 enriched microdomain and adherens junctions are

both components of the outer loops of myelin, the adherens junctions and tight

junctions are part of the paranodal loops of myelin, and the adherens junctions and

tight junctions are also found in the incisures and radial components of the myelin

membrane, respectively [16].

Ultimately, the unique subplasmalemmal distribution of each Na^+/K^+-ATPase

subunit isoform may confer unique physiological properties to specific cell types. On top

of these distinct localization patterns, the subunit isoforms also vary in their

comparative levels of expression. For example, neurons typically express Na^+/K^+-ATPase

α_1, α_2, and α_3; however the α_1 and α_3 isoforms are most abundant [72]. In the same

way, all three alpha isoforms of the CNS are expressed in the myelin membrane, as

identified in this study; however, as shown by Western blot analysis, myelin is rich in the α_3 isoform, while the α_1 and α_2 isoforms are less abundant. As in neurons, the α_2 isoform in myelin is the least abundant. With regards to the beta subunit in myelin, Na^+/K^+-ATPase β_2 and β_3 are more abundant than the β_1 isoform. Each individual Na^+/K^+-ATPase alpha or beta isoform, within a specific tissue or cell type, also experiences fluctuations in their expression over the course of development.

As discussed earlier, multiple subunit isoforms are often co-expressed within a tissue or specific cell type. The coexistence of different Na^+/K^+-ATPase subunit isoforms, and in turn various isozymes, may be essential due to differences in their sensitivity to inhibitors, substrate affinities, and varying cellular roles. Firstly, Na^+/K^+-ATPase is often targeted by cardiac glycosides, such as ouabain, in the treatment of congestive heart failure and other cardiomyopathies. These compounds can inhibit enzymatic activity by disrupting the catalytic site of the alpha subunit. They are also naturally occurring in biological systems. Interestingly, the α_1 isoform is ouabain-resistant; Na^+/K^+-ATPase α_2 and α_3, however, are ouabain-sensitive and can be inhibited by such compounds [75]. With regards to their substrate affinities, disparity in both Na^+ and K^+ ion affinities between isoforms have been experimentally proven. In a rat model, the α_1 isoform exhibited a greater K^+ affinity than its α_2 and α_3 counterparts; while the α_3 isoform has demonstrated a reduced affinity for Na^+ in comparison to α_1 and α_2 [24]. The enzymatic activity of each of the heterodimeric forms of Na^+/K^+-ATPase can also be modulated by associations with the FXYD1 protein, which is often co-expressed [76]. Thirdly, adaptations or isoform specific interactions are reflected in the distinct distribution of

the Na^+/K^+-ATPase beta subunit isoforms within oxidative and glycolytic tissues; in particular, the β_1 isoform is found in oxidative muscle fibers whereas the β_2 isoform resides primarily in the glycolytic fibers [77]. The slight differences in these enzymatic properties, between individual isoforms and isozymes, may support different physiological requirements and provide adaptability to inconsistent ionic and osmotic cellular environments [72]. Likewise, the chromosomal dispersion of the genes for each alpha subunit isoform, as well as their individual expression patterns, suggests selection in response to various physiological demands [72]. Negative and positive elements have been identified for the genes of each alpha isoform; they bind transcription factors and regulate both spatial and temporal expression. The existence of these elements also indicates that Na^+/K^+-ATPase expression is strongly associated with physiological requirements [72]. Alternative splicing has also been shown to generate truncated alpha and beta isoforms; both have been identified in several tissue types and retain their ATP binding and phosphorylation sites, suggesting that they maintain their ATPase activity [3]. The expression of these truncated proteins could have significant structural or functional importance. Finally, it is possible that co-expression may primarily offer functional redundancy, as Na^+/K^+-ATPase is responsible for several critical cellular functions and is a key regulator of homeostasis.

4.2.2 Comparison with Cell Types of the Brain

Na^+/K^+-ATPase α_1, α_2, and α_3, as well as the complementary β_1, β_2, and β_3 subunits, represent all known isoforms of Na^+/K^+-ATPase in the CNS. Table 4.1 summarizes the findings of this study, in addition to the known subunit isoform

expression of the major cell types of the CNS. Myelin, unlike these cell types, is the only

component of the CNS known to express all six subunit isoforms. Although Na^+/K^+-

ATPase α_3 expression has not been detected in oligodendrocytes [34;75;79;81], it is

found in the myelin sheath; thus, expression must occur post-myelination. The use of

antibodies with unique epitope binding sites, for each alpha and beta isoform, ensured

no cross-reactivity and provided confidence in the identification of each subunit

isoform. The specific epitopes for each antibody used in the study were described

previously in Table 2.1.

Table 4.1 The distribution of alpha and beta isoforms within the various cell types of the brain

The known expression of Na^+/K^+-ATPase subunit isoforms is represented by a positive (+) sign; alternatively, Na^+/K^+-ATPase subunit isoforms not known to exist in the specified tissue or cell type is represented by a negative (-) sign.

Cell Type	Isoform						References
	α_1	α_2	α_3	β_1	β_2	β_3	
Neurons	+	+	+	+	+	Only in retinal photoreceptors	[34;75;78-81]
Astrocytes	+	+	-	+	+	-	[75;78-81]
Oligodendrocytes	+	+	-	+	+	+	[34;75;79;81]
Myelin	+	+	+	+	+	+	This study

Although any of the three alpha isoforms could potentially associate with any of

the three beta isoforms to produce a functional ion pump, it is atypical to observe all

possible isozymes co-expressed within a single tissue or cell type [31]. In fact, all nine

heterodimeric forms of Na^+/K^+-ATPase have only been noted within cartilage tissue [72].

Only six of these isozymes were revealed, by this study, to exist in the myelin membrane

of healthy CD1 mice; these included $\alpha_1\beta_1$, $\alpha_2\beta_1$, $\alpha_2\beta_3$, $\alpha_3\beta_1$, $\alpha_3\beta_2$, and $\alpha_3\beta_3$. Of these,

$\alpha_1\beta_1$, $\alpha_2\beta_3$, and $\alpha_3\beta_1$ were the most abundant heterodimeric forms of Na^+/K^+-ATPase in

the myelin membrane, and $\alpha_2\beta_3$ and $\alpha_3\beta_3$ were unique when compared with neurons

and glial cells. The isozymes found in neurons, oligodendrocytes, astrocytes and other

mammalian tissues or cell types, are specified in Table 4.2. Neurons, oligodendrocytes

and astrocytes also express Na^+/K^+-ATPase heterodimers which can distinguish these

cells from the myelin membrane; both $\alpha_1\beta_2$ and $\alpha_1\beta_3$ exist in neurons, while $\alpha_1\beta_2$, $\alpha_1\beta_3$,

and $\alpha_2\beta_2$ have been identified in oligodendrocytes and/or astrocytes [72].

Table 4.2 The distribution of Na^+/K^+-ATPase isozymes within mammalian tissues

The known expression of Na^+/K^+-ATPase isozymes within various mammalian tissues and/or cell types.
This table was adapted from reference [72]. The results of this study are included; the six heterodimeric
forms of Na^+/K^+-ATPase, which were identified in the myelin membrane of CD1 mice, are listed.

Type of Tissue/Cell	Known Na^+/K^+-ATPase Isozymes
Renal tubule cells	$\alpha_1\beta_1$
Cardiac myocytes	$\alpha_1\beta_1$, $\alpha_1\beta_2$, $\alpha_1\beta_3$, $\alpha_2\beta_1$, $\alpha_2\beta_2$, $\alpha_2\beta_3$, $\alpha_3\beta_2$, $\alpha_3\beta_3$
Gut	$\alpha_1\beta_1$
Alveolar epithelial cells	$\alpha_1\beta_1$, $\alpha_1\beta_3$, $\alpha_2\beta_1$, $\alpha_2\beta_3$
Liver	$\alpha_1\beta_1$, $\alpha_1\beta_3$
Neurons	$\alpha_1\beta_1$, $\alpha_1\beta_2$, $\alpha_1\beta_3$, $\alpha_3\beta_1$, $\alpha_3\beta_2$
Oligodendrocytes and/or astrocytes	$\alpha_1\beta_1$, $\alpha_1\beta_2$, $\alpha_1\beta_3$, $\alpha_2\beta_1$, $\alpha_2\beta_2$
Ciliary epithelium	$\alpha_1\beta_1$, $\alpha_1\beta_2$, $\alpha_2\beta_1$, $\alpha_2\beta_2$, $\alpha_3\beta_1$ $\alpha_3\beta_2$
Chondrocytes	$\alpha_1\beta_1$, $\alpha_1\beta_2$, $\alpha_1\beta_3$, $\alpha_2\beta_1$, $\alpha_2\beta_2$, $\alpha_2\beta_3$, $\alpha_3\beta_1$, $\alpha_3\beta_2$, $\alpha_3\beta_3$
Osteoblasts	$\alpha_1\beta_1$, $\alpha_1\beta_2$
Osteoclasts	$\alpha_1\beta_1$
Vascular endothelial cells	$\alpha_1\beta_1$, $\alpha_1\beta_2$, $\alpha_3\beta_1$, $\alpha_3\beta_2$
Skeletal muscle	$\alpha_1\beta_1$, $\alpha_1\beta_2$, $\alpha_1\beta_3$, $\alpha_2\beta_1$, $\alpha_2\beta_2$, $\alpha_2\beta_3$
Smooth muscle	$\alpha_1\beta_1$, $\alpha_2\beta_1$
Testis	$\alpha_1\beta_1$, $\alpha_1\beta_2$, $\alpha_1\beta_3$, $\alpha_4\beta_3$
Prostatic epithelial cells	$\alpha_1\beta_1$, $\alpha_1\beta_2$
Myelin	$\alpha_1\beta_1$, $\alpha_2\beta_1$, $\alpha_2\beta_3$, $\alpha_3\beta_1$, $\alpha_3\beta_2$, and $\alpha_3\beta_3$

The assortment of Na^+/K^+-ATPase isozymes are generated by the expression of

different genes, variations in transcriptional modifications and processing, and the

successful formation of different heterodimeric combinations [3]. As noticed in Table

4.2, $\alpha_1\beta_1$ is present in all examined mammalian tissues and cell types to date; this observation supports the role of both α_1 and β_1 isoforms as the "housekeeping" Na^+/K^+-ATPase subunit isoforms [24;27;31;72]. Other isozymes have proposed functional roles according to the known ion affinities of their corresponding subunit isoforms, as well as known functions and physiological needs of the tissues or cell types in which they are expressed. In particular, heterodimeric forms which incorporate the α_3 isoform may provide additional ion transport capabilities in situations or locales of major fluctuations in ion concentration. As mentioned earlier, Na^+/K^+-ATPase α_3 demonstrates the lowest affinity for Na^+ ions, out of all the alpha isoforms [24]. Likewise, the $\alpha_3\beta_1$ isozyme has reduced affinity for both Na^+ and K^+ ions, and is found primarily in excitable tissues [72]. These qualities may be interpreted as the evolutionary adaptability of Na^+/K^+-ATPase to meet the requirements of excitable tissues, which experience extreme variations in their ionic environments; for example, the extreme fluctuations observed throughout the firing of action potentials [72]. Similarly, $\alpha_3\beta_1$, $\alpha_3\beta_2$, and $\alpha_3\beta_3$ are expressed in cartilage tissue or chondrocytes, where recovery from major variations in the concentration of Na^+ ions is necessary following mechanical joint loading [72]. It is therefore not surprising that the myelin membrane expresses all α_3-containing isozymes, as it is tightly associated with neuronal axons and may be needed to support the changes in ionic environments as action potentials are transmitted. Between the unique kinetic properties and sensitivity in inhibitors, each expressed isozyme appears to provide the necessary adaptations for their resident tissue requirements.

4.3 Protein-Protein Interactions in the Myelin Membrane

Proteins are responsible for carrying out cellular processes, and although they can have independent functions they often collaborate to maintain activity and control their environment. Considering there is a significant number of proteins, and exponentially more cellular functions, protein-protein interactions exhibit both structural and functional diversity. Firstly, proteins may interact with proteins of either identical or non-identical chains; these interactions generate either homo- or hetero-oligomers, respectively [82]. In turn, oligomers formed by homologous proteins can join in either an isologous or heterologous fashion. Isologous associations are formed on the equivalent surfaces of each protein unit, whereas heterologous connections occur at alternative interfaces [82]. Secondly, protein complexes may be functionally obligate; the individual protein components cannot exist alone, as they may not be stable without their specific binding partners. In contrast, non-obligate interactions are those produced from the assembly of proteins which can exist independently from one another [82;83]. A prime example of a non-obligate interactions are cellular signalling cascades; the individual proteins are generally not co-localized until the moment of interaction, and therefore must be stable on their own. Nonetheless, co-localized proteins, particularly homo-oligomers, can participate in non-obligate interactions [82]. Lastly, protein-protein interactions may be either permanent and form very stable complexes, or they can be transient and provide dynamic associations and disassociations in response to the environment or external factors [82;83]. These interactions may also be regulated by post-translational modifications, such as glutathionylation and carbonylation [84-86].

92

Despite the discrete types of protein complexes which can form, it is unusual for a particular interaction to be neatly categorized, as these complexes can vary in stability according to their surrounding environment.

Na^+/K^+-ATPase has several known binding partners and participates in various protein-protein interactions. The individual alpha and beta subunit isoforms of Na^+/K^+-ATPase, themselves, also interact and assemble to produce the functional enzyme. Thus, this enzyme is an example of a hetero-oligomer, or in this particular instance a heterodimer; it is also an example of a non-obligate and usually permanent interaction. Both alpha and beta subunits are produced independently, but the beta subunit is required for the successful insertion of the alpha subunit into the plasma membrane. It interacts with the alpha subunit via a heptad repeat motif, in order to form the αβ hetero-oligomer [87]. The beta subunit can exist within the plasma membrane regardless of alpha expression, although independent roles of this subunit are unknown [27]. It is, however, fundamentally important in cell-cell adhesion, as Na^+/K^+-ATPase $β_1$ also contains a glycine zipper motif which allows homo-oligomerization between beta subunits [87]. As a transmembrane protein of the plasma membrane, Na^+/K^+-ATPase has the potential to associate with cytosolic, extracellular, and other transmembrane proteins. Isozymes may also have unique or shared binding partners. Each of these types of associations is depicted in Figure 4.2.
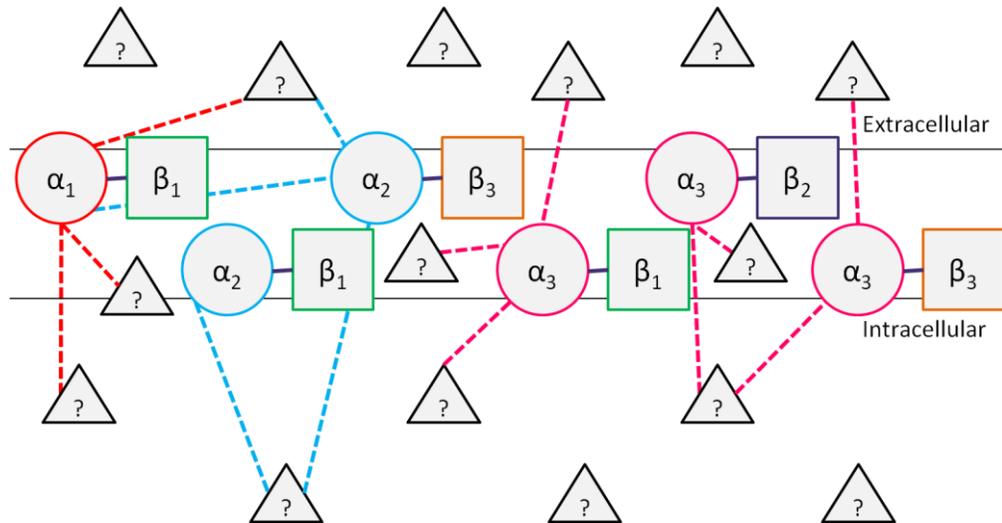
Figure 4.2 Potential protein-protein interactions involving Na$^+$/K$^+$-ATPase

Many unknown proteins may form complexes with Na$^+$/K$^+$-ATPase, or act as protein binding partners. The six heterodimeric forms of Na$^+$/K$^+$-ATPase, known to exist in the myelin membrane, are illustrated above. The dashed lines indicate the potential connections between the various subunit isoforms and other unknown proteins. Protein-protein interactions of the Na$^+$/K$^+$-ATPase alpha and beta subunit isoforms may include cytosolic, extracellular and/or other transmembrane proteins. The indicated associations are provided as examples and do not necessarily represent actual associations of these Na$^+$/K$^+$-ATPase isozymes.

4.3.1 Structural and Functional Properties

Co-immunoprecipitation of the three Na$^+$/K$^+$-ATPase alpha subunit isoforms revealed their involvement in several protein-protein interactions, within the myelin membrane. When analyzed by LC-MS/MS, a total of 13 major proteins were identified, with 100% probability and a minimum of two unique peptides recognized using the Scaffold 4 proteome software. The α_1 and α_2 isoforms were successfully detected within their respective isolated protein complexes; the remaining protein binding partners included additional Na$^+$/K$^+$-ATPase subunit isoforms, myelin specific proteins, and other protein types. The identified binding partners of each alpha isoform are listed in Table 4.3, along with their proposed structural and/or functional roles. Due to the transient nature of certain protein-protein interactions, it is likely that the number of identified

binding partners in myelin has been underestimated. Similarly, the conditions of the co-immunoprecipitation could have potentially disrupted various protein associations. For example, TX-100, although not used in this co-IP, has been reported to disrupt the Na$^+$/K$^+$-ATPase $\alpha_1\beta_2$ isozyme but not $\alpha_1\beta_1$ or $\alpha_2\beta_2$ [31].

Table 4.3 Known physiological functions of binding partners identified by co-immunoprecipitation and mass spectrometry in this study

Protein-protein interactions within the myelin membrane, which involved Na$^+$/K$^+$-ATPase, were identified by mass spectrometry. Each alpha isoform of Na$^+$/K$^+$-ATPase had both unique and shared binding partners. These binding partners are listed, along with their proposed structural and/or functional properties from the literature.

Na$^+$/K$^+$-ATPase α Isoform	Identified Binding Partner	Abbreviation	Structural and Functional Properties	References
α_1	Sodium/potassium-transporting ATPase subunit alpha-3	Na$^+$/K$^+$-ATPase α_3	Ion transport of Na$^+$ and K$^+$; lower affinity for Na$^+$	[24;72]
	Sodium/potassium-transporting ATPase subunit beta-1	Na$^+$/K$^+$-ATPase β_1	Transport and insertion of the α subunit into the plasma membrane; lower affinity for K$^+$	[27;72]
	Serine/arginine repetitive matrix protein 2	SRRM2	RNA splicing factor; binds components of pre-mRNA and the splicesome; plays a role in cell migration	[88]
	Peripheral myelin protein 22	PMP-22	Minor tetraspan membrane protein of PNS myelin; provides structural support and maintains compact myelin; component of membrane junctions with involvement in cell-cell interactions and cell proliferation	[1;89;90]
	Spermatogenesis-associated protein 7	SPAT7	Involved in normal retinal function; possible interactions with chromatin and the initiation of meiotic recombination in testis	[91;92]
	2',3'-cyclic nucleotide 3'-phosphodiesterase	CNP	Forms stable associations with tubulin and anchors microtubules to membranes; regulates tubulin polymerization	[11;93]
	Proteolipid protein 1	PLP1	Major tetraspan membrane protein of CNS myelin; provides structural support and maintains compact myelin;	[12;94]

			possible ionophore	
α₂	Sodium/potassium-transporting ATPase subunit alpha-3	Na$^+$/K$^+$-ATPase α$_3$	Ion transport of Na$^+$ and K$^+$; lower affinity for Na$^+$	[24;72]
	Cullin-associated NEDD8-dissociated protein 1	CAND1	Regulates the assembly and activity of Cullin-RING E3 ubiquitin-ligases; role in protein degradation pathways	[95-97]
α₃	Sodium/potassium-transporting ATPase subunit beta-1	Na$^+$/K$^+$-ATPase β$_1$	Transport and insertion of the α subunit into the plasma membrane; lower affinity for K$^+$	[27;72]
	Brain acid soluble protein 1	BASP1	Co-localizes with raft proteins; possible involvement in cell-cell-interactions; transcription regulator	[98;99]
	Protein MRVI1	MRVI1	Component of cGMP kinase signalling complexes; interacts with inositol 1,4,5-triphosphate receptor 1; mediates nitric oxide dependent inhibition of calcium signalling	[100-103]
	Peripheral myelin protein 22	PMP-22	Minor tetraspan membrane protein of PNS myelin; provides structural support and maintains compact myelin; component of membrane junctions with involvement in cell-cell interactions and cell proliferation	[1;89;90]
	Serine/arginine repetitive matrix protein 2	SRRM2	RNA splicing factor; binds components of pre-mRNA and the splicesome; plays a role in cell migration	[88]
	Proteolipid protein 1	PLP1	Major tetraspan membrane protein of CNS myelin; provides structural support and maintains compact myelin; possible ionophore	[12;94]
	Krueppel-like factor 6	KLF6	Contain zinc finger motifs that bind promoter and enhancer regions; regulate proliferation, differentiation and apoptosis	[104]

Na$^+$/K$^+$-ATPase interacts with an array of proteins within the myelin membrane. Its association with several myelin specific proteins alludes to the possibility of its direct or indirect involvement in the maintenance of myelin. Other binding partners may

provide significant structural and functional roles when associated with Na^+/K^+-ATPase, or vice versa. For example, SRRM2 is a RNA splicing factor which can bind sequence elements on pre-mRNA, as well as components of the splicesome, to form the complexes needed in excision-splicing [88]. The interaction of Na^+/K^+-ATPase with proteins involved in transcriptional processing is logical as the alternative splicing of the alpha and beta isoforms has been implicated in the generation of various Na^+/K^+-ATPase isozymes [3]. KLF6, one of the proteins associated with Na^+/K^+-ATPase α_3, is a transcription factor with proposed roles in promoting apoptosis in Schwann cells, following nerve injury; it appears to increase the susceptibility of a cell to apoptotic stressors [104]. Overexpression of KLF6 has also been linked to increased neurite growth [104]. Another binding partner, CAND1, is known to interact with diverse families of proteins, and consequently participate in a wide range of cellular processes. More specifically, CAND1 regulates Cullin3-mediated E3 ligase activity and suppresses Cullin-RING ubiquitin ligases by sequestering unneddylated Cullin1 [96]. Cullin-RING ubiquitin ligases are critical for targeting cellular proteins for ubiquitin-mediated degradation; hence, CAND1 delays or prevents the destruction of cellular proteins which are targeted for ubiquitination [97]. And lastly, MRVI1, also known as inositol 1,4,5-trisphosphate receptor-associated cGMP kinase substrate, not only interacts with Na^+/K^+-ATPase α_3 but has known associations with inositol 1,4,5-triphosphate receptor 1 [101]. Interestingly, inositol 1,4,5-triphosphate receptor 1 was a predicted functional partner of the α_1 and α_2 isoforms, but not α_3; these protein-protein interactions were revealed using STRING 9.1 (http://string-db.org/) [59]. Refer to Appendix C for more information.

97

Many of the proteins identified as Na^+/K^+-ATPase binding partners are responsible for cell to cell interactions, signal transduction, and the mediation of cellular responses. These proteins were also indicative of the distribution of Na^+/K^+-ATPase between the various microdomains of the myelin membrane. Specifically, PLP1 is a protein marker of the tetraspanin-enriched microdomain of compact myelin [16]; its association with both the α_1 and α_3 isoforms suggests that Na^+/K^+-ATPase also exists within this microdomain. Likewise, the partnership between the Na^+/K^+-ATPase α_3 and BASP1 indicates that this isoform is likely present in the lipid raft microdomains of the myelin membrane, as lipid rafts are found in all cell types and seem to sequester BASP1 in endothelial cells [99]. This result corresponds with the detection of Na^+/K^+-ATPase α_3 in the DRMs of mouse myelin, as demonstrated by Western blot analysis. Na^+/K^+-ATPase has also been identified in kidney caveolae; it forms complexes with caveolin-1 and associates with annexin-2 [58]. Caveolin-1 is also enriched in microdomains of the outer loop of myelin, in the PNS [16]. It is therefore possible that Na^+/K^+-ATPase could interact with caveolin-1 in the myelin membrane, and become localized to these caveolin-1 enriched microdomains.

The co-expression of the Na^+/K^+-ATPase beta subunit and E-cadherin is essential for the formation of tight junctions and desmosomes [105]. Similarly, in renal epithelia, Na^+/K^+-ATPase demonstrates co-localization with E-cadherin but not occludin; as a result, Na^+/K^+-ATPase has been proposed to regulate cellular junctions, including adherens junctions, via ion transport and signal transduction [58]. In particular, Na^+/K^+-ATPase has known involvement in EGFR/Src-Ras-Raf-ERK and PI3K-PDK-Akt cell

signalling pathways [24;58]. Ouabain can initiate the carbonylation of two amino acid

residues in the A-domain of Na^+/K^+-ATPase α_1, which results in stimulation of Src

signalling; however, this process appears to be regulated by reactive oxygen species, as

signalling is prevented by pre-treatment with N-acetyl-L-cysteine [86]. Finally, the

association of CNP with tubulin in brain tissue, and its roles in microtubule assembly and

organization, corresponds with the known interactions of Na^+/K^+-ATPase with

components of the cytoskeleton [93]. The non-random distribution of Na^+/K^+-ATPase

within biological membranes has been attributed to interactions with ankyrin, fodrin,

actin, and uvomorulin; these are cytoskeletal proteins which provoke the assembly of

the cytoskeleton together with Na^+/K^+-ATPase, in addition to mediating the specific

distribution of Na^+/K^+-ATPase within the plasma membrane [70;72].

The ability of Na^+/K^+-ATPase to respond to changes in physiological requirements

largely relies on its interaction with other cellular proteins. As previously mentioned,

reactive oxygen species can initiate signal transduction by Src, via Na^+/K^+-ATPase [86].

The induction of these signalling cascades can trigger a variety of cellular processes,

likely in response to oxidative stress. Similarly, cysteine residues in Na^+/K^+-ATPase

become S-glutathionylated when exposed to oxidized glutathione. S-glutathionylation

results in enzyme inhibition, as glutathione disrupts the ability of Na^+/K^+-ATPase to bind

adenine nucleotides [84]. This inhibition is not observed at high ATP levels, suggesting

that S-glutathionylation regulates Na^+/K^+-ATPase activity in situations of oxidative stress

and ATP depletion, such as in cases of hypoxia [84]. S-glutathionylation of Na^+/K^+-

ATPase can also be reversed by enzymes such as glutaredoxin 1; this deglutathionylation

has been demonstrated in the β_1 subunit following superoxide scavenging by superoxide dismutase [85]. The reversible glutathionylation of Na$^+$/K$^+$-ATPase by glutaredoxin 1 indicates that it is an oxidative regulator of Na$^+$/K$^+$-ATPase activity.

The major isozymes of Na$^+$/K$^+$-ATPase which were identified in this study, by Western blot analysis, included $\alpha_1\beta_1$, $\alpha_2\beta_3$, and $\alpha_3\beta_1$. Of these, both the $\alpha_1\beta_1$ and $\alpha_3\beta_1$ associations were confirmed by mass spectrometry, as the Na$^+$/K$^+$-ATPase β_1 subunit isoform was detectable in both the α_1 and α_3 isoform isolated protein complexes. Interestingly, the α_1 and α_2 isoforms demonstrated the ability to interact with other alpha subunits, specifically the α_3 isoform. This finding was anticipated, as the promiscuous nature of Na$^+$/K$^+$-ATPase alpha and beta subunits permits the assembly of oligomeric complexes. Different alpha isoforms have demonstrated the ability to form stable oligomers, proving the complexity of Na$^+$/K$^+$-ATPase and its molecular heterogeneity; however, the influence of Na$^+$/K$^+$-ATPase supracomplexes on enzymatic function remains unclear [3].

4.4 Na$^+$/K$^+$-ATPase Involvement in Demyelination

4.4.1 Temporal Na$^+$/K$^+$-ATPase Expression

The subunit isoforms of Na$^+$/K$^+$-ATPase not only demonstrate tissue specificity, but also display changes in expression over the stages of development. Of course, Na$^+$/K$^+$-ATPase provides important cellular functions that are required for normal development; therefore, patterns of expression are expected as a consequence of responding to changing physiological requirements. This enzyme has proven critical

during morphogenesis; in embryonic development the sodium-potassium pump collaborates with other sodium exchangers of trophoblasts, to produce the transepithelial flow of water and Na^+ ions necessary for the formation of the fluid or yolk-filled component of what eventually becomes the blastula [72]. In experiments which disrupted Na^+/K^+-ATPase activity during blastocyst formation, pre-natal development ceased.

Hormones, specifically thyroid hormones and glucocorticoids, appear to influence alpha isoform expression at various stages of development [106]. Thyroid hormone stimulates an increase in α_2 and α_3 isoform mRNA levels, whereas glucocorticoids have shown to suppress α_3 isoform gene transcription [70]. Combined, these two types of hormones adjust isoform expression in cardiac tissue; the α_3 isoform is transcribed to the greatest extent during fetal and neonatal development, while the α_2 isoform appears to take over during post-natal development [70]. Regardless, Na^+/K^+-ATPase α_1 remains the predominant alpha isoform at all stages of development. Similar changes in the gene transcription of the alpha isoforms have been observed in other tissues; for example, neuronal Na^+/K^+-ATPase α_3 mRNA and protein levels are significantly reduced with normal aging [36].

Both β_1 and β_2 isoforms are expressed in the CNS of rats at varying stages of post-natal development. The β_1 isoform is expressed equally with the β_2 isoform, in neurons, during the neonatal stage of development; its expression significantly increases after birth, and reaches mature levels as quickly as 6 days later [107]. In contrast, β_2 expression decreases continuously over post-natal development and

eventually becomes undetectable in the fully mature adult rat neurons [107]. Thyroid

hormones appear to have limited or no effect on the transcription of these beta subunit

isoforms [70]. Transcriptional regulation of the beta isoforms is possible; however, it

seems to be primarily driven by immediate physiological needs, rather than major

developmental changes. For example, myoblasts induce beta subunit biosynthesis in

response to increased intracellular Na^+ ion concentrations; as a result, Na^+/K^+-ATPase

alpha subunits can be promptly transported to the plasma membrane to restore ionic

balance [70]. Conversely, in situations where Na^+ entry becomes impaired, the Na^+/K^+-

ATPase isozymes are internalized in order to maintain ionic homeostasis [70].

Regardless of the transcriptional regulation of the Na^+/K^+-ATPase beta subunit,

these isoforms demonstrate developmental changes in their glycosylation. Bear in mind

that all isoforms of the beta subunit are heavily glycosylated, and that each isoform

varies in its number of potential N-glycosylation sequences according to its species of

origin [3;27]. In mammals, the β_1 subunit has three possible extracellular N-glycosylation

sites; on the other hand, the β_2 subunit of chicken, human, and mouse origin have four,

eight, and nine potential N-glycosylation sites, respectively [3;108]. The β_3 subunit is

much more variable between species, and little information is known regarding its

glycosylation. The fully glycosylated forms of each beta subunit are classically identified

as the mature beta subunits, whereas the unglycosylated core protein is, by definition,

the immature form. In this study, variations in expression of each glycosylation state of

the β_1 subunit were noted over post-natal development in mice. Unsurprisingly, the

unglycosylated core of Na^+/K^+-ATPase β_1 demonstrated limited expression in the later

months of development and was the least abundant of all forms. Conversely, the Na$^+$/K$^+$-ATPase β_1 subunits containing either one or two N-glycans were found in the greatest abundance. It is possible that these glycosylated, yet immature, β_1 subunits are held in reserve and become glycosylated when the mature form is needed.

4.4.2 Modifications to Na$^+$/K$^+$-ATPase Expression in a Demyelinating Model

Demyelination, as modelled by ND4 transgenic mice, is characterized by the destruction of the myelin sheath [1]. It is one of the fundamental causes of multiple sclerosis, and contributes significantly to the development of symptoms. This study identified several important dissimilarities in Na$^+$/K$^+$-ATPase expression between healthy CD1 control mouse myelin and transgenic ND4 mouse myelin. Although the patterns of expression for each subunit isoform evaluated using the ND4 model were relatively akin to those observed in the CD1 mouse myelin, when compared side-by-side the individual protein levels at each stage of development were strikingly different; these variations are illustrated in Figure 4.3. Na$^+$/K$^+$-ATPase α_1, α_2, and α_3 levels were 1.5 to 3.2 times higher at 3.00 months of age in the demyelinating model; however, this elevation was followed by a rapid decrease, with levels dropping below those observed in the healthy myelin over varying stages of post-natal development. The β_1 isoform had reduced expression in the ND4 myelin, with the exception of a spike at 9.00 months of age; here, the expression of β_1 was more than 2.5 times that measured in the CD1 myelin. Alternatively, β_2 isoform expression fluctuated throughout development but remained relatively close to levels demonstrated in healthy myelin. And lastly, expression of the β_3

isoform was extremely similar in both CD1 and ND4 myelin until 13.02 months of age,

when levels in ND4 myelin slightly increased.
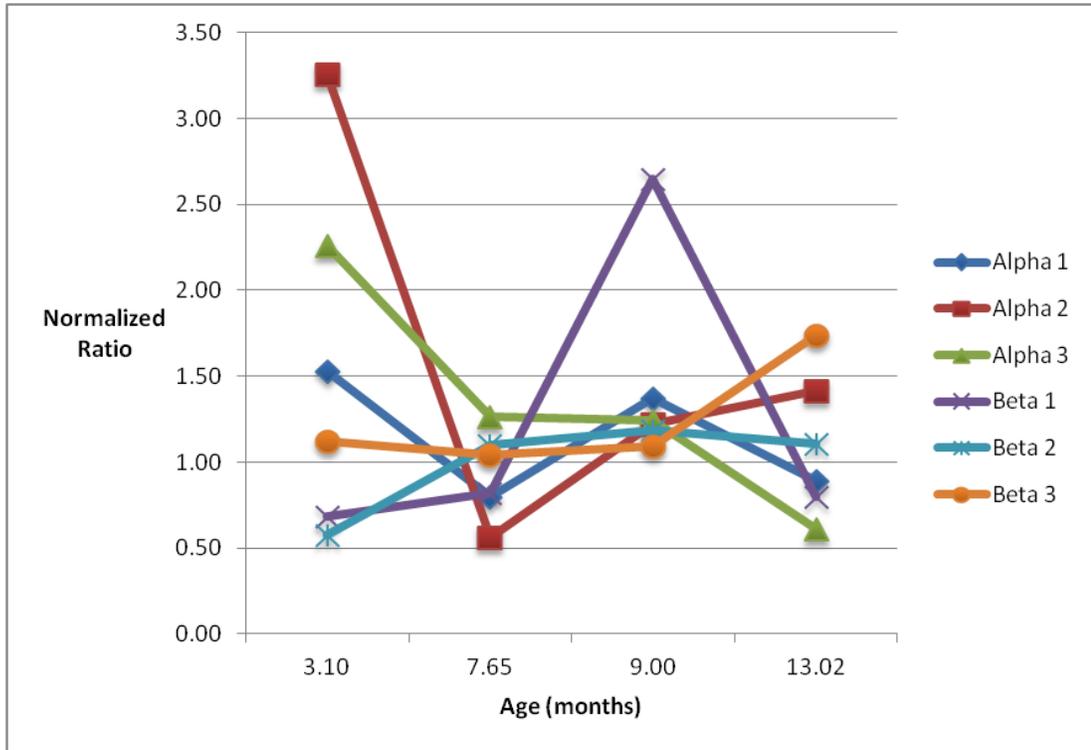
Figure 4.3 Ratio of corrected intensities for each Na$^+$/K$^+$-ATPase subunit isoform in ND4 myelin, relative to CD1 myelin, with aging

Intensity of each Na$^+$/K$^+$-ATPase subunit isoform in ND4 myelin relative to CD1 myelin, ensuring non-saturation and subtracting background. Data corresponds with the Western blots shown in Figure 3.8. Intensity was measured at 3.10, 7.65, 9.00 and 13.02 months of age. Each value was corrected by normalization with a β-actin protein loading control, and the CD1 myelin Na$^+$/K$^+$-ATPase subunit isoforms have relative intensities equal to 1.0.
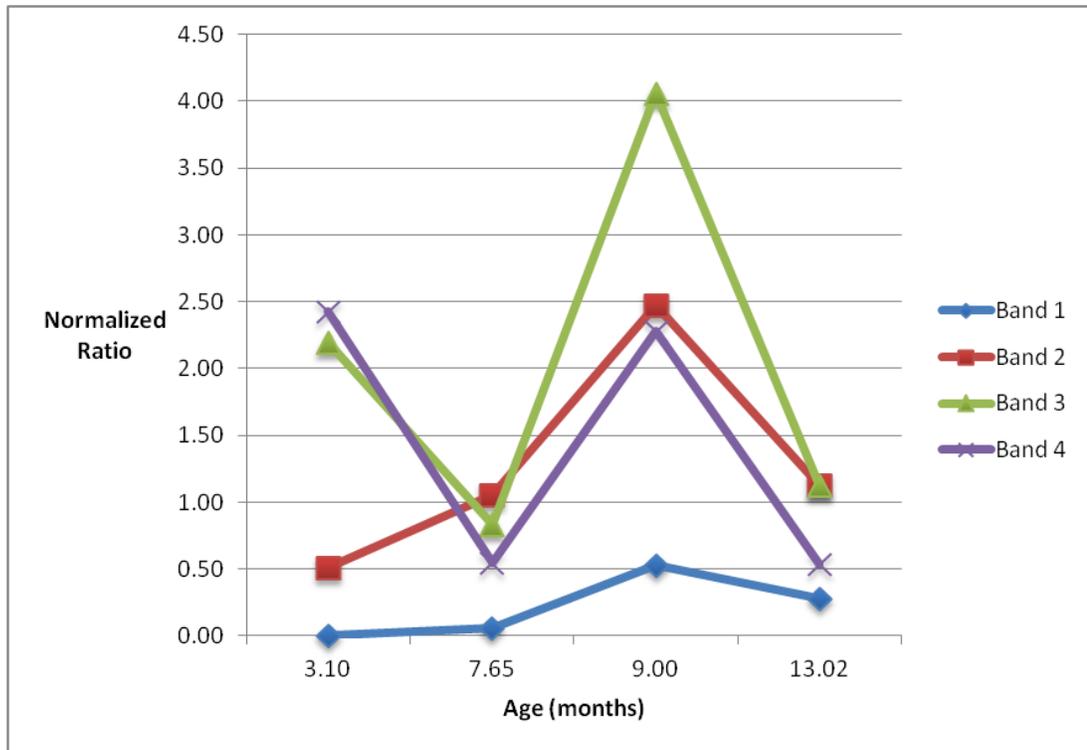
Figure 4.4 Ratio of corrected intensities for each Na$^+$/K$^+$-ATPase β_1 glycosylation state in ND4 myelin, relative to CD1 myelin, with aging

Intensity of each Na$^+$/K$^+$-ATPase β_1 glycosylation state in ND4 myelin relative to CD1 myelin, ensuring non-saturation and subtracting background. Data corresponds with the Western blots shown in Figure 3.8. Bands 1 to 4 represent the highest molecular mass form of Na$^+$/K$^+$-ATPase β_1 (3 N-glycans) to the lowest molecular mass form (core, non-glycosylated), respectively. Intensity was measured at 3.10, 7.65, 9.00 and 13.02 months of age. Each value was corrected by normalization with a β-actin protein loading control, and the CD1 myelin Na$^+$/K$^+$-ATPase β_1 glycosylation states have relative intensities equal to 1.0.

In the mouse model of demyelination, Na$^+$/K$^+$-ATPase β_1 demonstrated noteworthy differences in the expression of its various glycosylation states. These changes in expression are displayed in Figure 4.4. Aside from the mature, fully glycosylated form of Na$^+$/K$^+$-ATPase β_1, expression appears increased in the ND4 myelin at 9.00 months. Very little of the mature β_1 isoform exists in the ND4 myelin; at 9.00 months it reaches maximum expression, yet it remains to be only half as much as the protein levels observed in CD1 myelin. Ultimately, Na$^+$/K$^+$-ATPase β_1 does not reach full maturation in the demyelinating mouse model.

105

Mutated Na^+/K^+-ATPase beta subunits, with altered N-glycosylation sites, are able to maintain enzyme activity as well as their affinity for K^+ ions and their sensitivity to ouabain; however, these non-glycosylated subunits demonstrate an impaired ability to assemble into αβ complexes, and also increase the susceptibility of Na^+/K^+-ATPase to proteolysis [3]. This experimental observation suggests that glycosylation of the beta subunit may contribute to protein folding events necessary for maintaining proper Na^+/K^+-ATPase structures. An absence of the normal N-glycans of the β_1 isoform has also proven to disrupt its role in adherens junctions, by destroying its ability to bind ankyrin and increasing its susceptibility to endocytosis [109]. Respectively, a lack of Na^+/K^+-ATPase β_1 N-glycans has been held responsible for the impairment of mature cell-cell associations [110]. There is substantial evidence supporting the role of β-β interactions between the caveolar Na^+/K^+-ATPase αβ complexes of adjacent cells [58]; thus, glycosylation is not only vital for proper assembly of the alpha and beta Na^+/K^+-ATPase subunits, but is also important for the maintenance of cell-cell communication and adhesion. As interactions between unglycosylated beta subunits and components of adherens junctions and cytoskeletal elements can be more easily disrupted, the limited expression of mature Na^+/K^+-ATPase β_1 could potentially contribute to the formation of demyelinating lesions in ND4 mice. Glycosylation has also been proposed as a therapeutic target for the treatment of viral infections, cancer, and an array of human disorders [111;112]. By understanding the glycosylation changes of the Na^+/K^+-ATPase beta subunits in instances of demyelination, it may be possible to eventually establish methods for the therapeutic manipulation of N-glycans, as a treatment of MS.

Aside from demyelinating disorders, Na^+/K^+-ATPase has also been implicated in other neurological disorders, as it is ubiquitously expressed in the CNS. It has proposed involvement in the pathophysiology of bipolar mood disorder as well as potentially acting as a molecular target of prion infections, such as Creutzfeld-Jakob disease. Firstly, individuals with bipolar mood disorder are known to experience both generalized decreases in CNS glucose metabolism and ATP synthesis; these two processes could easily correspond to decreased, or impaired, Na^+/K^+-ATPase activity [72]. In fact, patients who have experienced digoxin or digitalis neurotoxicity, and animals administered ouabain, exhibit mania-like hyperactivity and symptoms of depression [72;113]. With regards to prion infections, animals injected with ouabain experience similar neurological changes to those observed in various spongiform encephalopathies [72].

4.4.3 Considerations for Evaluating Protein Expression

Evaluating and comparing Na^+/K^+-ATPase protein expression between myelin samples of different genetic backgrounds can present several challenges. To begin with, Na^+/K^+-ATPase expression is highly influenced by circadian rhythms, dehydration or over-hydration, diet, and hormonal changes [36]. Na^+/K^+-ATPase demonstrates diurnal patterns of expression; the neurons of the ventral suprachiasmatic nucleus experience increased enzymatic activity during the day and decreased activity at night [114]. Alternatively, extreme changes in ionic environments, such as those accompanying dehydration or over-hydration, can directly control Na^+/K^+-ATPase activity. It has also been claimed that a diet with increased saturated fatty acid composition, or decreased

107

polyunsaturated fatty acids, is able to inhibit Na^+/K^+-ATPase activity by becoming incorporated into biological membranes [36]. The influence of thyroid hormones and glucocorticoids on Na^+/K^+-ATPase expression was discussed previously; they appear to influence alpha isoform expression at various stages of development [106]. Similarly, estrogens have been implicated in increased Na^+/K^+-ATPase activity; it has been suggested that Na^+/K^+-ATPase becomes activated by estrogen-mediated signal cascades or by estrogen-dependent changes in membrane fluidity [36]. With particular regards to this study, Na^+/K^+-ATPase expression may also vary in ND4 myelin as efforts to remyelinate transpire. Injury to the myelin membrane may trigger changes in Na^+/K^+-ATPase subunit isoform expression. A similar effect has been documented in neurons; Na^+/K^+-ATPase α_3 expression increases post-axonal damage, and remains elevated during the period of regeneration [115]. Unfortunately, in this particular strain of ND4 mice, any remyelination or compensation mechanisms eventually become overwhelmed and lead to death.

Undoubtedly there are many factors, both environmental and endogenous, which can alter Na^+/K^+-ATPase activity and expression in a living animal model. Thus, standardized housing conditions for laboratory animals are imperative for reproducibility and minimizing bias [116]. Housing conditions such as animal feed and water, caging, bedding material, lighting, ventilation, temperature, noise, and sanitation must all be considered in animal research. Likewise, animals need to be euthanized under equivalent conditions, following a standard operating procedure. For the comparison of Na^+/K^+-ATPase expression in myelin isolated from both CD1 and ND4

mice, it was particularly important for all of the animals to be housed and sacrificed identically; samples from each mouse line needed to be euthanized at an equivalent age. Nonetheless, all efforts to maintain comparable standards of living can still not account for the fact that two genetically distinct lines (control and transgenic) of mice were compared; therefore, it is possible that innate differences may exist which could alter Na^+/K^+-ATPase activity and expression.

Finally, all densitometric data obtained in this study, by chemiluminescent or fluorescent detection, was normalized using β-actin. This housekeeping protein is one of many commonly used protein loading controls; others include β-tubulin, glyceraldehyde 3-phosphate dehydrogenase, cyclophillin, etc. [60;62]. As these proteins perform housekeeping roles, they are typically constitutively expressed. The use of an internal control takes technical artifacts, like pipetting errors during gel loading and inconsistent protein transfer to blotting membranes, into account [60]. Normalization using these controls can be easily applied to data, pending that all replicates destined for comparison contain the control protein band [61]. For all densitometric measurements of both samples and controls, non-saturation was ensured when measuring signal intensities, in addition to performing background subtraction. Unfortunately, variability in the expression of housekeeping proteins in certain tissues and disease states could undermine the validity of β-actin as an internal control. Specifically regarding the ND4 transgenic mice used in this study, by 10 months of age total myelin protein content can be reduced to as little as 17% of that found in normal healthy mice [23]. It is therefore difficult to imagine that when the total myelin protein content is disrupted to such an

extent, that β-actin levels remain normal. As a result, innovative approaches for the

accurate quantification of protein expression using densitometric analysis may need to

be developed.

Chapter 5 – Conclusions and Future Studies

In 1981, the question of whether or not Na^+/K^+-ATPase is a myelin-associated enzyme was put forth by Reiss *et al*. [117]. They found that Na^+/K^+-ATPase activity in purified myelin was significantly more than expected as a result of microsomal contamination. Other studies using electron microscopic cytochemistry, in addition to other subcellular fractionation techniques, were also suggestive of an association between Na^+/K^+-ATPase and myelin [118]. Now, over 30 years later, this study aimed to answer that original question by comprehensively examining the expression of myelin-associated Na^+/K^+-ATPase, and its individual subunit isoforms, using a mouse model. Mouse myelin closely resembles human myelin; in fact, they share 308 common proteins [119]. As a result, the study of myelin proteins using a mouse model can provide relevant information pertaining to human demyelinating diseases.

It was discovered that Na^+/K^+-ATPase α_1, α_2, and α_3, as well as the complementary β_1, β_2, and β_3 subunits, are expressed in mouse myelin prepared by both sucrose and Percoll gradient isolation methods. These six subunit isoforms represent all known forms of Na^+/K^+-ATPase in the CNS; they are uniquely co-expressed within the myelin sheath, when compared with neurons, astrocytes and oligodendrocytes [34;75;78-81]. Similarly, six different isozymes of Na^+/K^+-ATPase were identified in myelin; these included $\alpha_1\beta_1$, $\alpha_2\beta_1$, $\alpha_2\beta_3$, $\alpha_3\beta_1$, $\alpha_3\beta_2$, and $\alpha_3\beta_3$. The most abundant isozymes were $\alpha_1\beta_1$, $\alpha_2\beta_3$, and $\alpha_3\beta_1$. All six $\alpha\beta$ complexes were also distinct when compared with neurons and glia; more specifically, $\alpha_2\beta_3$ and $\alpha_3\beta_3$ are unique to

myelin, whereas $\alpha_1\beta_2$, $\alpha_1\beta_3$, and $\alpha_2\beta_2$ are known to exist in neurons and/or glia but were not identified in the myelin membrane [72].

Several protein-protein interactions involving Na$^+$/K$^+$-ATPase were revealed using mouse myelin. In particular, the various alpha isoforms demonstrated interactions with other Na$^+$/K$^+$-ATPase alpha and beta subunit isoforms, in addition to associating with certain myelin-specific proteins and other protein types. These protein binding partners of Na$^+$/K$^+$-ATPase have known cellular functions, including RNA splicing, involvement in cell-cell migration and adhesion, the mediation of cytoskeletal interactions, and the regulation of protein degradation and apoptosis. Furthermore, several of these binding partners are known to localize in adherens junctions, tight junctions and caveolae. Na$^+$/K$^+$-ATPase also demonstrated associations with protein markers of lipid raft and tetraspanin-enriched microdomains [32;58;73;74]. The results of this study suggest that Na$^+$/K$^+$-ATPase likely localizes in the corresponding microdomains of the myelin membrane.

When the temporal expression of each subunit isoform of Na$^+$/K$^+$-ATPase was examined by Western blot analysis, this protein displayed noticeable changes over the course of normal development. This result corresponds with the known variations in Na$^+$/K$^+$-ATPase expression and activity observed in other tissues and cell types; these fluctuations occur in response to physiological demands, as well as normal aging processes [36;70]. The Na$^+$/K$^+$-ATPase subunit isoforms of the myelin membrane also showed differences in expression between healthy and diseased myelin. The divergence in the expression levels of the Na$^+$/K$^+$-ATPase subunit isoforms, in ND4 mouse myelin,

may be a contributing factor to the demyelinating processes which occur in these transgenic mice; alternatively, it could be consequence of other biochemical changes which take place during demyelination. Regardless of cause or effect, ND4 myelin exhibited severe impairment in Na^+/K^+-ATPase β_1 subunit maturation. Expression of its mature, fully glycosylated form was drastically reduced over the post-natal development of ND4 mice; at maximum expression, the diseased myelin only contained approxmately 50% as much of the mature Na^+/K^+-ATPase β_1, as measured in the healthy CD1 mouse myelin.

Ultimately, the experimental evidence suggests that Na^+/K^+-ATPase provides significant structural and functional roles within the myelin membrane. The co-expression of all six CNS isoforms, in addition to several different heterodimeric forms, implies that this enzyme is essential to the normal physiology of the myelin sheath. It is likely that each isoform and isozyme confers distinctive properties required to meet the unique physiological demands of the myelin membrane. Likewise, the observed disruption of Na^+/K^+-ATPase expression in ND4 mice may indicate Na^+/K^+-ATPase involvement in demyelinating processes.

In the future, differences in Na^+/K^+-ATPase expression between various control and demyelinating animal models should be further evaluated. By examining myelin from a greater range of developmental timepoints, in addition to performing more replicates and using different models of demyelination, the significance of the changes in Na^+/K^+-ATPase subunit isoform expression will be established. Similarly, an investigation pursuing the effects of beta subunit N-glycosylation on demyelination

would be worthwhile. As changes in the N-glycans of Na$^+$/K$^+$-ATPase β_1 have been noted

between healthy and diseased myelin, it would be beneficial to test whether or not

manipulation of these carbohydrate constituents can trigger a diseased state

reminiscent of demyelination, or specifically multiple sclerosis. Alternatively,

manipulation of the N-glycans or N-glycosylation sequences of the Na$^+$/K$^+$-ATPase beta

subunits could offer therapeutic benefit in the treatment of demyelination.

Glycosylation has been previously proposed in the literature as a medicinal target for

the treatment of a variety of human disorders [111;112].

Lastly, the characterization of Na$^+$/K$^+$-ATPase in the myelin membrane needs to

continue with the development of an effective method for evaluating its enzymatic

activity. To date, typical enzymatic assays for Na$^+$/K$^+$-ATPase, such as the *p*-nitrophenyl

phosphatase activity assay, have not been validated for measuring Na$^+$/K$^+$-ATPase

activity in preparations of myelin vesicles. A preliminary investigation into the enzymatic

activity of Na$^+$/K$^+$-ATPase, in the myelin membrane, is described in Appendix E. Na$^+$/K$^+$-

ATPase inhibitors, aside from ouabain, need to be identified such that enzymatic activity

can be accurately measured. Recall that although Na$^+$/K$^+$-ATPase is generally inhibited

by cardiac glycosides, Na$^+$/K$^+$-ATPase α_2 and α_3 are ouabain-sensitive, whereas the α_1

isoform is ouabain-resistant [75]. Therefore, the measurement of the total Na$^+$/K$^+$-

ATPase activity, as well as the activity of each individual catalytic alpha subunit isoform,

will require the use of several different inhibitors.

References

1. M.H. Ross & W. Pawlina, Histology: A Text and Atlas: With Correlated Cell and Molecular Biology, Lippincott Wiliams & Wilkins, Baltimore, MD, 2006.

2. J.A. Black, J. Newcombe & S.G. Waxman, Astrocytes within multiple sclerosis lesions upregulate sodium channel Nav1.5, Brain 133 (2010) 835-846.

3. G. Blanco & R.W. Mercer, Isozymes of the Na+/K+-ATPase: heterogeneity in structure, diversity in function, Am.J.Physiol. 275 (1998) F633-50.

4. C.D. Klaassen & J.B. Watkins, Casarett & Doull's Essentials of Toxicology, McGraw-Hill Medical, New York, 2010.

5. M. Simons & J. Trotter, Wrapping it up: the cell biology of myelination, Curr.Opin.Neurobiol. 17 (2007) 533-540.

6. N. Baumann & D. Pham-Dinh, Biology of Oligodendrocyte and Myelin in the Mammalian Central Nervous System, Physiol.Rev. 81 (2001) 871-927.

7. J. Lieff, Searching for the Mind with Jon Lieff, M.D.: Myelin Variations, Accessed July 5, 2014 (2014) <http://jonlieffmd.com/blog/new-myelin-code-adds-to-brain-complexity>.

8. S.A. Goldman & J. Osorio, So many progenitors, so little myelin. Nat.Neurosci. 17 (2014) 483-485.

9. S. Mitew, C.M. Hay, H. Peckham, J. Xiao, M. Koenning & B. Emery, Mechanisms regulating the development of oligodendrocytes and central nervous system myelin, Neuroscience 276 (2013) 29-47.

10. W. Stoffel & A. Bosio, Myelin glycolipids and their functions, Curr.Opin.Neurobiol. 7 (1997) 654-661.

11. O. Jahn, S. Tenzer & H. Werner, Myelin Proteomics: Molecular Anatomy of an Insulating Sheath, Mol.Neurobiol. 40 (2009) 55-72.

12. T.I. Gudz, T.E. Schneider, T.A. Haas & W.B. Macklin, Myelin proteolipid protein forms a complex with integrins and may participate in integrin receptor signaling in oligodendrocytes, Neuroscience 22 (2002) 7398-7407.

13. S.J. Singer & G.L. Nicolson, The fluid mosaic model of the structure of cell membranes, Science 175 (1972) 720-731.

14. P. Sengupta, B. Baird & D. Holowka, Lipid rafts, fluid/fluid phase separation, and their relevance to plasma membrane structure and function, Semin.Cell Dev.Biol. 18 (2007) 583-590.

15. A.T. Hammond, F.A. Heberle, T. Baumgart, D. Holowka, B. Baird & G.W. Feigenson, Crosslinking a lipid raft component triggers liquid ordered-- liquid disordered phase separation in model plasma membranes. Proc.Natl.Acad.Sci.U.S.A. 102 (2005) 6320-6325.

16. L.S. DeBruin & G. Harauz, White Matter Rafting—Membrane Microdomains in Myelin, Neurochem.Res. 32 (2007) 213-228.

17. Multiple Sclerosis Society of Canada, Types of MS, Accessed April 21, 2014 (2013) <http://mssociety.ca/en/information/types.htm#rrms_cis>.

18. Mayo Clinic, Multiple Sclerosis: Types, Accessed April 21, 2014 (2013) <http://www.mayoclinic.org/multiple-sclerosis/types.html>.

19. M. Rodriguez, Advances in Multiple Sclerosis and Experimental Demyelinating Diseases, Springer, Berlin, 2008.

20. M. Bradl & C. Linington, Animal Models of Demyelination, Brain Pathol. 6 (1996) 303-311.

21. E. Lavi & C.S. Constantinescu, Experimental Models of Multiple Sclerosis, Springer, New York, NY, 2005.

22. F.G. Mastronardi, C.A. Ackerley, L. Arsenault, B.I. Roots & M.A. Moscarello, Demyelination in a Transgenic Mouse - A Model for Multiple-Sclerosis, J.Neurosci.Res. 36 (1993) 315-324.

23. M. Futai, Y. Wada & J.H. Kaplan, Handbook of ATPases, Wiley, Weinheim, 2004.

24. A. Zouzoulas, A.G. Therien, R. Scanzano, C.M. Deber & R. Blostein, Modulation of Na, K-ATPase by the γ subunit, J.Biol.Chem. 278 (2003) 40437-40441.

25. P. Beguin, U. Hasler, A. Beggah, J.D. Horisberger & K. Geering, Membrane integration of Na,K-ATPase alpha-subunits and beta-subunit assembly, J.Biol.Chem. 273 (1998) 24921-24931.

26. J.H. Kaplan, Biochemistry of Na, K-ATPase, Annu.Rev.Biochem. 71 (2002) 511-535.

27. P.L. Jorgensen, K.O. Håkansson & S.J.D. Karlish, Structure and mechanism of Na, K-ATPase: functional sites and their interactions, Annu.Rev.Physiol. 65 (2003) 817-849.

28. A. Mobasheri, E. Trujillo, M.F. Arteaga & P. Martin-Vasallo, Na+, K+-ATPase Subunit Composition in a Human Chondrocyte Cell Line; Evidence for the Presence of alpha 1, alpha 3, beta 1, beta 2 and beta 3 Isoforms, Int. J. Mol. Sci. 13 (2012) 5019-5034.

29. K.B. Axelsen & M.G. Palmgren, Evolution of substrate specificities in the P-type ATPase superfamily, J.Mol.Evol. 46 (1998) 84-101.

30. E. Tokhtaeva, R.J. Clifford, J.H. Kaplan, G. Sachs & O. Vagin, Subunit isoform selectivity in assembly of Na,K-ATPase alpha-beta heterodimers, J.Biol.Chem. 287 (2012) 26115-26125.

31. L. Reinhard, H. Tidow, M.J. Clausen & P. Nissen, Na , K -ATPase as a docking station: protein–protein complexes of the Na , K -ATPase, Cell Mol. Life Sci. 70 (2013) 205-222.

32. J.P. Morth, B.P. Pedersen, M.J. Buch-Pedersen, J.P. Andersen, B. Vilsen, M.G. Palmgren & P. Nissen, A structural overview of the plasma membrane Na+, K+-ATPase and H+-ATPase ion pumps, Nat. Rev. Mol. Cell Bio. 12 (2011) 60-70.

33. P. Martin-Vasallo, W. Dackowski, J.R. Emanuel & R. Levenson, Identification of a putative isoform of the Na, K-ATPase beta subunit. Primary structure and tissue-specific expression. J.Biol.Chem. 264 (1989) 4613-4618.

34. H.X. Pu, F. Cluzeaud, R. Goldshleger, S.J.D. Karlish, N. Farman & R. Blostein, Functional role and immunocytochemical localization of the γa and γb forms of the Na, K-ATPase γ subunit, J.Biol.Chem. 276 (2001) 20370-20378.

35. M.G. Harrington, A.N. Fonteh, X. Arakaki, R.P. Cowan, L.E. Ecke, H. Foster, A.F. Hühmer & R.G. Biringer, Capillary Endothelial Na +/K+-ATPase Transporter Homeostasis and a New Theory for Migraine Pathophysiology, Headache 50 (2010) 459-478.

36. R.F. Rakowski, D.C. Gadsby & P. De Weer, Voltage dependence of the Na/K pump, J.Membr.Biol. 155 (1997) 105-112.

37. S.P. Gupta, Quantitative Structure-Activity Relationship Studies on Na+,K+-ATPase Inhibitors, Chem.Rev. 112 (2012) 3171-3192.

38. E.E. Benarroch, Na+,K+ -ATPase Functions in the nervous system and involvement in neurologic disease, Neurology 76 (2011) 287-293.

39. N. Glorioso, F. Filigheddu, C. Troffa, A. Soro, P.P. Parpaglia, A. Tsikoudakis, R.H. Myers, V.L.M. Herrera & N. Ruiz-Opazo, Interaction of alpha(1)-Na,K-ATPase and Na,K,2Cl-cotransporter genes in human essential hypertension, Hypertension 38 (2001) 204-209.

40. T.P. Huynh, V. Mah, V.B. Sampson, D. Chia, M.C. Fishbein, S. Horvath, M. Alavi, D.C. Wu, J. Harper, T. Sarafian, S.M. Dubinett, S.A. Langhans, L. Goodglick & A.K. Rajasekaran, Na,K-ATPase is a target of cigarette smoke and reduced expression predicts poor patient outcome of smokers with lung cancer, Am.J.Physiol.-Lung Cell.Mol.Physiol. 302 (2012) L1150-L1158.

41. S. Vucic, D. Burke & M.C. Kiernan, Fatigue in multiple sclerosis: Mechanisms and management, Clin. Neurophysiol. 121 (2010) 809-817.

42. X. Wu & H. Koiwa, One-step casting of Laemmli discontinued sodium dodecyl sulfate-polyacrylamide gel electrophoresis gel, Anal.Biochem. 421 (2012) 347-349.

43. D. Koticha, M. Mabuchi & M. Carelli, Transfer membrane improves fluorescent detection of proteins, Biosci. Tech. 31 (2006) 18.

44. J.C. Gingrich, D.R. Davis & Q. Nguyen, Multiplex detection and quantitation of proteins on western blots using fluorescent probes, Biotechniques 29 (2000) 636-642.

45. S.C. Masters, Protein-Protein Interactions: Co-Immunoprecipitation from Transfected Cells, Humana Press, Totowa, NJ, 2004.

46. R.J.F. Branco, A.M.G.C. Dias & A.C.A. Roque, Understanding the molecular recognition between antibody fragments and protein A biomimetic ligand, J. Chromatogr. 1244 (2012) 106-115.

47. G. Chen & B.N. Pramanik, LC- MS for protein characterization: current capabilities and future trends, Expert Rev. Proteomic 5 (2008) 435-444.

48. W.T. Norton, Isolation of myelin from nerve tissue, Meth. Enzymol. 31 (1974) 435-444.

49. T. Kristian, Isolation of mitochondria from the CNS, Curr. Protoc. Neurosci. 52 (2010) 7.22.1-7.22.12.

50. P.R. Dunkley, P.E. Jarvie, J.W. Heath, G.J. Kidd & J.A.P. Rostas, A rapid method for isolation of synaptosomes on Percoll gradients, Brain Res. 372 (1986) 115-129.

51. L.S. DeBruin, J.D. Haines, L.A. Wellhauser, G. Radeva, V. Schonmann, D. Bienzle & G. Harauz, Developmental partitioning of myelin basic protein into membrane microdomains, J.Neurosci.Res. 80 (2005) 211-225.

52. L.S. DeBruin, J.D. Haines, D. Bienzle & G. Harauz, Partitioning of myelin basic protein into membrane microdomains in a spontaneously demyelinating mouse model for multiple sclerosis, Biochem. Cell Biol. 84 (2006) 993-1005.

53. R.C. Switzer, C.R. Merril & S. Shifrin, A highly sensitive silver stain for detecting proteins and peptides in polyacrylamide gels, Anal.Biochem. 98 (1979) 231-237.

54. A. Keller, A. Nesvizhskii, E. Kolker & R. Aebersold, Empirical statistical model to estimate the accuracy of peptide identifications made by MS/MS and database search. Anal.Chem. 74, 20 (2002) 5383-5392.

55. A. Nesvizhskii, A. Keller, E. Kolker & R. Aebersold, A statistical model for identifying proteins by tandem mass spectrometry. Anal.Chem. 75, 17 (2003) 4646-4658.

56. T.S. Elliott, F.M. Townsley, A. Bianco, R.J. Ernst, A. Sachdeva, S.J. Elssser, L. Davis, K. Lang, R. Pisa, S. Greiss, K.S. Lilley & J.W. Chin, Proteome labeling and protein identification in specific tissues and at specific developmental stages in an animal, Nat.Biotechnol. 32, 5 (2014) 465-472.

57. A.J. Laude & I.A. Prior, Plasma membrane microdomains: organization, function and trafficking, Mol.Membr.Biol. 21 (2004) 193-205.

58. L.J. Liu, A.V. Ivanov, M.E. Gable, F. Jolivel, G.A. Morrill & A. Askari, Comparative Properties of Caveolar and Noncaveolar Preparations of Kidney Na+/K+- ATPase, Biochemistry 50 (2011) 8664-8673.

59. L.J. Jensen, M. Kuhn, M. Stark, S. Chaffron, C. Creevey, J. Muller, T. Doerks, P. Julien, A. Roth, M. Simonovic, P. Bork & C. von Mering, STRING 8--a global view on proteins and their functional interactions in 630 organisms, Nucleic Acids Res. 37 (2009) D412-6.

60. S.C. Taylor, T. Berkelman, G. Yadav & M. Hammond, A Defined Methodology for Reliable Quantification of Western Blot Data, Mol.Biotechnol. 55 (2013) 217-226.

61. A. Degasperi, M.R. Birtwistle, N. Volinsky, J. Rauch, W. Kolch & B.N. Kholodenko, Evaluating strategies to normalise biological replicates of Western blot data, Plos One 9 (2014) e87293.

62. L. Wu, X. Hu, H. Tang, Z. Han & Y. Chen, Valid application of western blotting, Mol.Biol.Rep. 41 (2014) 3517-3520.

63. Conn, P.M. Cell Culture. P. M. Conn(ed). San Diego, California:Academic Press (1990).

64. Graham, J.M. & D. Rickwood. Subcellular Fractionation: A Practical Approach. Oxford: Oxford University Press (1997).

65. G.J. Siegel, B.W. Agranoff, R.W. Albers, S.K. Fisher & M.D. Uhler, Basic Neurochemistry: Molecular, Cellular and Medical Aspects., Lippincott-Raven, Philadelphia, 1999.

66. W.T. Norton & S.E. Poduslo, Myelination in the Rat Brain: Method of Myelin Isolation 1, J.Neurochem. 21 (1973) 749-757.

67. P.R. Dunkley, P.E. Jarvie & P.J. Robinson, A rapid Percoll gradient procedure for preparation of synaptosomes, Nat. Protoc. 3 (2008) 1718-1728.

68. Academic OneFile, Phosphatase, protease inhibitors, Biosci. Tech. 32 (2007) 21.

69. B.M. Morrison, Y. Lee & J.D. Rothstein, Oligodendroglia: metabolic supporters of axons, Trends Cell Biol. 23 (2013) 644-651.

70. Lee, A.G. Biomembranes. London, England: Jai Press Ltd. (1996).

71. G. Schmalzing, K. Ruhl & S.M. Gloor, Isoform-Specific Interactions of Na,K-ATPase Subunits are Mediated Via Extracellular Domains and Carbohydrates, Proc.Natl.Acad.Sci.U.S.A. 94 (1997) 1136-1141.

72. A. Mobasheri, J. Avila, I. Cózar-Castellano, M. Brownleader, M. Trevan, M. Francis, J. Lamb & P. Martín-Vasallo, Na , K -ATPase isozyme diversity; comparative biochemistry and physiological implications of novel functional interactions, Biosci.Rep. 20 (2000) 51-91.

73. W. Souza, L. Barbosa, L. Liu, W. Araujo, J. de-Freitas-Junior, N. Fortunato-Miranda, C. Fontes & J. Morgado-Díaz, Ouabain-Induced Alterations of the Apical Junctional Complex Involve α1 and β1 Na,K-ATPase Downregulation and ERK1/2 Activation Independent of Caveolae in Colorectal Cancer Cells, J. Membrane Biol. 247 (2014) 23-33.

74. O. Vagin, L.A. Dada, E. Tokhtaeva & G. Sachs, The Na-K- ATPase alpha1 beta1 heterodimer as a cell adhesion molecule in epithelia, Am. J. Physiol.-Cell Ph. 302 (2012) C1271-C1281.

75. S. Alberti, E.A. Gregorio, C.T. Spadella & C. Cojocel, Localization and irregular distribution of Na,K-ATPase in myelin sheath from rat sciatic nerve, Tissue Cell 39 (2007) 195-201.

76. E. Cirri, A. Katz, N.K. Mishra, T. Belogus, Y. Lifshitz, H. Garty, S.J.D. Karlish & H. Apell, Phospholemman (FXYD1) raises the affinity of the human α1β1 isoform of Na,K- ATPase for Na ions, Biochemistry 50 (2011) 3736-3748.

77. M. Kristensen & C. Juel, Na , K -ATPase Na affinity in rat skeletal muscle fiber types, J.Membr.Biol. 234 (2010) 35-45.

78. J.H. Peng, Y. Zeng & J.C. Parker, Highly Ouabain-Sensitive α3 Isoform of Na , K -ATPase in Human Brain, J.Neurochem. 58 (1992) 1180-1183.

79. P. Martín-Vasallo, R.K. Wetzel, L.M. García-Segura, E. Molina-Holgado, E. Arystarkhova & K.J. Sweadner, Oligodendrocytes in brain and optic nerve express the β3 subunit isoform of Na, K-ATPase, Glia 31 (2000) 206-218.

80. P.E. Knapp, O.S. Itkis & M. Mata, Neuronal interaction determines the expression of the α-2 isoform of Na, K-ATPase in oligodendrocytes, Dev.Brain Res. 125 (2000) 89-97.

81. K. Taguchi, H. Kumanogoh, S. Nakamura & S. Maekawa, Ouabain-induced isoform-specific localization change of the Na, K-ATPase α subunit in the synaptic plasma membrane of rat brain, Neurosci.Lett. 413 (2007) 42-45.

82. I.M.A. Nooren & J.M. Thornton, Diversity of protein-protein interactions, EMBO J. 22 (2003) 3486-3492.

83. S. Jones & J.M. Thornton, Principles of protein-protein interactions, Proc.Natl.Acad.Sci.U.S.A. 93 (1996) 13-20.

84. I.Y. Petrushanko, S. Yakushev, V.A. Mitkevich, Y.V. Kamanina, R.H. Ziganshin, X. Meng, A.A. Anashkina, A. Makhro, O.D. Lopina, M. Gassmann, A.A. Makarov & A. Bogdanova, S-glutathionylation of the Na,K-ATPase catalytic alpha subunit is a determinant of the enzyme redox sensitivity, J.Biol.Chem. 287 (2012) 32195-32205.

85. G.A. Figtree, C.C. Liu, S. Bibert, E.J. Hamilton, A. Garcia, C.N. White, K.K.M. Chia, F. Cornelius, K. Geering & H.H. Rasmussen, Reversible oxidative modification: a key mechanism of Na+-K+ pump regulation, Circ Res. 105 (2009) 185-193.

86. Y. Yan, A.P. Shapiro, S. Haller, V. Katragadda, L. Liu, J. Tian, V. Basrur, D. Malhotra, Z.J. Xie, N.G. Abraham, J.I. Shapiro & J. Liu, Involvement of reactive oxygen species in a feed-forward mechanism of Na/K-ATPase-mediated signaling transduction, J.Biol.Chem. 288 (2013) 34249-34258.

87. S.P. Barwe, A. Skay, R. Mcspadden, T.P. Huynh, S.A. Langhans, L.J. Inge & A.K. Rajasekaran, Na,K- ATPase β-subunit cis homo-oligomerization is necessary for epithelial lumen formation in mammalian cells, J.Cell.Sci. 125 (2012) 5711-5720.

88. L.A. Shehadeh, K. Yu, L. Wang, A. Guevara, C. Singer, J. Vance & S. Papapetropoulos, SRRM2, a Potential Blood Biomarker Revealing High Alternative Splicing in Parkinson's Disease, Plos One 5 (2010) e9104.

89. F. Taioli, I. Cabrini, T. Cavallaro, M. Acler & G.M. Fabrizi, Inherited demyelinating neuropathies with micromutations of peripheral myelin protein 22 gene, Brain 134 (2011) 608-617.

90. L. Notterpek, K.J. Roux, S.A. Amici, A. Yazdanpour, C. Rahner & B.S. Fletcher, Peripheral Myelin Protein 22 is a Constituent of Intercellular Junctions in Epithelia, Proc.Natl.Acad.Sci.U.S.A. 98 (2001) 14404-14409.

91. H. Wang, A.I. den Hollander, Y. Moayedi, A. Abulimiti, Y. Li, R.W.J. Collin, C.B. Hoyng, I. Lopez, M. Bray, R.A. Lewis, J.R. Lupski, G. Mardon, R.K. Koenekoop & R. Chen, Mutations in SPATA7 Cause Leber Congenital Amaurosis and Juvenile Retinitis Pigmentosa, Am. J. Hum. Genet. 84 (2009) 380-387.

92. X. Zhang, H. Liu, Y. Zhang, Y. Qiao, S. Miao, L. Wang, J. Zhang, S. Zong & S.S. Koide, A novel gene, RSD-3/HSD-3.1, encodes a meiotic-related protein expressed in rat and human testis, J.Mol.Med. 81 (2003) 380-387.

93. M. Bifulco, C. Laezza, S. Stingo & J. Wolff, 2',3'- Cyclic Nucleotide 3'-Phosphodiesterase: A Membrane-Bound, Microtubule-Associated Protein and Membrane Anchor for Tubulin, Proc.Natl.Acad.Sci.U.S.A. 99 (2002) 1807-1812.

94. Y. Miyamoto, T. Torii, A. Tanoue & J. Yamauchi, Pelizaeus–Merzbacher disease-associated proteolipid protein 1 inhibits oligodendrocyte precursor cell differentiation via extracellular-signal regulated kinase signaling, Biochem.Biophys.Res.Commun. 424 (2012) 262-268.

95. X. Mao, N. Gluck, B. Chen, P. Starokadomskyy, H. Li, G.N. Maine & E. Burstein, COMMD1 (copper metabolism MURR1 domain-containing protein 1) regulates Cullin RING ligases by preventing CAND1 (Cullin-associated Nedd8-dissociated protein 1) binding, J.Biol.Chem. 286 (2011) 32355-32365.

96. S.H. Kim, H. Kim, S. Kim & J. Yim, Drosophila Cand1 regulates Cullin3-dependent E3 ligases by affecting the neddylation of Cullin3 and by controlling the stability of Cullin3 and adaptor protein, Dev.Biol. 346 (2010) 247-257.

97. J. Merlet, J. Burger, J.E. Gomes & L. Pintard, Regulation of cullin-RING E3 ubiquitin-ligases by neddylation and dimerization. Cell. Mol. Life Sci. 66 (2009) 1924-1938.

98. B. Carpenter, K.J. Hill, M. Charalambous, K.J. Wagner, D. Lahiri, D.I. James, J.S. Andersen, V. Schumacher, B. Royer-pokora, M. Mann, A. Ward & S.G.E. Roberts, BASP1 is a transcriptional cosuppressor for the Wilms' tumor suppressor protein WT1, Mol.Cell.Biol. 24 (2004) 537-549.

99. R.R. Sprenger, R.D. Fontijn, J. Van Marle, H. Pannekoek & A.J.G. Horrevoets, Spatial segregation of transport and signalling functions between human endothelial caveolae and lipid raft proteomes, Biochem.J. 400 (2006) 401-410.

100. A. Geiselhöringer, M. Werner, K. Sigl, P. Smital, R. Wörner, L. Acheo, J. Stieber, P. Weinmeister, R. Feil, S. Feil, J. Wegener, F. Hofmann & J. Schlossmann, IRAG is essential for relaxation of receptor-triggered smooth muscle contraction by cGMP kinase, EMBO J. 23 (2004) 4222-4231.

101. M. Antl, M. Von Brühl, C. Eiglsperger, M. Werner, I. Konrad, T. Kocher, M. Wilm, F. Hofmann, S. Massberg & J. Schlossmann, IRAG mediates NO/cGMP-dependent inhibition of platelet aggregation and thrombus formation, Blood 109 (2007) 552-559.

102. J.D. Shaughnessy, D.A. Largaespada, E. Tian, C.F. Fletcher, B.C. Cho, P. Vyas, N.A. Jenkins & N.G. Copeland, Mrvi1, a common MRV integration site in BXH2 myeloid leukemias, encodes a protein with homology to a lymphoid-restricted membrane protein Jaw1, Oncogene 18 (1999) 2069-2084.

103. P. Carninci, The Transcriptional Landscape of the Mammalian Genome, Science 309 (2005) 1559-1563.

104. T. Gui, Y. Wang, L. Zhang, W. Wang, H. Zhu & W. Ding, Krüppel-Like Factor 6 Rendered Rat Schwann Cell More Sensitive to Apoptosis via Upregulating FAS Expression, Plos One 8 (2013) e82449.

105. S.A. Rajasekaran, L.G. Palmer, S.Y. Moon, A. Peralta-Soler, G.L. Apodaca, J.F. Harper, Y. Zheng & A.K. Rajasekaran, Na,K- ATPase activity is required for formation of tight junctions, desmosomes, and induction of polarity in epithelial cells, Mol.Biol.Cell 12 (2001) 3717-3732.

106. L.A. Dunbar & M.J. Caplan, Ion pumps in polarized cells: sorting and regulation of the Na+, K+- and H+, K+-ATPases, J.Biol.Chem. 276 (2001) 29617-29620.

107. E. Lecuona, S. Luquín, J. Avila, L.M. García-Segura & P. Martín-Vasallo, Expression of the beta 1 and beta 2 (AMOG) subunits of the Na,K-ATPase in neural tissues: cellular and developmental distribution patterns, Brain Res.Bull. 40 (1996) 167-174.

108. D.C. Chow & J.G. Forte, Functional significance of the beta- subunit for heterodimeric p-type ATPases, J.Exp.Biol. 198 (1995) 1-17.

109. O. Vagin, E. Tokhtaeva & G. Sachs, The role of the β1 subunit of the Na, K-ATPase and its glycosylation in cell-cell adhesion, J.Biol.Chem. 281 (2006) 39573-39587.

110. O. Vagin, G. Sachs & E. Tokhtaeva, The roles of the Na,K- ATPase beta 1 subunit in pump sorting and epithelial integrity, J.Bioenerg.Biomembr. 39 (2007) 367-372.

111. G. Walsh & R. Jefferis, Post-translational modifications in the context of therapeutic proteins, Nat.Biotechnol. 24 (2006) 1241-1252.

112. M.M. Fuster & J.D. Esko, The sweet and sour of cancer: glycans as novel therapeutic targets, Nat. Rev. Cancer 5 (2005) 526-542.

113. Y.C. Wang, E.N. Wang, C.C. Wang, C.L. Huang & A.C.W. Huang, Effects of lithium and carbamazepine on spatial learning and depressive behavior in a rat model of bipolar disorder induced by ouabain, Pharmacol.Biochem.Behav. 105 (2013) 118-127.

114. H.Y. Wang & R. Huang, Diurnal modulation of the Na+/K+- ATPase and spontaneous firing in the rat retinorecipient clock neurons, J.Neurophysiol. 92 (2004) 2295-2301.

115. M.F. Arteaga, R. Gutiérrez, J. Avila, A. Mobasheri, L. Díaz-Flores & P. Martín-Vasallo, Regeneration influences expression of the Na +,K +-atpase subunit isoforms in the rat peripheral nervous system, Neuroscience 129 (2004) 691-702.

116. H.J.M. Blom, C.J.A.H.V. van Vorstenbosch, V. Baumans, M.J.C. Hoogervorst, A.C. Beynen & L.F.M. van Zutphen, Description and validation of a preference test system to evaluate housing conditions for laboratory mice, Appl.Anim.Behav.Sci. 35 (1992) 67-82.

117. D.S. Reiss, M.B. Lees & V.S. Sapirstein, Is Na + ATPase a myelin-associated enzyme? J.Neurochem. 36 (1981) 1418-1426.

118. K. Domanska-Janik & J.M. Bourre, Effect of lipid peroxidation on Na +, K +-ATPase, 5'-nucleotidase and CNPase in mouse brain myelin, Biochim. Biophys. Acta 1034 (1990) 200-206.

119. A. Ishii, R. Dutta, G.M. Wark, S.I. Hwang, D.K. Han, B.D. Trapp, S.E. Pfeiffer & R. Bansal, Human myelin proteome and comparative analysis with mouse myelin, Proc.Natl.Acad.Sci.U.S.A. 106 (2009) 14605-14610.

Appendix A – Structure, Physical and Chemical Properties

of Detergents

Table A.1 Structure, physical and chemical properties of detergents used in this study

Detergent	Type	Structure	Molecular mass (g/mol)	Critical Micelle Concentration (mM)
CHAPS	Zwitterionic		614.9	6-10
SDS	Anionic		288.4	7-10
Tween-20	Non-ionic		1228	0.059
TX-100	Non-ionic		650	0.2-0.9

Appendix B – Protein Sequence Analysis of Na⁺/K⁺-ATPase

B.1 The Alpha Subunit

CLUSTAL O(1.2.1) multiple sequence alignment

```
Alpha1   MGKGVGRDKYEPAAVSEHGDKKGKKAKKERDMDELKKEVSMDDHKLSLDELHRKYGTDLS   60
Alpha2   MGRGAGRE-YSPAAT-TAENGGGKKKQKEKELDELKKEVAMDDHKLSLDELGRKYQVDLS   58
Alpha3   MGDKKDDK-SSP---------KKSKAKERRDLDDLKKEVAMTEHKMSVEEVCRKYNTDCV   50
         **       .  .*           .*  ::.::*:*****:* :**:*::*: *** .*

Alpha1   RGLTPARAAEILARDGPNALTPPPTTPEWVKFCRQLFGGFSMLLWIGAILCFLAYGIRSA   120
Alpha2   KGLTNQRAQDILARDGPNALTPPPTTPEWVKFCRQLFGGFSILLWIGALLCFLAYGILAA   118
Alpha3   QGLTHSKAQEILARDGPNALTPPPTTPEWVKFCRQLFGGFSILLWIGAILCFLAYGIQAG   110
         :***   :*  :***********************:*****:********* :.

Alpha1   TEEEPPNDDLYLGVVLSAVVIITGCFSYYQEAKSSKIMESFKNMVPQQALVIRNGEKMSI   180
Alpha2   MEDEPSNDNLYLGIVLAAVVIVTGCFSYYQEAKSSKIMDSFKNMVPQQALVIREGEKMQI   178
Alpha3   TEDDPSGDNLYLGIVLAAVVIITGCFSYYQEAKSSKIMESFKNMVPQQALVIREGEKMQV   170
          *::*   *:****:**:****:**********************:***************:****.:

Alpha1   NAEDVVVGDLVEVKGGDRIPADLRIISANGCKVDNSSLTGESEPQTRSPDFTNENPLETR   240
Alpha2   NAEEVVVGDLVEVKGGDRVPADLRIISSHGCKVDNSSLTGESEPQTRSPEFTHENPLETR   238
Alpha3   NAEEVVVGDLVEIKGGDRVPADLRIISAHGCKVDNSSLTGESEPQTRSPDCTHDNPLETR   230
         ***:*********:*****:********:..*******************:  *.:******

Alpha1   NIAFFSTNCVEGTARGIVVYTGDRTVMGRIATLASGLEGGQTPIAEEIEHFIHLITGVAV   300
Alpha2   NICFFSTNCVEGTARGIVIATGDRTVMGRIATLASGLEVGQTPIAMEIEHFIQLITGVAV   298
Alpha3   NITFFSTNCVEGTARGVVVATGDRTVMGRIATLASGLEVGKTPIAIEIEHFIQLITGVAV   290
         ** ************:*:  ***************** *:**** ******:*******

Alpha1   FLGVSFFILSLILEYTWLEAVIFLIGIIVANVPEGLLATVTVCLTLTAKRMARKNCLVKN   360
Alpha2   FLGVSFFVLSLILGYSWLEAVIFLIGIIVANVPEGLLATVTVCLTLTAKRMARKNCLVKN   358
Alpha3   FLGVSFFILSLILGYTWLEAVIFLIGIIVANVPEGLLATVTVCLTLTAKRMARKNCLVKN   350
         *******:***** *:*:******************************************

Alpha1   LEAVETLGSTSTICSDKTGTLTQNRMTVAHMWFDNQIHEADTTENQSGVSFDKTSATWFA   420
Alpha2   LEAVETLGSTSTICSDKTGTLTQNRMTVAHMWFDNQIHEADTTEDQSGATFDKRSPTWTA   418
Alpha3   LEAVETLGSTSTICSDKTGTLTQNRMTVAHMWFDNQIHEADTTEDQSGTSFDKSSHTWVA   410
         ********************************************:***.:*** * ** *

Alpha1   LSRIAGLCNRAVFQANQENLPILKRAVAGDASESALLKCIEVCCGSVMEMREKYSKIVEI   480
Alpha2   LSRIAGLCNRAVFKAGQENISVSKRDTAGDASESALLKCIELSCGSVRKMRDRNPKVAEI   478
Alpha3   LSHIAGLCNRAVFKGGQDNIPVLKRDVAGDASESALLKCIELSSGSVKLMRERNKKVAEI   470
         **:**********:. *:*: : ** .**************:..***   **::   *:.**

Alpha1   PFNSTNKYQLSIHKNPNASEPKHLLVMKGAPERILDRCSSILLHGKEQPLDEELKDAFQN   540
Alpha2   PFNSTNKYQLSIHEREDSPQS-HVLVMKGAPERILDRCSTILVQGKEIPLDKEMQDAFQN   537
Alpha3   PFNSTNKYQLSIHETEDPNDNRYLLVMKGAPERILDRCATILLQGKEQPLDEEMKEAFQN   530
         *************:  :  :  ::***************::**::*** ***:*:::****
```

```
Alpha1  AYLELGGLGERVLGFCHLLLPDEQFPEGFQFDTDDVNFPVDNLCFVGLISMIDPPRAAVP   600
Alpha2  AYMELGGLGERVLGFCQLNLPSGKFPRGFKFDTDELNFPTEKLCFVGLMSMIDPPRAAVP   597
Alpha3  AYLELGGLGERVLGFCHYYLPEEQFPKGFAFDCDDVNFTTDNLCFVGLMSMIDPPRAAVP   590
        **:************:   **. :**.** ** *::** .::******:***********

Alpha1  DAVGKCRSAGIKVIMVTGDHPITAKAIAKGVGIISEGNETVEDIAARLNIPVNQVNPRDA   660
Alpha2  DAVGKCRSAGIKVIMVTGDHPITAKAIAKGVGIISEGNETVEDIAARLNIPVSQVNPREA   657
Alpha3  DAVGKCRSAGIKVIMVTGDHPITAKAIAKGVGIISEGNETVEDIAARLNIPVSQVNPRDA   650
        **********************************************************.*****.*

Alpha1  KACVVHGSDLKDMTSEELDDILRYHTEIVFARTSPQQKLIIVEGCQRQGAIVAVTGDGVN   720
Alpha2  KACVVHGSDLKDMTSEQLDEILRDHTEIVFARTSPQQKLIIVEGCQRQGAIVAVTGDGVN   717
Alpha3  KACVIHGTDLKDFTSEQIDEILQNHTEIVFARTSPQQKLIIVEGCQRQGAIVAVTGDGVN   710
        ****:**:****:***::*:**: ***********************************

Alpha1  DSPALKKADIGVAMGIVGSDVSKQAADMILLDDNFASIVTGVEEGRLIFDNLKKSIAYTL   780
Alpha2  DSPALKKADIGIAMGISGSDVSKQAADMILLDDNFASIVTGVEEGRLIFDNLKKSIAYTL   777
Alpha3  DSPALKKADIGVAMGIAGSDVSKQAADMILLDDNFASIVTGVEEGRLIFDNLKKSIAYTL   770
        ***********:**** ******************************************

Alpha1  TSNIPEITPFLIFIIANIPLPLGTVTILCIDLGTDMVPAISLAYEQAESDIMKRQPRNPK   840
Alpha2  TSNIPEITPFLLFIIANIPLPLGTVTILCIDLGTDMVPAISLAYEAAESDIMKRQPRNSQ   837
Alpha3  TSNIPEITPFLLFIMANIPLPLGTITILCIDLGTDMVPAISLAYEAAESDIMKRQPRNPR   830
        ***********:**:*********:*********************** ************ :

Alpha1  TDKLVNERLISMAYGQIGMIQALGGFFTYFVILAENGFLPFHLLGIRETWDDRWVNDVED   900
Alpha2  TDKLVNERLISMAYGQIGMIQALGGFFTYFVILAENGFLPSRLLGIRLDWDDRTTNDLED   897
Alpha3  TDKLVNERLISMAYGQIGMIQALGGFFSYFVILAENGFLPGNLVGIRLNWDDRTVNDLED   890
        **************************:************ .*:***  ****  .**:**

Alpha1  SYGQQWTYEQRKIVEFTCHTAFFVSIVVVQWADLVICKTRRNSVFQQGMKNKILIFGLFE   960
Alpha2  SYGQEWTYEQRKVVEFTCHTAFFASIVVVQWADLIICKTRRNSVFQQGMKNKILIFGLLE   957
Alpha3  SYGQQWTYEQRKVVEFTCHTAFFVSIVVVQWADLIICKTRRNSVFQQGMKNKILIFGLFE   950
        ****:*******:*********.*********.************************:*

Alpha1  ETALAAFLSYCPGMGAALRMYPLKPTWWFCAFPYSLLIFVYDEVRKLIIRRRPGGWVEKE  1020
Alpha2  ETALAAFLSYCPGMGVALRMYPLKVTWWFCAFPYSLLIFIYDEVRKLILRRYPGGWVEKE  1017
Alpha3  ETALAAFLSYCPGMDVALRMYPLKPSWWFCAFPYSFLIFVYDEIRKLILRRNPGGWVEKE  1010
        **************  .*******  :*********:***:***:****:**  *******

Alpha1  TYY  1023
Alpha2  TYY  1020
Alpha3  TYY  1013
        ***
```

Figure B.1 Multiple sequence alignment of mouse Na$^+$/K$^+$-ATPase α subunits

Alignments were generated with Clustal Omega (1.2.1) on the EMBL-EBI website using UniProtKB accession numbers, Q8VDN2, Q6PIE5, and Q6PIC6 for alpha 1, 2, 3, respectively. The amino acids are coloured as follows: red (small and/or hydrophobic, *i.e.*, A, V, F, P,M, I, L, W, and G), blue (acidic, *i.e.*, D and E), magenta (basic, *i.e.*, R and K, and including H), and green (polar, *i.e.*, S, T, N, Q, and C). In the alignment, the consensus symbol asterisk (*) indicates positions which have a single, fully conserved residue; symbol colon (:) indicates conservation between groups of strongly similar properties; and symbol period (.) indicates conservation between groups of weakly similar properties.

3 (96.3%) **7** (100%) **9** (100%) **21** (78%) **22** (83.7%) **24** (92.9%) **25** (87.5%) **27** (90.5%) **28** (84.6%) **30** (89.7%) **36** (82.6%) **37** (84.6%) **45** (100%) **53** (100%) **54** (84.3%) **61** (100%) **67** (100%) **74** (100%) **91** (100%) **94** (100%) **118** (100%) **153** (100%)**156** (100%) **162** (100%) **173** (100%) **177** (100%) **194** (94.4%) **198** (94.1%) **204** (100%) **212** (100%) **227** (100%) **240** (100%) **255** (100%) **264** (100%) **269** (100%) **349** (87.3%) **350** (100%) **353** (95.3%) **354** (100%) **359** (85.7%) **377** (100%) **385**(100%) **413** (100%) **423** (100%) **430** (100%) **444** (91.8%) **445** (100%) **458** (100%) **471** (100%) **473** (92.8%) **476** (100%) **487** (100%) **494** (100%) **502** (100%) **508** (90.7%) **513** (75.6%) **517** (90.8%) **526** (100%) **535** (86.4%) **551** (94.1%) **596** (100%) **605** (100%) **607** (90.7%) **612** (100%) **625** (95.4%) **629** (100%) **647** (100%) **658** (100%) **661** (95.4%) **671** (86.4%) **683** (100%) **692** (100%) **698** (100%) **707** (100%) **726** (82.6%) **727** (87.5%) **743** (100%) **766** (100%) **773** (82.6%) **774** (90.9%) **833**(100%) **834** (100%) **837** (100%) **840** (100%) **843** (76.8%) **848** (100%) **887** (98.5%) **893** (100%) **911** (100%) **912** (100%) **938** (100%) **940** (90.9%) **941** (100%) **950** (100%) **952** (100%) **979** (100%) **984** (49.7%) **1005** (100%) **1006** (83.7%) **1010**(82.6%) **1011** (30.6%) **1012** (30.4%) **1019** (79.9%)

Figure B.2 The predicted trypsin cleavage sites for mouse Na$^+$/K$^+$-ATPase α_1

Trypsin cleavage sites were predicted by PeptideCutter (http://web.expasy.org/peptide_cutter/) using the UniProtKB accession number Q8VDN2 for Na$^+$/K$^+$-ATPase α_1. Cleavage is predicted to occur on the right side (C-terminal direction) of the indicated amino acids.

3 (100%) **7** (100%) **22** (92.9%) **23** (78%) **24** (75.5%) **26** (84.3%) **28** (79.9%) **34** (82.6%) **35** (84.6%) **43** (100%) **51** (90.9%) **52** (84.3%) **59** (93.9%) **65** (100%) **72** (100%) **89** (100%) **92** (100%) **151** (100%) **154** (100%) **160** (100%) **171** (98.5%) **175**(100%) **192** (94.4%) **196** (100%) **202** (100%) **210** (100%) **225** (100%) **238** (100%) **253** (100%) **262** (100%) **267** (100%) **347** (87.3%) **348** (100%) **351** (95.3%) **352** (100%) **357** (85.7%) **375** (100%) **383** (100%) **411** (73.9%) **412** (100%) **421** (100%)**428** (100%) **432** (86.4%) **442** (65%) **443** (100%) **456** (100%) **466** (100%) **467** (75%) **469** (100%) **471** (100%) **474** (100%) **485** (100%) **493** (78.4%) **505** (90.7%) **510** (75.6%) **514** (90.8%) **523** (100%) **529** (83.8%) **548** (94.1%) **561** (100%) **564**(100%) **567** (100%) **579** (94.7%) **593** (100%) **602** (100%) **604** (90.7%) **609** (100%) **622** (95.4%) **626** (100%) **644** (100%) **655** (100%) **658** (95.4%) **668** (86.4%) **680** (91.8%) **689** (100%) **695** (100%) **704** (100%) **723** (82.6%) **724** (87.5%) **740**(100%) **763** (100%) **770** (82.6%) **771** (90.9%) **830** (100%) **831** (100%) **834** (100%) **840** (76.8%) **845** (100%) **879** (100%) **884** (100%) **890** (100%) **908** (100%) **909** (84.5%) **935** (100%) **937** (90.9%) **938** (100%) **947** (100%) **949** (100%) **976** (100%)**981** (92.4%) **1002** (100%) **1003** (83.7%) **1007** (100%) **1008** (87.3%) **1016** (79.9%)

Figure B.3 The predicted trypsin cleavage sites for mouse Na$^+$/K$^+$-ATPase α_2

Trypsin cleavage sites were predicted by PeptideCutter (http://web.expasy.org/peptide_cutter/) using the UniProtKB accession number Q6PIE5 for Na$^+$/K$^+$-ATPase α_2. Cleavage is predicted to occur on the right side (C-terminal direction) of the indicated amino acids.

4 (78%) **5** (84.6%) **8** (100%) **12** (86.6%) **13** (90.9%) **15** (100%) **17** (82%) **19** (100%) **20** (100%) **26** (82.6%) **27** (84.6%) **35** (100%) **43** (45.3%) **44** (84.3%) **57** (100%) **64** (100%) **81** (100%) **84** (100%) **143** (100%) **146** (100%) **152** (100%) **163** (98.5%)**167** (100%) **184** (100%) **188** (100%) **194** (100%) **202** (100%) **217** (100%) **230** (100%) **245** (100%) **254** (100%) **259** (100%) **271** (100%) **339** (87.3%) **340** (100%) **343** (95.3%) **344** (100%) **349** (85.7%) **367** (100%) **375** (100%) **403** (100%) **420**(100%) **424** (100%) **434** (91.8%) **435** (100%) **448** (100%) **458** (100%) **461** (100%) **463** (100%) **465** (84.1%) **466** (79.6%) **477** (100%) **492** (100%) **498** (90.7%) **503** (75.6%) **507** (90.8%) **516** (100%) **525** (100%) **541** (94.1%) **557** (94%) **586** (100%)**595** (100%) **597** (90.7%) **602** (100%) **615** (95.4%) **619** (100%) **637** (100%) **648** (100%) **651** (95.4%) **661** (86.4%) **682** (100%) **688** (100%) **697** (100%) **716** (82.6%) **717** (87.5%) **733** (100%) **756** (100%) **763** (82.6%) **764** (90.9%) **823** (100%) **824**(100%) **827** (100%) **830** (100%) **833** (76.8%) **838** (100%) **877** (100%) **883** (100%) **901** (100%) **902** (84.5%) **928** (100%) **930** (90.9%) **931** (100%) **940** (100%) **942** (100%) **969** (100%) **974** (49.7%) **995** (84.6%) **996** (83.7%) **1000** (100%) **1001**(100%) **1009** (79.9%)

Figure B.4 The predicted trypsin cleavage sites for mouse Na$^+$/K$^+$-ATPase α$_3$

Trypsin cleavage sites were predicted by PeptideCutter (http://web.expasy.org/peptide_cutter/) using the UniProtKB accession number Q6PIC6 for Na$^+$/K$^+$-ATPase α$_3$. Cleavage is predicted to occur on the right side (C-terminal direction) of the indicated amino acids.

B.2 The Beta Subunit

CLUSTAL O(1.2.1) multiple sequence alignment

```
Beta1   -----MARGKAKEEGSWKKFIWNSEKKEFLGRTGGSWFKILLFYVIFYGCLAGIFIGTIQ 55
Beta2   MVIQKEKKSCGQVVEEWKEFVWNPRTHQFMGRTGTSWAFILLFYLVFYGFLTAMFSLTMW 60
Beta3   -MTKTEKKSFHQSLAEWKLFIYNPSSGEFLGRTSKSWGLILLFYLVFYGFLAALFTFTMW 59
             :.  :    .** *::*   . :*:***. **  *****::*** *:..*   *:

Beta1   VMLLTISELKPTYQDRVAPPGLTQIPQIQK-TEISFRPNDPKSYEAYVLNIIRFLEKYKD 114
Beta2   VMLQTVSDHTPKYQDRLATPGLMIRPKTEN-LDVIVNISDTESWGQHVQKLNKFLEPYND 119
Beta3   AMLQTLNDEVPKYRDQIPSPGLMVFPKPQTALEYTFSMSEPQTYKKLVEDLESFLKPYSV 119
         .** *:.:  *.*:*::  ***   *: :.  :  .  .: ::: *  .:  **: *.

Beta1   SAQKDDMIFEDCGNVPSEPKERGDINHERGERKVCRFKLDWLGNCSGLND-DSYGYREGK 173
Beta2   SIQAQKNDV--CR--PGRYYEQPDNGVLNYPKRACQFNRTQLGDCSGIGDPTHYGYSTGQ 175
Beta3   EEQKNL-TS--CP--DGAPFIQH-----GPDYRACQFPVSLLEECSGVTD-ANFGYSKGQ 168
         . * :      *    .   :         :.*:*    * :***: *    :**   *:

Beta1   PCIIIKLNRVLGFKPKPPKNESLETYPLMMKYNPNVLPVQCTGKRDEDKDKVGNIEYFGM 233
Beta2   PCVFIKMNRVINFYAGANQ---------------SMNVTCVGKRDEDAENLGHFVMFPA 219
Beta3   PCILVKMNRIIDLIPDGYP-------------QISCLPKEE-----NATIATYPE 205
         **:::*:**:: :               : *  *.:     . : :
```

```
Beta1 GGYYGFPLQYYPYYGKLLQPKYLQPLLAVQ--FTNLTVDTEIRVECKAYGE-N-IGYSEK 289
Beta2 NG--SIDLMYFPYYGKKFHVNYTQPLVAVK--FLNVTPNVEVNVECRINA-ANIATDDER 274
Beta3 FG--VLDLKYFPYYGKKRHVGYRQPLVAVQVKFDSGLNKKEVTVECHIAGTRNLKNKNER 263
       *    : * *:*****   :   * ***:**:  * .   . *: ***:   .  *     .*:

Beta1 DRFQGRFDVKIEIKS- 304
Beta2 DKFAGRVAFKLRINKT 290
Beta3 DKFLGRVSFKVTARA- 278
      *:* **.  .*:   .
```

Figure B.5 Multiple sequence alignment of mouse Na$^+$/K$^+$-ATPase β subunits

Alignments were generated with Clustal Omega (1.2.1) on the EMBL-EBI website using UniProtKB accession numbers, P14094, P14231, and P97370 for beta 1, 2, 3, respectively. The amino acids are coloured as follows: red (small and/or hydrophobic, *i.e.*, A, V, F, P,M, I, L, W, and G), blue (acidic, *i.e.*, D and E), magenta (basic, *i.e.*, R and K, and including H), and green (polar, *i.e.*, S, T, N, Q, and C). In the alignment, the consensus symbol asterisk (*) indicates positions which have a single, fully conserved residue; symbol colon (:) indicates conservation between groups of strongly similar properties; and symbol period (.) indicates conservation between groups of weakly similar properties.

3 (100%) **5** (100%) **7** (82%) **13** (100%) **14** (100%) **21** (87.3%) **22** (84.6%) **27** (100%) **34** (100%) **65** (49.7%) **71** (100%) **85** (100%) **91** (51%) **96** (100%) **107** (100%) **111** (92.8%) **113** (87%) **118** (100%) **134** (90.7%) **136** (100%) **143** (100%) **146**(88.4%) **147** (84.5%) **150** (100%) **152** (100%) **170** (85.3%) **173** (51.9%) **179** (100%) **182** (100%) **187** (40.6%) **189** (8.1%) **192** (100%) **204** (100%) **217** (84.7%) **218** (100%) **222** (37.7%) **224** (89.7%) **249** (100%) **254** (100%) **274** (100%) **278** (100%)**289** (83.2%) **291** (100%) **295** (100%) **299** (100%) **303** (100%)

Figure B.6 The predicted trypsin cleavage sites for mouse Na$^+$/K$^+$-ATPase β$_1$

Trypsin cleavage sites were predicted by PeptideCutter (http://web.expasy.org/peptide_cutter/) using the UniProtKB accession number P14094 for Na$^+$/K$^+$-ATPase β$_1$. Cleavage is predicted to occur on the right side (C-terminal direction) of the indicated amino acids.

5 (84.3%) **7** (87.3%) **8** (90.9%) **18** (100%) **25** (100%) **32** (100%) **72** (100%) **76** (79.4%) **85** (34.9%) **87** (100%) **109** (100%) **112** (91.4%) **125** (88.7%) **130** (32.6%) **133** (100%) **147** (90.7%) **148** (100%) **154** (100%) **181** (100%) **184** (100%) **203**(84.7%) **204** (100%) **233** (92.9%) **234** (100%) **247** (100%) **262** (100%) **274** (89.7%) **276** (64.2%) **280** (100%) **284** (100%) **286** (100%) **289** (100%)

Figure B.7 The predicted trypsin cleavage sites for mouse Na$^+$/K$^+$-ATPase β$_2$

Trypsin cleavage sites were predicted by PeptideCutter (http://web.expasy.org/peptide_cutter/) using the UniProtKB accession number P14231 for Na$^+$/K$^+$-ATPase β$_2$. Cleavage is predicted to occur on the right side (C-terminal direction) of the indicated amino acids.

3 (93.1%) **6** (87.3%) **7** (90.9%) **17** (100%) **31** (100%) **34** (100%) **71** (100%) **73** (90.6%) **86** (8
.1%) **104** (100%) **105** (82%) **115** (49.7%) **123** (88.7%) **142** (100%) **166** (93.9%) **174** (100%)
177 (100%) **194** (90.7%) **212** (100%) **219** (92.9%) **220**(54.5%) **221** (70%) **226** (100%) **235** (
100%) **242** (84.1%) **243** (84.6%) **255** (100%) **258** (100%) **260** (80.3%) **263** (89.7%) **265** (64.
2%) **269** (100%) **273** (89.5%) **277** (100%)

Figure B.8 The predicted trypsin cleavage sites for mouse Na$^+$/K$^+$-ATPase β$_3$

Trypsin cleavage sites were predicted by PeptideCutter (http://web.expasy.org/peptide_cutter/) using the
UniProtKB accession number P97370 for Na$^+$/K$^+$-ATPase β$_3$. Cleavage is predicted to occur on the right
side (C-terminal direction) of the indicated amino acids.

Appendix C – Predicted Functional Partners

C.1 Predicted Functional Partners of Na⁺/K⁺-ATPase Subunits

Table C.1 Predicted functional partners of Na$^+$/K$^+$-ATPase α and β subunits

Functional partners predicted for Na$^+$/K$^+$-ATPase α and β subunits in mice, using STRING 9.1 (http://string-db.org/). Each suggested protein partner is listed in order of greatest evidence to least evidence.

Na$^+$/K$^+$-ATPase Subunit	Predicted Functional Partner		
	Protein	Gene	Evidence
Alpha 1	Sodium/potassium-transporting ATPase subunit beta-1	Atp1b1	Co-expression Experiments Databases Textmining
	FXYD domain-containing ion transport regulator 2	Fxyd2	Experiments Databases Textmining
	Sodium/potassium-transporting ATPase subunit beta-2	Atp1b2	Databases Textmining
	Sodium/potassium-transporting ATPase subunit beta-3	Atp1b3	Experiments Databases Textmining
	Sodium/potassium-transporting ATPase subunit alpha-2	Atp1a2	Co-occurrence Co-expression Databases Textmining Homology
	Sodium/potassium-transporting ATPase subunit alpha-3	Atp1a3	Co-occurrence Databases Textmining Homology
	Sodium/potassium-transporting ATPase subunit alpha-4	Atp1a4	Co-occurrence Databases Homology
	Solute carrier family 8 (sodium/calcium exchanger), member 1	Scl8a1	Experiments Textmining
	Klotho	Kl	Experiments Textmining
	Inositol 1,4,5-triphosphate receptor 1	Itpr1	Experiments Textmining
Alpha 2	Sodium/potassium-transporting	Atp1b2	Co-expression

	ATPase subunit beta-2		Databases Textmining
	Sodium/potassium-transporting ATPase subunit beta-1	Atp1b1	Co-expression Databases Textmining
	FXYD domain-containing ion transport regulator 2	Fxyd2	Experiments Databases Textmining
	Sodium/potassium-transporting ATPase subunit beta-3	Atp1b3	Experiments Databases Textmining
	Sodium/potassium-transporting ATPase subunit alpha-3	Atp1a3	Co-occurrence Co-expression Databases Textmining Homology
	Sodium/potassium-transporting ATPase subunit alpha-4	Atp1a4	Co-occurrence Databases Textmining Homology
	Sodium/potassium-transporting ATPase subunit alpha-1	Atp1a1	Co-occurrence Co-expression Databases Textmining Homology
	Solute carrier family 8 (sodium/calcium exchanger), member 1	Slc8a1	Experiments Textmining
	Inositol 1,4,5-triphosphate receptor 1	Itpr1	Experiments Textmining
	Potassium inwardly-rectifying channel, subfamily J, member 9	Kcnj9	Textmining
Alpha 3	FXYD domain-containing ion transport regulator 2	Fxyd2	Experiments Databases Textmining
	Sodium/potassium-transporting ATPase subunit beta-2	Atp1b2	Co-expression Databases Textmining
	Sodium/potassium-transporting ATPase subunit beta-3	Atp1b3	Experiments Databases Textmining
	Sodium/potassium-transporting ATPase subunit beta-1	Atp1b1	Co-expression Databases

			Textmining
	Sodium/potassium-transporting ATPase subunit alpha-2	Atp1a2	Co-occurrence Co-expression Databases Textmining Homology
	Sodium/potassium-transporting ATPase subunit alpha-1	Atp1a1	Co-occurrence Databases Textmining Homology
	Sodium/potassium-transporting ATPase subunit alpha-4	Atp1a4	Co-occurrence Databases Textmining Homology
	Agrin	Agrn	Textmining
	BR serine/threonine kinase 2	Brsk2	Co-expression Textmining
	Dynein, axonemal, heavy chain 8	Dnahc8	Textmining
Beta 1	Sodium/potassium-transporting ATPase subunit alpha-1	Atp1a1	Co-expression Experiments Databases Textmining
	FXYD domain-containing ion transport regulator 2	Fxyd2	Experiments Databases
	Sodium/potassium-transporting ATPase subunit alpha-2	Atp1a2	Co-expression Databases Textmining
	Sodium/potassium-transporting ATPase subunit alpha-3	Atp1a3	Co-expression Databases Textmining
	Sodium/potassium-transporting ATPase subunit alpha-4	Atp1a4	Databases Textmining
	Sodium/potassium-transporting ATPase subunit beta-2	Atp1b2	Databases Textmining Homology
	Sodium/potassium-transporting ATPase subunit beta-3	Atp1b3	Databases Textmining Homology
	Sodium/potassium transporting ATPase interacting 1	Nkain1	Textmining
	FXYD domain-containing ion transport regulator 7	Fxyd7	Experiments Textmining
	Sodium/potassium transporting	Nkain4	Textmining

	ATPase interacting 4		
Beta 2	Sodium/potassium-transporting ATPase subunit alpha-2	Atp1a2	Co-expression Databases Textmining
	Sodium/potassium-transporting ATPase subunit alpha-1	Atp1a1	Databases Textmining
	Sodium/potassium-transporting ATPase subunit alpha-3	Atp1a3	Co-expression Databases Textmining
	Sodium/potassium-transporting ATPase subunit alpha-4	Atp1a4	Databases Textmining
	FXYD domain-containing ion transport regulator 2	Fxyd2	Experiments Databases
	Sodium/potassium-transporting ATPase subunit beta-3	Atp1b3	Co-expression Databases Textmining Homology
	Sodium/potassium-transporting ATPase subunit beta-1	Atp1b1	Databases Textmining Homology
	WD repeat containing, antisense to TP53	Wrap53	Textmining
	Lymphocyte antigen 6 complex, locus G6C	Ly6g6c	Textmining
	Rabaptin, RAB GTPase binding effector protein 2	Rabep2	Textmining
Beta 3	Sodium/potassium-transporting ATPase subunit alpha-3	Atp1a3	Experiments Databases Textmining
	Sodium/potassium-transporting ATPase subunit alpha-2	Atp1a2	Experiments Databases Textmining
	Sodium/potassium-transporting ATPase subunit alpha-1	Atp1a1	Experiments Databases Textmining
	Sodium/potassium-transporting ATPase subunit alpha-4	Atp1a4	Experiments Databases
	FXYD domain-containing ion transport regulator 2	Fxyd2	Experiments Databases
	Sodium/potassium-transporting ATPase subunit beta-2	Atp1b2	Co-expression Databases Textmining Homology

	Sodium/potassium-transporting ATPase subunit beta-1	Atp1b1	Databases Textmining Homology
	Cartilage associated protein	Crtap	Co-expression
	RAS related protein 1b	Rap1b	Co-expression

C.2 Predicted Protein-Protein Interactions of Na⁺/K⁺-ATPase

Subunits

Figure C.1 The predicted functional partners of Na$^+$/K$^+$-ATPase α_1

Image generated using STRING 9.1.

Figure C.2 The predicted functional partners of Na$^+$/K$^+$-ATPase α_2

Image generated using STRING 9.1.

Figure C.3 The predicted functional partners of Na$^+$/K$^+$-ATPase α_3

Image generated using STRING 9.1.

Figure C.4 The predicted functional partners of Na$^+$/K$^+$-ATPase β_1

Image generated using STRING 9.1.

Figure C.5 The predicted functional partners of Na$^+$/K$^+$-ATPase β$_2$
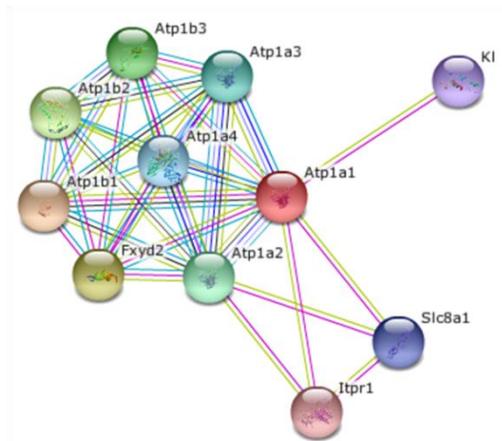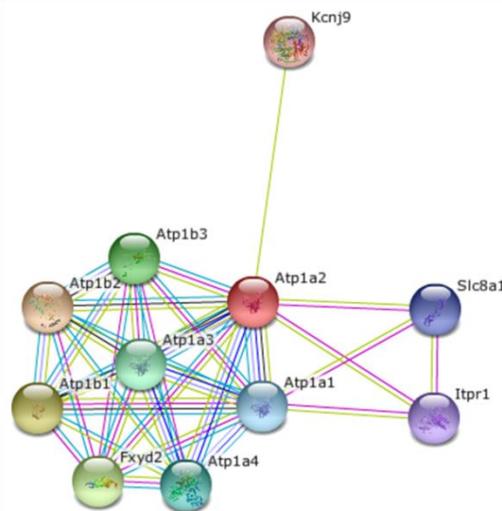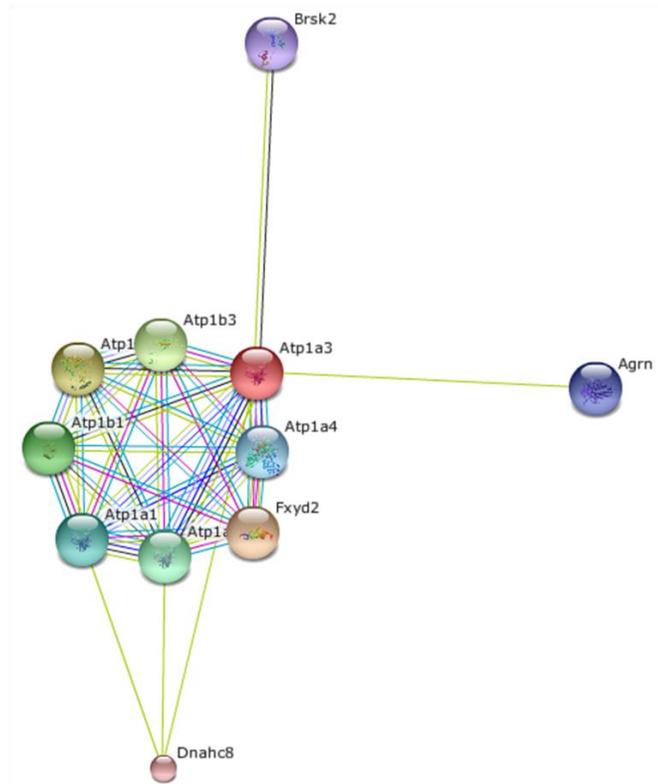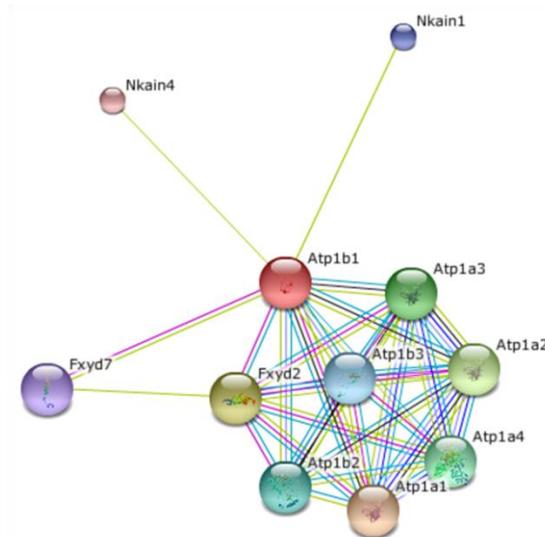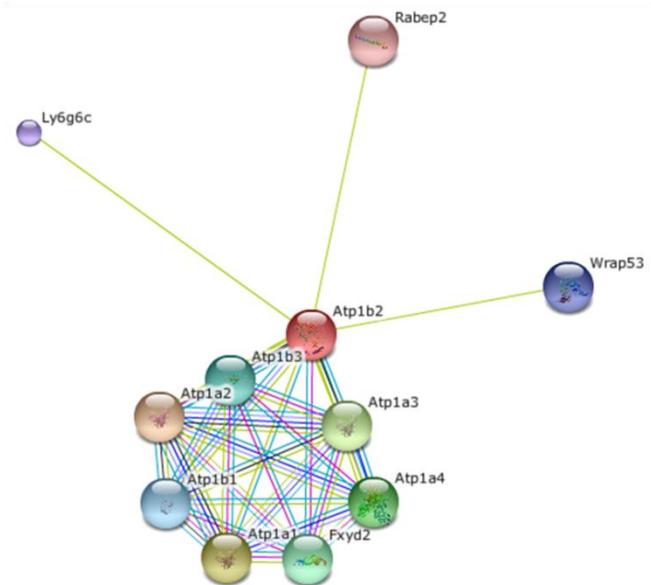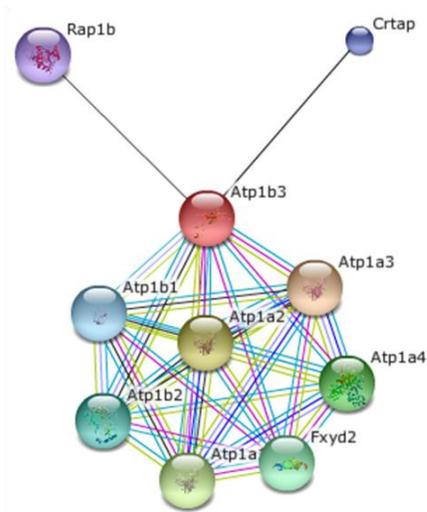
Image generated using STRING 9.1.

Figure C.6 The predicted functional partners of Na$^+$/K$^+$-ATPase β$_3$

Image generated using STRING 9.1.

Appendix D – Raw Data for Densitometric Analyses

Table D.1 Western blot intensity data for CD1 and ND4 myelin comparison

Raw data from densitometric analysis of CD1 and ND4 Western blot analysis. Intensities are provided for each Na$^+$/K$^+$-ATPase subunit isoform, as well as each glycosylation state of the β_1 subunit; Band 1 to Band 4 represent the highest molecular mass protein band to the lowest molecular mass (unglycosylated core) protein band, respectively. Intensities were normalized to β-actin protein loading controls, and standard deviation of the pixel intensities in each sample was calculated by Image Lab Version 5.0 (Bio-Rad).

	Age	Type of Data	Measurement	Subunit Isoform									
				Alpha 1	Alpha 2	Alpha 3	Beta 1	Beta 2	Beta 3	Beta 1 Band 1	Beta 1 Band 2	Beta 1 Band 3	Beta 1 Band 4
CD1 Control Myelin	3.10 months	Raw Data	Intensity of Fluorescent Signal (β-Actin control)	1964105	2708061	1851844	1851844	1964105	2708061	1851844	1851844	1851844	1851844
			Standard Deviation of Fluorescent Signal	799.0206	979.5301	801.8033	801.8033	799.0206	979.5301	801.8033	801.8033	801.8033	801.8033
			Intensity of Enhanced Chemiluminescent Signal (Sample)	483129.5	36782.64	1083381	1856270	2225996	3205753	250723	162529	176851	47232
			Standard Deviation of Chemiluminescent Signal	3024.82	824.3722	4967.65	763.5356	7210.989	8782.518	979.4812	637.9062	625.3855	421.3716
		Normalized Data	Relative Intensity Factor	0.25	0.34	0.23	0.23	0.25	0.34	0.23	0.23	0.23	0.23
			Relative Intensity of Enhanced Chemiluminescent Signal	1961504	108311.6	4665167	7993317	9037536	9439782	1079643	699869.2	761541.4	203386.6
			Standard Deviation of Relative Intensity	12306.66	2427.794	21486.45	4773.681	29506.54	26085.77	4243.588	2763.564	2713.095	1816.612
	7.65 months	Raw Data	Intensity of Fluorescent Signal	7974260	6808667	1760731	1760731	7974260	6808667	1760731	1760731	1760731	1760731

139

			(β-Actin control)										
			Standard Deviation of Fluorescent Signal	2567.282	2207.072	734.084	734.084	2567.282	2207.072	734.084	734.084	734.084	734.084
			Intensity of Enhanced Chemiluminescent Signal (Sample)	1175295	925577.6	2333128	1352819	6709981	6613303	94498.76	285076.6	367779.1	70889.52
			Standard Deviation of Chemiluminescent Signal	9068.39	8504.181	10404.16	2258.68	18604.01	12467.35	1004.61	1836.48	3503.16	811.3904
		Normalized Data	Relative Intensity Factor	1.00	0.85	0.22	0.22	1.00	0.85	0.22	0.22	0.22	0.22
			Relative Intensity of Enhanced Chemiluminescent Signal	1175295	1084030	10566615	6126846	6709981	7745452	427980	1291097	1665653	321054.9
			Standard Deviation of Relative Intensity	9076.281	9966.23	47325.39	10543.55	18729.01	14815.96	4553.324	8334.723	15880.82	3677.182
	9.00 months	Raw Data	Intensity of Fluorescent Signal (β-Actin control)	4012486	4145130	4702827	4702827	4012486	4145130	4702827	4702827	4702827	4702827
			Standard Deviation of Fluorescent Signal	1796.694	1850.12	2090.94	2090.94	1796.694	1850.12	2090.94	2090.94	2090.94	2090.94
			Intensity of Enhanced Chemiluminescent Signal (Sample)	1248363	694249.2	3619293	455475.7	5135876	3998997	45878.65	145469.6	87800.8	5208.42
			Standard Deviation of Chemiluminescent Signal	8557.57	5894.32	12913.14	570.544	12736.53	8775.83	263.1928	649.2042	607.0426	116.3775
		Normalized Data	Relative Intensity Factor	0.50	0.52	0.59	0.59	0.50	0.52	0.59	0.59	0.59	0.59
			Relative Intensity of Enhanced Chemiluminescent Signal	2480948	1335573	6136986	772318.8	10206841	7693134	77793.27	246662.7	148877.8	8831.559
			Standard Deviation of Relative Intensity	17043.23	11354.95	22065.28	1026.566	25721.39	17228.29	447.6162	1106.26	1031.447	197.3724

Group	Months	Data Type	Measurement										
	13.02 months	Raw Data	Intensity of Fluorescent Signal (β-Actin control)	2266047	1818010	1281897	1281897	2266047	1818010	1281897	1281897	1281897	1281897
			Standard Deviation of Fluorescent Signal	1123.899	789.0717	929.5972	929.5972	1123.899	789.0717	929.5972	929.5972	929.5972	929.5972
			Intensity of Enhanced Chemiluminescent Signal (Sample)	2697860	676230.2	3598350	650954.6	4566681	1653301	47033.25	198043	82480.5	49149.06
			Standard Deviation of Chemiluminescent Signal	17006.02	5156.71	14758.39	1029.21	10633.07	4943.56	586.7155	1153.26	1489.24	421.3461
		Normalized Data	Relative Intensity Factor	0.28	0.23	0.16	0.16	0.28	0.23	0.16	0.16	0.16	0.16
			Relative Intensity of Enhanced Chemiluminescent Signal	9493819	2966119	22384155	4049375	16070232	7251803	292578.4	1231960	513084.1	305740.2
			Standard Deviation of Relative Intensity	60029.45	22655.26	93231.07	7043.682	38257.44	21910.97	3655.926	7229.464	9271.542	2630.416
ND4 Transgenic Myelin	3.10 months	Raw Data	Intensity of Fluorescent Signal (β-Actin control)	2317390	3653502	1234209	1234209	2317390	3653502	1234209	1234209	1234209	1234209
			Standard Deviation of Fluorescent Signal	958.5079	1127.46	736.5056	736.5056	958.5079	1127.46	736.5056	736.5056	736.5056	736.5056
			Intensity of Enhanced Chemiluminescent Signal (Sample)	873924.1	161674.6	1630287	842295.5	1510235	4864355	570	55844	258577	76477
			Standard Deviation of Chemiluminescent Signal	4653.235	1382.791	7264.35	595.6856	4815.513	12951.38	381.5696	404.2201	938.8458	383.2174
		Normalized Data	Relative Intensity Factor	0.29	0.46	0.15	0.15	0.29	0.46	0.15	0.15	0.15	0.15
			Relative Intensity of Enhanced Chemiluminescent Signal	3007218	352876.6	10533328	5442093	5196798	10617108	3682.785	360809.6	1670673	494119.9

			Standard Deviation of Relative Intensity	16060.26	3020.092	47354.18	5035.797	16709.26	28457.38	2465.332	2620.537	6147.289	2493.474
7.65 months	Raw Data		Intensity of Fluorescent Signal (β-Actin control)	6932256	5945920	969985.3	969985.3	6932256	5945920	969985.3	969985.3	969985.3	969985.3
			Standard Deviation of Fluorescent Signal	2417.751	1938.347	504.4575	504.4575	2417.751	1938.347	504.4575	504.4575	504.4575	504.4575
			Intensity of Enhanced Chemiluminescent Signal (Sample)	813033.6	455770	1621032	609532.3	6395463	6002612	2926.9	166333.5	168380.8	21381.14
			Standard Deviation of Chemiluminescent Signal	6539.262	3467.39	7943.9	902.6996	18032.15	11167.67	205.0394	911.4549	1151.38	227.9837
	Normalized Data		Relative Intensity Factor	0.87	0.75	0.12	0.12	0.87	0.75	0.12	0.12	0.12	0.12
			Relative Intensity of Enhanced Chemiluminescent Signal	935242.6	611247.5	13326520	5010972	7356780	8050291	24062.08	1367430	1384260	175774.6
			Standard Deviation of Relative Intensity	7529.263	4654.493	65673.62	7865.382	20900.7	15205.5	1685.677	7526.752	9492.845	1876.484
9.00 months	Raw Data		Intensity of Fluorescent Signal (β-Actin control)	5854361	5618304	6088181	6088181	5854361	5618304	6088181	6088181	6088181	6088181
			Standard Deviation of Fluorescent Signal	2544.906	2239.23	2174.6	2174.6	2544.906	2239.23	2174.6	2174.6	2174.6	2174.6
			Intensity of Enhanced Chemiluminescent Signal (Sample)	2500319	1152316	5814317	1562077	8893667	5939907	31243.42	466539.3	461119.8	15398.23
			Standard Deviation of Chemiluminescent Signal	15829.75	9213.09	16031.52	2536.84	20138.52	13223.55	305.6617	2257.18	3513.76	332.7187
	Normalized Data		Relative Intensity Factor	0.73	0.70	0.76	0.76	0.73	0.70	0.76	0.76	0.76	0.76
			Relative Intensity of Enhanced Chemiluminescent	3405699	1635523	7615554	2045998	12114115	8430721	40922.43	611070.1	603971.7	20168.5

Category	Time	Data Type	Measurement										
			Signal										
			Standard Deviation of Relative Intensity	21612.56	13092.7	21173.44	3402.153	27931.7	19067.07	400.6204	2964.485	4607.353	435.8523
	13.02 months	Raw Data	Intensity of Fluorescent Signal (β-Actin control)	2821045	2185337	2443929	2443929	2821045	2185337	2443929	2443929	2443929	2443929
			Standard Deviation of Fluorescent Signal	1343.626	970.8208	1115.91	1115.91	1343.626	970.8208	1115.91	1115.91	1115.91	1115.91
			Intensity of Enhanced Chemiluminescent Signal (Sample)	2998635	1148146	4201894	993252.2	6297561	3457138	25295	425775.8	178040.8	50861.83
			Standard Deviation of Chemiluminescent Signal	17870.8	7724.68	14417.33	1622.31	14580.09	10064.49	344.8458	1964.29	1961.05	357.1174
		Normalized Data	Relative Intensity Factor	0.35	0.27	0.31	0.31	0.35	0.27	0.31	0.31	0.31	0.31
			Relative Intensity of Enhanced Chemiluminescent Signal	8476252	4189565	13710298	3240868	17801338	12615038	82534.68	1389258	580926.5	165956.3
			Standard Deviation of Relative Intensity	50676.52	28248.61	47456.8	5496.362	42076.66	37150.28	1125.823	6440.567	6404.176	1167.694
Normal-ized ND4 to CD1 Myelin Ratios	3.10 months	Normalized Data	Ratio of Diseased to Healthy Relative Intensities	1.53	3.26	2.26	0.68	0.58	1.12	0.00	0.52	2.19	2.43
			Standard Deviation of Normalized Ratio	0.01	0.08	0.01	0.00	0.00	0.00	0.00	0.00	0.01	0.02
	7.65 months	Normalized Data	Ratio of Diseased to Healthy Relative Intensities	0.80	0.56	1.26	0.82	1.10	1.04	0.06	1.06	0.83	0.55
			Standard Deviation of Normalized Ratio	0.01	0.01	0.01	0.00	0.00	0.00	0.00	0.01	0.01	0.01
	9.00 months	Normalized Data	Ratio of Diseased to Healthy Relative Intensities	1.37	1.22	1.24	2.65	1.19	1.10	0.53	2.48	4.06	2.28
			Standard Deviation of Normalized Ratio	0.01	0.01	0.01	0.01	0.00	0.00	0.01	0.02	0.04	0.07
	13.02 months	Normalized Data	Ratio of Diseased to Healthy Relative	0.89	1.41	0.61	0.80	1.11	1.74	0.28	1.13	1.13	0.54

			Intensities										
			Standard Deviation of Normalized Ratio	0.01	0.01	0.00	0.00	0.00	0.01	0.01	0.01	0.02	0.01

Appendix E – Na⁺/K⁺-ATPase Endpoint and Kinetic Enzyme Assays

E.1 Introduction

Evaluation of the enzymatic activity of Na^+/K^+-ATPase is a necessary step in the characterization of this protein within the myelin membrane. The specific enzymatic activity of Na^+/K^+-ATPase has been determined in other tissue and cell types by using the K^+-dependent *p*-nitrophenyl phosphatase (pNPPase) activity assay; it measures the enzymatic activity of phosphatases [2]. This assay takes advantage of the chemical reaction depicted in Figure E.1. The presence of phosphatases, such as Na^+/K^+-ATPase, catalyzes the conversion of 4-nitrophenyl to 4-nitrophenol [4]. This chromogenic product absorbs strongly at 410 nm, when deprotonated to produce *p*-nitrophenolate [4]. Without deprotonation, 4-nitrophenol only weakly absorbs light at 405 nm. Thus, this reaction can be manipulated by the addition of a strong base, such as sodium hydroxide (NaOH), to ensure full deprotonation and allow an endpoint measurement of absorption, such that Na^+/K^+-ATPase activity can be determined.

Figure E.1 The reaction utilized in the K⁺-dependent *p*-nitrophenyl phosphatase activity assay

Alternatively, the evaluation of enzyme kinetics using the pNPPase assay requires that the pH conditions of the reaction maximize both enzymatic activity and

spectrophotometric detection. Although the pKa of 4-nitrophenol is approximately 7.2, it is expected that physiological pH will provide the greatest Na^+/K^+-ATPase activity [6]. Studies of Na^+/K^+-ATPase activity in other tissue and cell types also generally use inhibitors to distinguish between the total ATPase activity and Na^+/K^+-ATPase activity. More specifically, the difference in enzyme activity between a reaction containing Na^+, K^+, and Mg^{2+}, and one without K^+ but with 10^{-4} M ouabain, is often considered the enzymatic activity attributed to Na^+/K^+-ATPase [7].

E.2 Materials and Methods

E.2.1 Materials

Ouabain octahydrate, sodium azide (NaN_3) and *p*-nitrophenyl phosphate di(tris) (pNPP) were purchased from Sigma-Aldrich (St. Louis, MO, USA). NaOH was obtained from VWR Scientific Products (West Chester, PA, USA). All other materials were sourced as previously described in section 2.1.

E.2.2 Methodology

Myelin was isolated from CD1 mouse brains using a modified version of the sucrose gradient method developed by Norton [5]; this protocol was described previously in section 2.3.1. The K^+-dependent *p*-nitrophenyl phosphatase activity assay was conducted using 96-well microplates, with 50 mM pNPP always prepared fresh using ultrapure water. Blanks consisted of 75 µL of 2X reaction buffer (100 mM Tris/HCl, 0.1 mM EGTA, 5 mM $MgCl_2$, and 15 mM KCl) and 65 µL of water; the pH of the reaction

buffer was adjusted as needed for each experiment; ranging from 7.4 to 8.2. Samples

included 75 µL of 2X reaction buffer, 1-65 µL myelin protein (30 µg total), and were

brought to a total volume of 140 µL with water. In samples with inhibitor, 10 µL of water

was omitted and replaced with 10 µL of varying concentrations of either Na_3VO_4, NaN_3,

or ouabain; the sample or sample and inhibitor mixtures were incubated at 37^oC for 10

minutes prior to initiating the reaction. The reaction was initiated by the addition of 10

µL of 50 mM pNPP; it was also added to blanks. For endpoint measurements, the

reactions were incubated at 37^oC for 20 minutes, stopped with the addition of 50 µL of

2N NaOH, and immediately measuring the absorbance at 410 nm. Alternatively, kinetic

measurements were taken every 30 seconds at 410 nm, over a 30 minute period, while

the reaction mixtures were maintained at 37^oC. After 30 minutes, the reactions were

stopped by the addition of 50 µL of 2N NaOH, and the absorbance was measured again

at 410 nm. Controls which contained myelin protein but omitted the addition of 10 µL of

50 mM pNPP, by substituting it with water, were also prepared. The extinction

coefficient of p-nitrophenolate at 410 nm (18300 $M^{-1}cm^{-1}$) was used to calculate enzyme

activity.

E.3 Results

The enzyme activity of Na^+/K^+-ATPase in myelin, was evaluated kinetically at pH

7.6, 7.8, 8.0 and 8.2, over a 30 minute period. The results of this kinetic pNPPase activity

assay are shown in Figure E.2. The activity of Na^+/K^+-ATPase at each pH was determined

using the slope of the line of best fit of the linear portion of each reaction curve. These

values, along with the activities determined using the absorbances at 410 nm after samples were stopped with NaOH, are shown in Table E.1. There was no significant change in absorbance over time in the blanks.
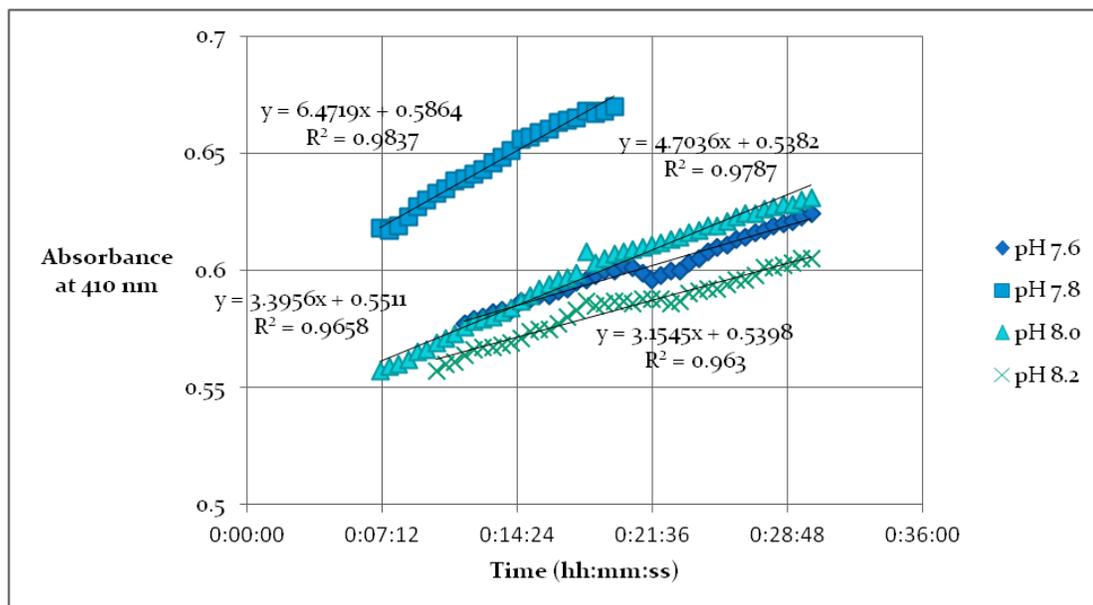
Figure E.2 Determination of the rate of change in absorbance over time, in myelin samples of varying pH, at 410 nm

As expected, the blanks showed little or no enzymatic activity. Likewise, the control samples without pNPP did not demonstrate an increase in absorbance over time. The determined enzyme, and specific, activities from the pNPPase activity assays suggests that pH 7.8 is optimal for the continued kinetic analysis of Na^+/K^+-ATPase; this pH provides not only the highest measured absorbances, but also the greatest slope. The final measured absorbances at 410 nm established that alterations in the pH of the reaction buffer have little influence on the final measurement, post-addition of NaOH.

Table E.1 Calculated enzymatic activity of Na^+/K^+-ATPase, over a range of pH values

	Endpoint Assay		Kinetic Assay	
	Enzyme Activity (μmol min^{-1})	Specific Activity (μmol min^{-1} mg^{-1})	Enzyme Activity (μmol min^{-1})	Specific Activity (μmol min^{-1} mg^{-1})
pH 7.6	3.64E-04	1.21E-02	3.03E-03	1.01-01

148

pH 7.8	3.71E-04	1.24E-02	5.94E-03	1.98E-01
pH 8.0	3.56E-04	1.19E-02	4.24E-03	1.41E-01
pH 8.2	3.55E-04	1.18E-02	2.82E-03	9.41E-02

Endpoint pNPPase activity assays demonstrated that not only was phosphatase activity greater in brain homogenate samples when compared to purified myelin samples of equal protein content, but that enzyme activity exhibited a positive dose-response; increased total myelin protein generated a linear increase in enzyme activity (results not shown). The addition of 100 mM Na_3VO_4, 15 mM NaN_3, or 10 mM ouabain to the purified myelin samples also generated little or no change in enzyme activity, although it did demonstrate significant decreases in the phosphatase activity of brain homogenate samples of equal protein content (results not shown).

E.4 Discussion and Conclusions

Steady-state kinetics offers a very good approximation of the rates of enzymatic reactions [3]. Although pH 7.8 appears to be ideal for kinetic evaluation of Na^+/K^+-ATPase using the pNPPase activity assay, the kinetic lag observed in Figure E.2 dictates that further method development is required. The kinetic lag may be a consequence of investigating Na^+/K^+-ATPase activity within vesicles; recall that the isolated myelin exists as vesicles and for the reaction substrate (pNPP) to interact with Na^+/K^+-ATPase, a membrane protein, it may need to be incorporated into these vesicles [8]. The substrate must be able to reach the active site of the enzyme, in order for this assay to be successfully applied. A delay in pNPPase activity may therefore be the result of the time requirement of this integration. The myelin vesicles themselves may also cause light

149

scattering during spectrophotometric analysis, which would in turn cause fluctuations in the measured absorbances at 410 nm. As a result, it may be necessary to further purify Na^+/K^+-ATPase from the myelin membrane, such that its activity can be more accurately assessed.
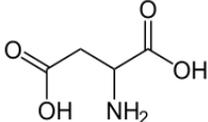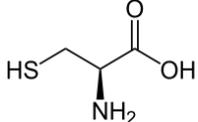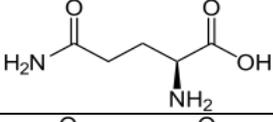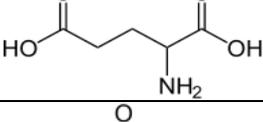
Ouabain-sensitivity has historically been used to identify the phosphatase activity of a sample which is attributable to Na^+/K^+-ATPase [7]. Unfortunately, this doe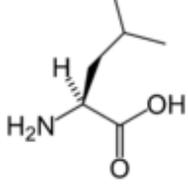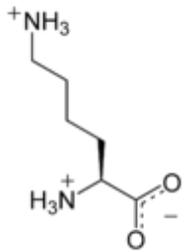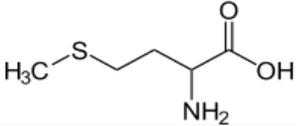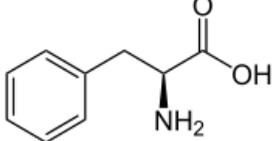s not account for any enzymatic activity associated with the α_1 isoform, as it is ouabain-resistant. Only Na^+/K^+-ATPase α_2 and α_3 are ouabain-sensitive and will be successfully inhibited [1]. Other inhibitors need to be examined for the accurate determination of Na^+/K^+-ATPase activity within the myelin membrane. These may include sodium vanadate, sodium azide, and potassium nitrate; they are inhibitors of P-type ATPase activity, F_0F_1-type ATPase activity, and V-type ATPase activity, respectively. By using a variety of phosphatase or ATPase inhibitors, it may also be possible to determine the enzymatic activity attributable to each of the three Na^+/K^+-ATPase alpha isoforms in myelin.

Once a kinetic activity assay for Na^+/K^+-ATPase of myelin origin has been successfully developed, the reactions can be manipulated, and a variety of analyses can be performed using the acquired data. Specific enzymatic activity, as well as initial rates, V_{max}, and the apparent Michaelis constant (K_M) will be calculated. Dose-response experiments may be performed using a range of substrate concentrations. Similarly, the half maximal inhibitory concentration (IC_{50}) of ouabain and other ATPase inhibitors can be determined.

E.5 References

1. S. Alberti, E.A. Gregorio, C.T. Spadella & C. Cojocel, Localization and irregular distribution of Na,K-ATPase in myelin sheath from rat sciatic nerve, Tissue Cell 39 (2007) 195-201.

2. M.L. Caspers, M. Bussone, M.J. Dow, L.J. Ulanski & P. Grammas, Alterations of cerebromicrovascular Na +, K +- ATPase activity due to fatty acids and acute hypertension, Brain Res. 602 (1993) 215-220.

3. A. Fersht, Enzyme Structure and Mechanism, W. H. Freeman and Company, San Francisco, 1977.

4. M.G. Marichal, A.R. Delcastillo, P.M. Vasallo & E.B. Arias, Characterization of K+-dependent and K+-independent p-nitrophenylphosphatase activity of synaptosomes, Neurochem.Res. 18 (1993) 751-758.

5. W.T. Norton, Isolation of myelin from nerve tissue, Meth. Enzymol. 31 (1974) 435-444.

6. S. Nouri & F. Haghseresht, Adsorption of p -Nitrophenol in Untreated and Treated Activated Carbon, Adsorption 10 (2004) 79-86.

7. K. Renkawek, W.O. Renier, J.H.H.M. Pont, O.J.M. Vogels & F.J.M. Gabreels, Neonatal Status Convulsivus, Spongiform Encephalopathy, and Low Activity of Na /K -ATPase in the Brain, Epilepsia 33 (1992) 58-64.

8. Siegel, G.J., B.W. Agranoff, R.W. Albers, S.K. Fisher & M.D. Uhler. Basic Neurochemistry: Molecular, Cellular and Medical Aspects. Philadelphia: Lippincott-Raven (1999).

Appendix F – Peptide Fragmentation in Mass Spectrometry

Figure F.1 Peptide fragmentation in mass spectrometry

The major y and b ions generated during protein identification by mass spectrometry are produced by fragmentation at amide bonds. The assignment of y and b ion values to amino acid residues or peptide fragments is indicated in red.

Table F.1 Residue masses of amino acids for protein identification in mass spectrometry

The monoisotopic masses of amino acid residues are used for the sequencing of peptides in mass spectrometry. The 20 common amino acids often fragment at amide bonds generating the major y and b fragment ions which have mass-to-charge ratios that correspond to these monoisotopic masses.

Amino Acid	Symbol	Type	Structure	Monoisotopic Mass of Residue
Alanine	A	Non-polar, aliphatic		71.03711
Arginine	R	Positively charged		156.10111
Asparagine	N	Polar, uncharged		114.04293

Aspartate	D	Negatively charged		115.02694
Cysteine	C	Polar, uncharged		103.00919
Glutamine	Q	Polar, uncharged		128.05858
Glutamate	E	Negatively charged		129.04259
Glycine	G	Non-polar, aliphatic		57.02146
Histidine	H	Positively charged		137.05891
Isoleucine	I	Non-polar, aliphatic		113.08406
Leucine	L	Non-polar, aliphatic		113.08406
Lysine	K	Positively charged		128.09496
Methionine	M	Non-polar, aliphatic		131.04049
Phenylalanine	F	Aromatic		147.06841
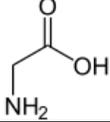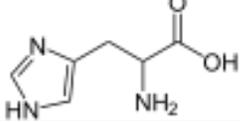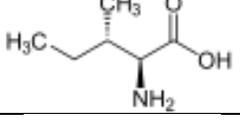
|				
Proline	P	Non-polar, aliphatic		97.05276
Serine	S	Polar, uncharged		87.03203
Threonine	T	Polar, uncharged		101.04768
Tryptophan	W	Aromatic		186.07931
Tyrosine	Y	Aromatic		163.06333
Valine	V	Non-polar, aliphatic		99.06841
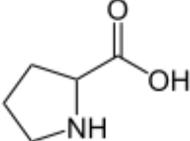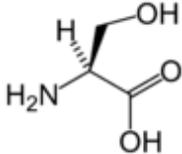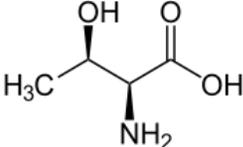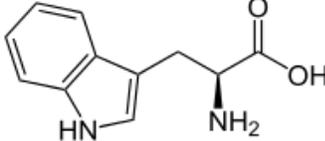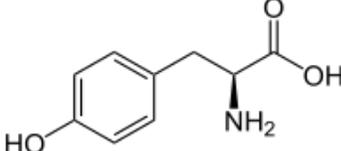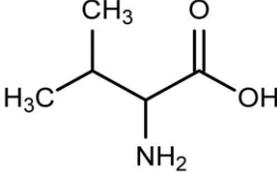
Appendix G – Additional Western Blots
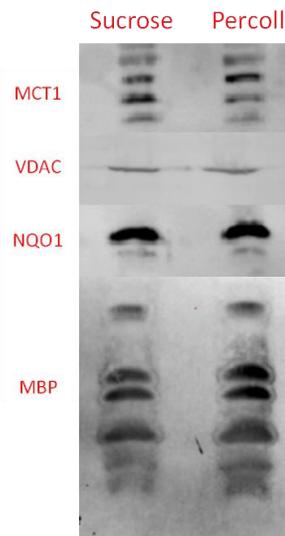
Figure G.1 Protein expression in myelin isolated using sucrose and Percoll gradient methods

Enhanced chemiluminescent Western blot detection of MCT1, VDAC, NQO1, and MBP in partially delipidated myelin samples, of equivalent protein content, from sucrose-gradient and Percoll-gradient isolation methods. Equal volumes (12.5 µL), and therefore equal protein (approximately 50 µg of total myelin protein), of each sample were separated on 14% SDS-PAGE and transferred to nitrocellulose membrane. The corresponding primary and secondary antibodies used are described in Table 2.3. Each Western blot was imaged using the VersaDoc 4000 (Bio-Rad) with an exposure time of 30-400 seconds, ensuring non-saturation.
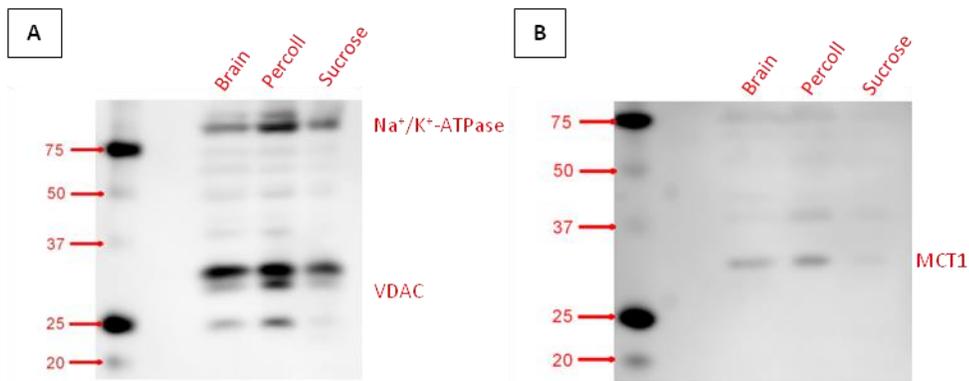
Figure G.2 Comparison of isolated myelin with brain homogenate

Enhanced chemiluminescent Western blot detection of: **A)** Na+/K+-ATPase and VDAC; **B)** MCT1; in partially delipidated brain homogenate and myelin samples, of equivalent protein content, from sucrose-gradient and Percoll-gradient isolation methods. Equal volumes (18.75 µL), and therefore equal protein (approximately 75 µg of total myelin protein), of each sample were separated on 14% SDS-PAGE and transferred to nitrocellulose membrane. The corresponding primary and secondary antibodies used are described in Table 2.3. Each Western blot was imaged using the VersaDoc 4000 (Bio-Rad) with an exposure time of 30-400 seconds, ensuring non-saturation.
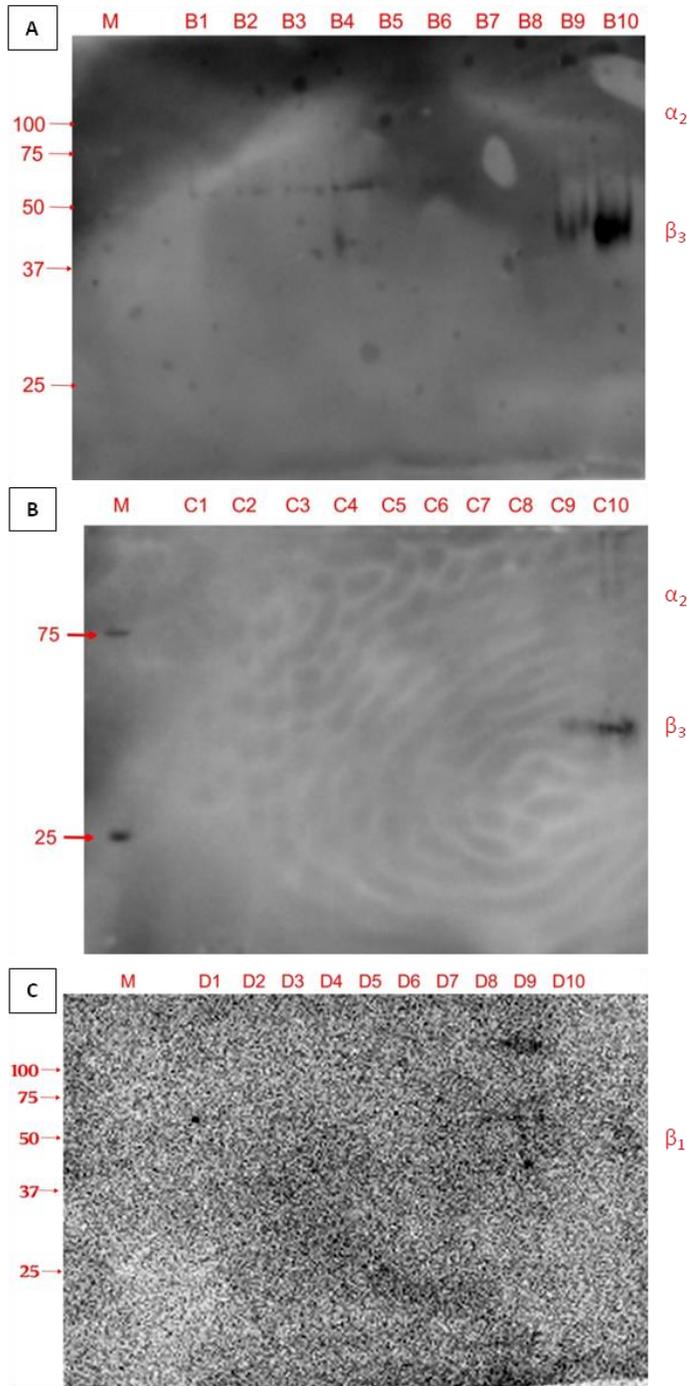
Figure G.3 Detection of Na$^+$/K$^+$-ATPase subunit isoforms in myelin DRMs

Enhanced chemiluminescent Western blot detection of: **A)** Na$^+$/K$^+$-ATPase α_2 and β_3; **B)** Na$^+$/K$^+$-ATPase α_2 and β_3; **C)** Na$^+$/K$^+$-ATPase β_1. Equal volumes (20 μL) of each acetone-precipitated lipid raft fraction (B1-10, C1-10, and D1-10), isolated as CHAPS DRMs, were separated on 12% SDS-PAGE and transferred to nitrocellulose membrane. Fractions B3, B4, C3, C4, D3 and D4 represent the low density, raft fractions; alternatively, fractions B9, B10, C9, C10, D9 and D10 represented the non-raft, high density fractions. The corresponding primary and secondary antibodies used are described in Table 2.3. Each Western blot was imaged using the VersaDoc 4000 (Bio-Rad) with an exposure time of 30-200 seconds, ensuring non-saturation.

# Appendix H – Comparison of Densitometric Data Without β-Actin Control

Table H.1 Western blot intensity data for alternate sample sets without a β-actin control

Raw data from densitometric analysis of CD1 and ND4 Western blot analysis, without normalization to β-actin. Intensities are provided for each Na$^+$/K$^+$-ATPase subunit isoform, as well as each glycosylation state of the β$_1$ subunit; Band 1 to Band 4 represent the highest molecular mass protein band to the lowest molecular mass (unglycosylated core) protein band, respectively. Standard deviation of the pixel intensities in each sample was calculated by Image Lab Version 5.0 (Bio-Rad).

	Age	Data Set	Measurement	Subunit Isoform									
				Alpha 1	Alpha 2	Alpha 3	Beta 1	Beta 2	Beta 3	Beta 1 Band 1	Beta 1 Band 2	Beta 1 Band 3	Beta 1 Band 4
CD1 Control Myelin	3.10 months	1	Intensity of Enhanced Chemiluminescent Signal (Sample)	949982	177210.5	3338678	369958.2	3736108	2786185	54978.14	68599	55692.29	29271
			Standard Deviation of Chemiluminescent Signal	6188.159	2576.144	13824.59	588.9315	10654.79	7338.029	496.1169	572.695	762.3669	312.121
		2	Intensity of Enhanced Chemiluminescent Signal (Sample)	483129.5	36782.64	1083381	1856270	2225996	3205753	250723	162529	176851	47232
			Standard Deviation of Chemiluminescent Signal	3024.82	824.3722	4967.65	763.5356	7210.989	8782.518	979.4812	637.9062	625.3855	421.3716
	7.65 months	1	Intensity of Enhanced Chemiluminescent Signal (Sample)	2385123	17775.33	3762310	1212395	6004631	3298992	43489.79	290223.8	473463.4	143777.6
			Standard Deviation of Chemiluminescent Signal	15042.21	2149.99	16047.69	2054.5	14520.01	8695.68	363.794	1350.82	3290.72	806.4366
		2	Intensity of Enhanced Chemiluminescent Signal (Sample)	1175295	925577.6	2333128	1352819	6709981	6613303	94498.76	285076.6	367779.1	70889.52
			Standard Deviation of Chemiluminescent Signal	9068.39	8504.181	10404.16	2258.68	18604.01	12467.35	1004.61	1836.48	3503.16	811.3904
	9.00 months	1	Intensity of Enhanced Chemiluminescent Signal (Sample)	455076.3	366972	2568857	317021.5	5010588	4812661	28243.8	113739.1	81498.15	11115.8
			Standard Deviation of Chemiluminescent Signal	2195.755	2800.039	13599.17	623.7382	11997.7	9867.872	335.1071	750.8703	938.0963	155.6221

|													
		2	Intensity of Enhanced Chemiluminescent Signal (Sample)	1248363	694249.2	3619293	455475.7	5135876	3998997	45878.65	145469.6	87800.8	5208.42
			Standard Deviation of Chemiluminescent Signal	8557.57	5894.32	12913.14	570.544	12736.53	8775.83	263.1928	649.2042	607.0426	116.3775
	13.02 months	1	Intensity of Enhanced Chemiluminescent Signal (Sample)	2545489	34753.5	2764283	312825.4	3780305	3199185	44710.23	123206.2	35265.69	391.9821
			Standard Deviation of Chemiluminescent Signal	17300.53	1325.992	11451.41	536.1424	10378.71	9319.39	472.5498	560.7273	521.9172	49.98207
		2	Intensity of Enhanced Chemiluminescent Signal (Sample)	2697860	676230.2	3598350	650954.6	4566681	1653301	47033.25	198043	82480.5	49149.06
			Standard Deviation of Chemiluminescent Signal	17006.02	5156.71	14758.39	1029.21	10633.07	4943.56	586.7155	1153.26	1489.24	421.3461
ND4 Transgenic Myelin	3.10 months	1	Intensity of Enhanced Chemiluminescent Signal (Sample)	2791077	166966.3	4204345	413235.6	2247258	4700973	6645.86	79621.71	176561	30409.86
			Standard Deviation of Chemiluminescent Signal	18301.66	4499.504	16928.69	1009.66	6156.039	11436.92	204.3782	580.6925	1912.33	317.0696
		2	Intensity of Enhanced Chemiluminescent Signal (Sample)	873924.1	161674.6	1630287	842295.5	1510235	4864355	570	55844	258577	76477
			Standard Deviation of Chemiluminescent Signal	4653.235	1382.791	7264.35	595.6856	4815.513	12951.38	381.5696	404.2201	938.8458	383.2174
	7.65 months	1	Intensity of Enhanced Chemiluminescent Signal (Sample)	1426324	87658.67	2845655	414859.3	5230054	4985924	-6062.7	205027.6	133935	11218.42
			Standard Deviation of Chemiluminescent Signal	9267.994	1842.78	13517.72	908.0418	13567.35	10727.75	153.5906	1039.3	1163.36	173.7648
		2	Intensity of Enhanced Chemiluminescent Signal (Sample)	813033.6	455770	1621032	609532.3	6395463	6002612	2926.9	166333.5	168380.8	21381.14
			Standard Deviation of Chemiluminescent Signal	6539.262	3467.39	7943.9	902.6996	18032.15	11167.67	205.0394	911.4549	1151.38	227.9837
	9.00 months	1	Intensity of Enhanced Chemiluminescent Signal (Sample)	1804484	483497.7	3350180	855650.9	10624075	6537429	28272.75	260014.3	346565.8	19455
			Standard Deviation of Chemiluminescent Signal	7956.94	2906.148	16027.87	1930.13	19336.02	13971.82	370.173	1394.09	3616.76	265.9338
		2	Intensity of Enhanced Chemiluminescent Signal (Sample)	2500319	1152316	5814317	1562077	8893667	5939907	31243.42	466539.3	461119.8	15398.23

|													
			Standard Deviation of Chemiluminescent Signal	15829.75	9213.09	16031.52	2536.84	20138.52	13223.55	305.6617	2257.18	3513.76	332.7187
	13.02 months	1	Intensity of Enhanced Chemiluminescent Signal (Sample)	1550445	338870.9	2635873	669467.8	7384027	4600099	55969.46	319809	90608.92	9454.8
			Standard Deviation of Chemiluminescent Signal	9899.051	3626.769	12132.26	1128.22	16507.52	12479.78	602.2975	1287.1	923.8873	101.5365
		2	Intensity of Enhanced Chemiluminescent Signal (Sample)	2998635	1148146	4201894	993252.2	6297561	3457138	25295	425775.8	178040.8	50861.83
			Standard Deviation of Chemiluminescent Signal	17870.8	7724.68	14417.33	1622.31	14580.09	10064.49	344.8458	1964.29	1961.05	357.1174
Ratio (CD1 Control Myelin to ND4 Transgenic Myelin)	3.10 months	1	Ratio of Diseased to Healthy Intensities	2.938031	0.942192	1.259284	1.116979	0.601497	1.687244	0.120882	1.160683	3.170295	1.038907
		2	Ratio of Diseased to Healthy Intensities	1.808882	4.395406	1.504814	0.453757	0.678454	1.517383	0.002273	0.343594	1.462118	1.619178
	7.65 months	1	Ratio of Diseased to Healthy Intensities	0.598009	4.931479	0.756358	0.342182	0.871003	1.511348	-0.13941	0.706446	0.282883	0.078026
		2	Ratio of Diseased to Healthy Intensities	0.69177	0.492417	0.694789	0.450565	0.953127	0.907657	0.030973	0.583469	0.457831	0.301612
	9.00 months	1	Ratio of Diseased to Healthy Intensities	3.965235	1.317533	1.304152	2.699031	2.120325	1.358381	1.001025	2.28606	4.252437	1.750211
		2	Ratio of Diseased to Healthy Intensities	2.002878	1.659801	1.606479	3.429549	1.731675	1.485349	0.681001	3.207126	5.251886	2.956411
	13.02 months	1	Ratio of Diseased to Healthy Intensities	0.609095	9.750699	0.953547	2.140069	1.953288	1.437897	1.251827	2.595722	2.569322	24.12049
		2	Ratio of Diseased to Healthy Intensities	1.111486	1.697862	1.167728	1.525839	1.379024	2.091051	0.537811	2.149917	2.15858	1.034848
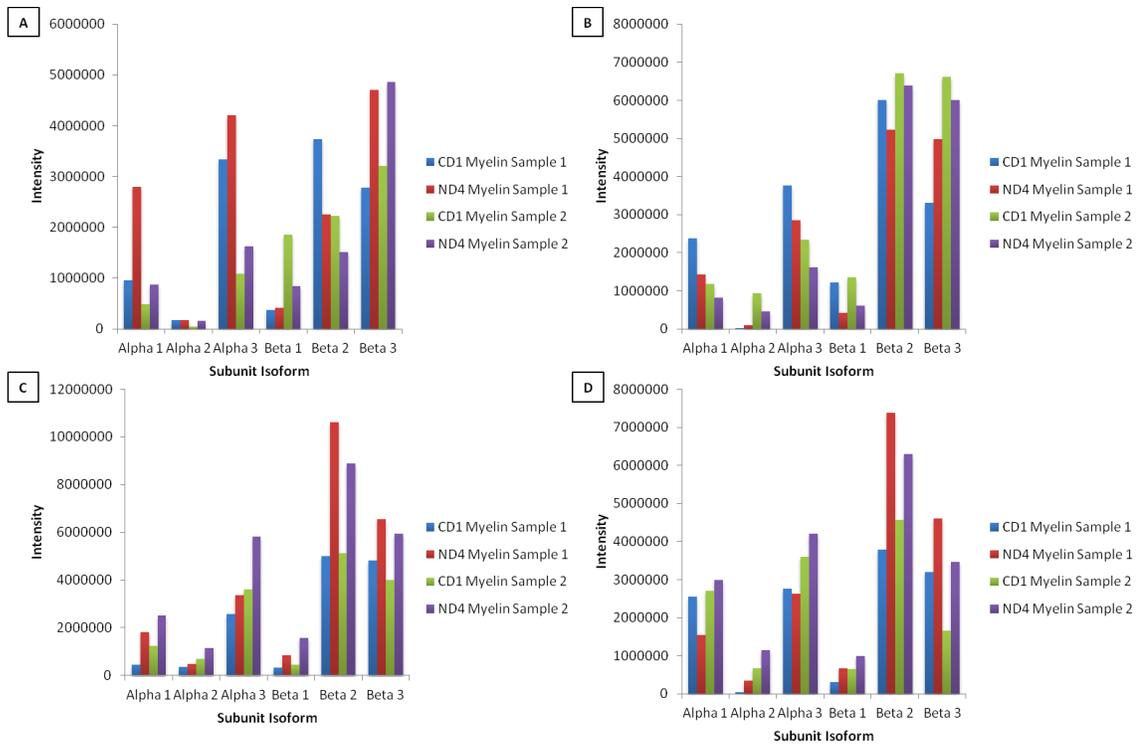
Figure H.1 Compared intensities of each Na$^+$/K$^+$-ATPase subunit isoform, between two sets of CD1 and ND4 myelin samples, in each age group

Intensity of each Na$^+$/K$^+$-ATPase subunit isoform, ensuring non-saturation and subtracting background. Comparisons were for CD1 and ND4 myelin at: **A)** 3.00 months of age; **B)** 7.65 months of age; **C)** 9.00 months of age; **D)** 13.02 months of age.
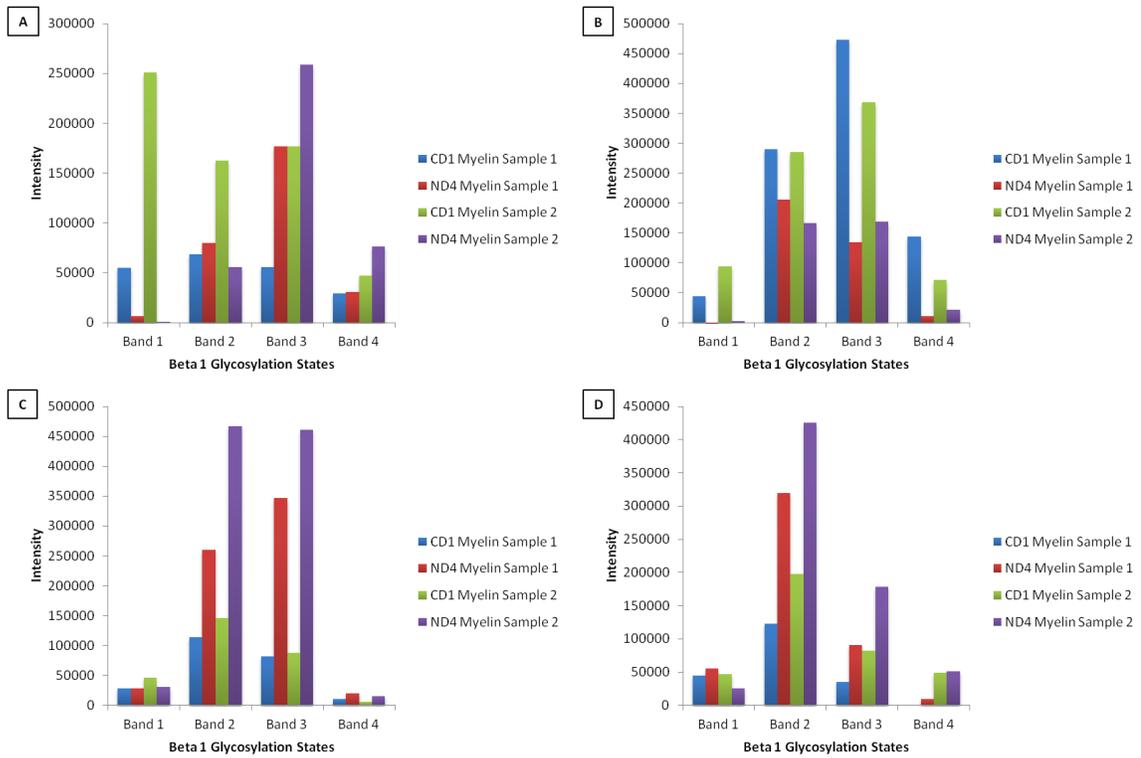
Figure H.2 Compared intensities of each Na$^+$/K$^+$-ATPase β$_1$ glycosylation state, between two sets of CD1 and ND4 myelin samples, in each age group

Intensity of each Na$^+$/K$^+$-ATPase β$_1$ glycosylation state, ensuring non-saturation and subtracting background. Bands 1 to 4 represent the highest molecular weight form of Na$^+$/K$^+$-ATPase β$_1$ (3 N-glycans) to the lowest molecular weight form (core, non-glycosylated), respectively. Comparisons were for CD1 and ND4 myelin at: **A)** 3.00 months of age; **B)** 7.65 months of age; **C)** 9.00 months of age; **D)** 13.02 months of age.
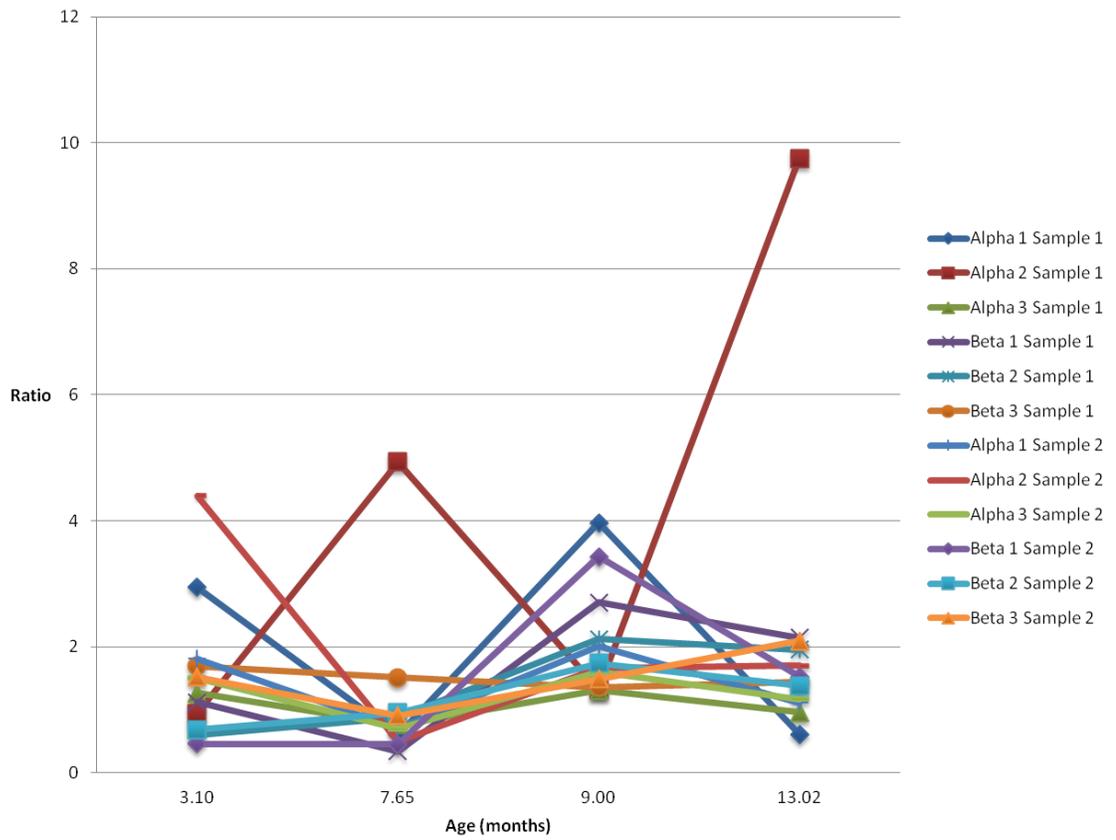
Figure H.3 Ratio of intensities for each Na$^+$/K$^+$-ATPase subunit isoform in ND4 myelin, relative to CD1 myelin, with aging

Intensity of each Na$^+$/K$^+$-ATPase subunit isoform in ND4 myelin relative to CD1 myelin, ensuring non-saturation and subtracting background. Results from two separate Western blot data sets are shown (Sample 1 and Sample 2). Intensity was measured at 3.10, 7.65, 9.00 and 13.02 months of age.
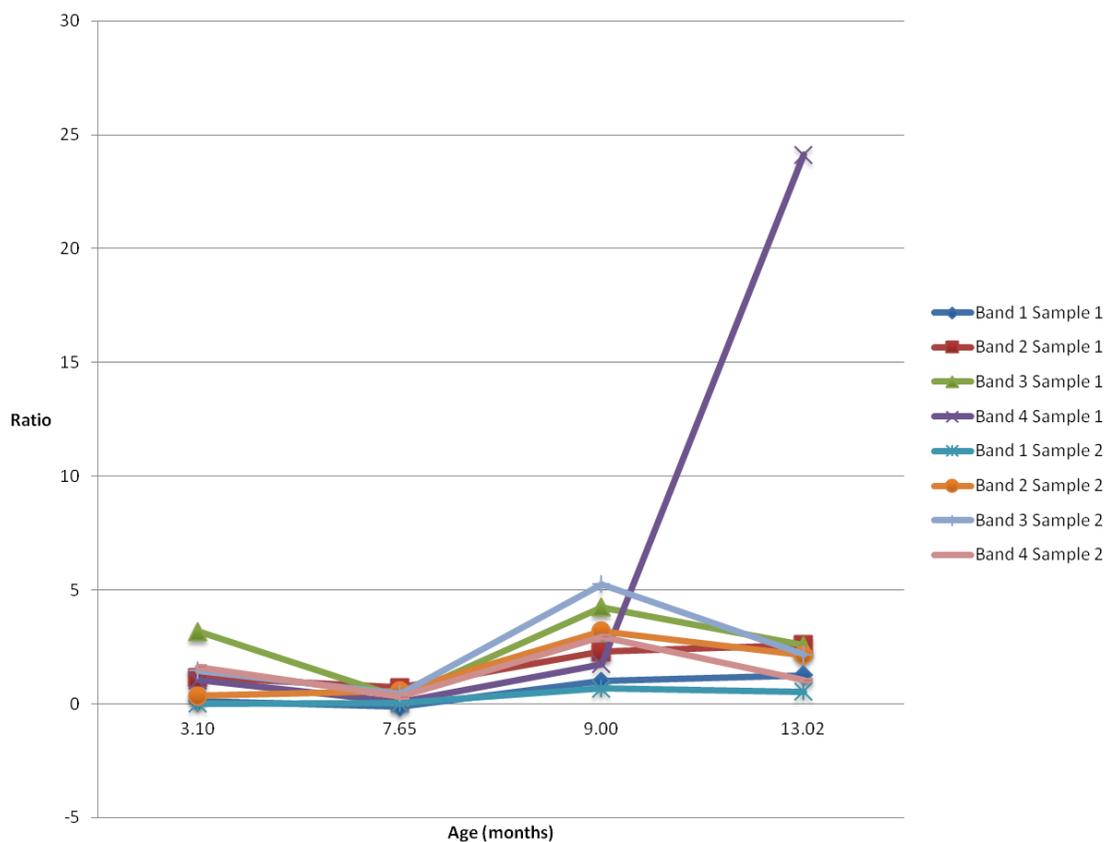
Figure H.4 Ratio of intensities for each Na$^+$/K$^+$-ATPase β$_1$ glycosylation state in ND4 myelin, relative to CD1 myelin, with aging

Intensity of each Na$^+$/K$^+$-ATPase β$_1$ glycosylation state in ND4 myelin relative to CD1 myelin, ensuring non-saturation and subtracting background. Bands 1 to 4 represent the highest molecular weight form of Na$^+$/K$^+$-ATPase β$_1$ (3 N-glycans) to the lowest molecular weight form (core, non-glycosylated), respectively. Results from two separate Western blot data sets are shown (Sample 1 and Sample 2). Intensity was measured at 3.10, 7.65, 9.00 and 13.02 months of age.